National Library
of Canada

Bibliothèque nationale
du Canada

Canadian Theses Service

Services des thèses canadiennes

Ottawa, Canada
K1A 0N4

CANADIAN THESES

THÈSES CANADIENNES

NOTICE

The quality of this microfiche is heavily dependent upon the quality of the original thesis submitted for microfilming. Every effort has been made to ensure the highest quality of reproduction possible.

If pages are missing, contact the university which granted the degree.

Some pages may have indistinct print especially if the original pages were typed with a poor typewriter ribbon or if the university sent us an inferior photocopy.

Previously copyrighted materials (journal articles, published tests, etc.) are not filmed.

Reproduction in full or in part of this film is governed by the Canadian Copyright Act, R.S.C. 1970, c. C-30. Please read the authorization forms which accompany this thesis.

AVIS

La qualité de cette microfiche dépend grandement de la qualité de la thèse soumise au microfilmage. Nous avons tout fait pour assurer une qualité supérieure de reproduction.

S'il manque des pages, veuillez communiquer avec l'université qui a conféré le grade.

La qualité d'impression de certaines pages peut laisser à désirer, surtout si les pages originales ont été dactylographiées à l'aide d'un ruban usé ou si l'université nous a fait parvenir une photocopie de qualité inférieure.

Les documents qui font déjà l'objet d'un droit d'auteur (articles de revue, examens publiés, etc.) ne sont pas microfilmés.

La reproduction, même partielle, de ce microfilm est soumise à la Loi canadienne sur le droit d'auteur, SRC 1970, c. C-30. Veuillez prendre connaissance des formules d'autorisation qui accompagnent cette thèse.

THIS DISSERTATION
HAS BEEN MICROFILMED
EXACTLY AS RECEIVED

LA THÈSE A ÉTÉ
MICROFILMÉE TELLE QUE
NOUS L'AVONS REÇUE

NL 339 (r. 86/01)

Canadä

0-315-22920-9

National Library of Canada
Canadian Theses Division
Ottawa, Canada
K1A 0N4

Bibliothèque nationale du Canada
Division des thèses canadiennes

54

PERMISSION TO MICROFILM — AUTORISATION DE MICROFILMER

- Please print or type — Écrire en lettres moulées ou dactylographier

Full Name of Author — Nom complet de l'auteur
CHIU STEPHEN KAM-LING

Date of Birth — Date de naissance
Oct 8 1954

Country of Birth — Lieu de naissance
HONG KONG

Permanent Address — Résidence fixe
Alberta Research Council
8615 - 8ST NE CALGARY AB

Title of Thesis — Titre de la thèse
Seismic Tomography of the Lithosphere

University — Université
University of Alberta

Degree for which thesis was presented — Grade pour lequel cette thèse fut présentée
Ph. D

Year this degree conferred — Année d'obtention de ce grade
1985

Name of Supervisor — Nom du directeur de thèse
Dr. E.R Kanasewich

Permission is hereby granted to the NATIONAL LIBRARY OF CANADA to microfilm this thesis and to lend or sell copies of the film.

The author reserves other publication rights, and neither the thesis nor extensive extracts from it may be printed or otherwise reproduced without the author's written permission.

L'autorisation est, par la présente, accordée à la BIBLIOTHÈQUE NATIONALE DU CANADA de microfilmer cette thèse et de prêter ou de vendre des exemplaires du film.

L'auteur se réserve les autres droits de publication; ni la thèse ni de longs extraits de celle-ci ne doivent être imprimés ou autrement reproduits sans l'autorisation écrite de l'auteur.

Date
July 24 '85

Signature
Stephen Chiu

NL-91 (4/77)

THE UNIVERSITY OF ALBERTA

SEISMIC TOMOGRAPHY OF THE LITHOSPHERE

by

© STEPHEN KAM-LING CHIU

A THESIS

SUBMITTED TO THE FACULTY OF GRADUATE STUDIES AND RESEARCH

IN PARTIAL FULFILMENT OF THE REQUIREMENTS FOR THE DEGREE

OF DOCTOR OF PHILOSOPHY

IN

GEOPHYSICS

DEPARTMENT OF PHYSICS

EDMONTON, ALBERTA

FALL 1985

The Royal Society
6 Carlton House Terrace, London, SW1Y 5AG
Telephone 01-839 5561 Telex 917876

P1276/RGT/VWC

31st May 1985

AIRMAIL

Mr S. Chiu
Physics Department
University of Alberta
EDMONTON
Alberta
Canada
T6G 2J1

Dear Sir,

Thank you for your letter dated 18th May 1985 requesting permission to reproduce material from the Royal Society's Philosophical Transactions. The Society will have no objection provided:

1. You have obtained the author's permission
2. A reference is made to the original publication.

Yours faithfully,

R.G.THEOBALD
Publications Sales Officer

CANADIAN SUPERIOR OIL LTD.

1985 03 29

Physics Department
University of Alberta
Edmonton, Alberta
T6G 2J1

Attention: Mr. Stephen Chiu

Dear Mr. Chiu:

Subject: The Western Canada Sedimentary Basin
Permission to use Fig. 2

Thank you for your letter concerning the subject request. I personally have no objections, but it is my understanding that you shall have to obtain official permission from the Royal Society. The publication in which the subject paper is contained is entitled The Evolution of Sedimentary Basins. To quote from the fly leaf, "request for the copying or reprinting of any article for any purpose should be sent to the Royal Society". Their address is: Royal Society, 6 Carlton House Terrace, London SW1Y5AG.

Sincerely,

J. W. PORTER

JWP/sc

Three Calgary Place, 355 Fourth Avenue S.W. Calgary, Alberta T2P 0J1 Telephone: (403) 267-4110

Physics Department
University of Alberta
Edmonton, Alberta
July 2, 1985

Dear C. Macrides:

I would like to use two of your diagrams in my Ph. D thesis. Can I have your written permission to use Figures 32 and 35 in your Master's thesis- "Interpretation of seismic refraction profiles in southern Saskatchewan", University of Alberta.

I greatly appreciate your assistance.

Sincerely,

Stephen Chiu

Stephen Chiu

I hereby give my permission to Stephen Chiu for using figures 32 and 35 of my M.Sc. thesis in his Ph.D. thesis.

Costas G. Macrides
July 3, 1985

Physics Department
University of Alberta
Edmonton, Alberta
Canada
T6G 2J1
March 19, 1985

Earth Physics Branch
Ottawa, Ont.
K1A 0Y3

Dear Dr. A. G. Green,

I would like to use two of your diagrams in my Ph.D thesis. Can I have your written permission to use the figure 4 and 5 in your paper- "Evolution of the Churchill Province and Western margin of the Superior Province in Canada and the North-Central United States", Tectonophysics, 1985 (in press)

I greatly appreciate your assistance in this matter.

Sincerely,

Stephen Chiu

Stephen Chiu

You have my permission to use figures 4 and 5 of Green et al (1985) in your thesis. I enclose prints of these figures for your use.

All the best

Alan Green

Physics Department
University of Alberta
Edmonton, Alberta
Canada
T6G 2J1
March 19, 1985

Earth Physics Branch
Ottawa, Ont.
K1A 0Y3

Dear Dr. P. A. Camfield,

I would like to use one of your diagram in my Ph.D thesis. Can I have your written permission to use the figure 2 in your paper- "A possible Proterozoic plate boundary in North America", Can. J. Earth Sci. 14, 1977.

I greatly appreciate your assistance in this matter.

Sincerely,

Stephen Chiu

Stephen Chiu

85/03/27

Dear Mr. Chiu,

As long as you note in the caption the source of the figure, I am pleased to give you my permission to use the above diagram. I am sure that Ian Gough would have no objection. I trust that you will note our most recent work (enclosed) — the conductive body links to the Rottenstone - LaRonge Belt, not to the Wollaston Domain or the Needle Falls Shear Zone.

Sincerely yours,

P. A. Camfield

THE UNIVERSITY OF ALBERTA

RELEASE FORM

NAME OF AUTHOR STEPHEN KAM-LING CHIU

TITLE OF THESIS SEISMIC TOMOGRAPHY OF THE LITHOSPHERE

DEGREE FOR WHICH THESIS WAS PRESENTED DOCTOR OF PHILOSOPHY

YEAR THIS DEGREE GRANTED FALL 1985

Permission is hereby granted to THE UNIVERSITY OF ALBERTA LIBRARY to reproduce single copies of this thesis and to lend or sell such copies for private, scholarly or scientific research purposes only.

The author reserves other publication rights, and neither the thesis nor extensive extracts from it may be printed or otherwise reproduced without the author's written permission.

(SIGNED) Stephen Chiu

PERMANENT ADDRESS:

Alberta Research Council
8615 - 8ST N.E.
Calgary, AB

DATED July 8 1985

THE UNIVERSITY OF ALBERTA

FACULTY OF GRADUATE STUDIES AND RESEARCH

The undersigned certify that they have read, and recommend to the Faculty of Graduate Studies and Research, for acceptance, a thesis entitled SEISMIC TOMOGRAPHY OF THE LITHOSPHERE submitted by STEPHEN KAM-LING CHIU in partial fulfilment of the requirements for the degree of DOCTOR OF PHILOSOPHY in GEOPHYSICS.

E. R. Kanasewich

Supervisor

....

....

....

Zolta Hajnal

External Examiner

Date...July 8/85..................

ABSTRACT

A tomographic method has been developed to obtain simultaneously body wave velocities and three-dimensional structure of interfaces from seismic refraction or/and reflection data. The medium consists of layers with piecewise continuous arbitrary three-dimensional curved interfaces separating homogeneous material with different elastic properties. The interface is defined by a polynomial surface.

The elastic waves are assumed to be refracted or reflected at curved interfaces in which the ray paths satisfy Snell's law. The ray tracing for each source-receiver pair is determined by solving a system of non-linear equations. This method of three-dimensional ray tracing is fast, accurate, and efficient in computing a large group of seismic rays including converted phases and multiples.

A damped least-squares inversion scheme is formulated to reconstruct the interval velocity and three-dimensional structure of the interface by minimizing the difference between the observations and computed travel times. The results from synthetic models indicate that the solutions converge quickly to the true model. In addition, it has been found to give rapid convergence even in the case of complex faulted models using noisy data. Typically, there are three to six iterations.

A Spatial Seismic Refraction Recording method (S^2R^2) was suggested by E. R. Kanasewich as a means of delineating the three-dimensional structure of any lithospheric interface such as the Moho discontinuity. The S^2R^2 produces a superabundance of common ray intersections at the target horizon. In this thesis the tomographic method has been developed to permit reliable imaging of three-dimensional structures with elastic wave data from spatial seismic refraction recording.

A crustal model of a portion of the Williston Basin in south-central Saskatchewan was obtained by seismic tomography. It indicates significant faulting in the crust and several normally faulted blocks at the Moho discontinuity. The faults are also associated with linear aeromagnetic anomalies. The area is notable for its thick crust, local seismicity, and a linear conductivity anomaly.

Furthermore, the seismic tomographic method was applied to a Vibroseis seismic section obtained in 1984 on Vancouver Island as a part of PROJECT LITHOPROBE. It has been demonstrated that this method is particularly useful for imaging the three-dimensional subsurface of subducting plates by taking advantage of crooked lines in a nominally two-dimensional seismic reflection survey.

ACKNOWLEDGEMENTS

I sincerely thank Dr. E. R. Kanasewich for his tireless effort, guidance, and encouragement throughout the entire programme. I would also like to express my gratitude to the CO-CRUST group, the LITHOPROBE group, and many persons who assisted in the 1981 and 1984 field operations.

Mr. Charles McCloughan and Mark Baxter offered many constructive suggestions and assistance during the preparation of seismic records and computer programs for constructing various regional maps. Their help is greatly appreciated. I also wish to acknowledge my wife, Theory, for her understanding and encouragement during this part of our life.

During the course of this research, the author was supported by a Graduate Teaching Assistantship from the Department of Physics, University of Alberta.

Finally, I would like to thank my parents who made it all possible.

Table of Contents

Chapter Page

1. INTRODUCTION 1

2. FORMULATION OF SEISMIC TOMOGRAPHY 4

2.1 Introduction 4

2.2 The forward modelling 6

2.3 Inversion procedure 10

2.4 Singular Value Decompostion (SVD) 14

2.5 Treating the ranking deficient case 17

2.6 Resolution and covariance matrices 22

2.7 Conclusions 26

3. REGIONAL SETTING, DATA ACQUISITION AND PROCESSING IN THE SASKATCHEWAN REGION 27

3.1 Geology of the Williston Basin 27

3.2 Deep structures 29

3.3 Geophysical characteristics 31

3.4 Extension of Canadian Shield beneath the Williston Basin 33

3.5 Ideal theoretical refraction recordings (S^2R^2) ..38

3.6 Previous seismic studies 43

3.7 Data acquisition 45

3.8 Spectral analysis 46

3.9 Bandpass filtering 50

4. INVERSION OF SASKATCHEWAN SPATIAL REFRACTION DATA ...52

4.1 Comments on refracted waves from the crust 52

4.2 Summary of inline refraction data 53

4.3 Test model 55

4.4 Presentation and comments on spatial refraction data 64

4.5 Analyses of wide-angle reflections 68
4.6 Determination of structure of the Moho 78
4.7 Discussion of the results 84
4.8 Conclusions 87
5. 3-D IMAGING OF VANCOUVER ISLAND REFLECTION DATA 88
5.1 Introduction 88
5.2 Synthetic model 89
5.3 Application to Vancouver Island reflection data .96
5.4 Conclusion 114
6. CONCLUSIONS 116
BIBLIOGRAPHY 118
APPENDIX ---COMPUTER PROGRAMS 129

List of Figures

Figure Page

3.1 (a) Principal physiographic divisions in Western Canada and the study area (rectangle). (b) The Western Canada sedimentary basin. Total preserved thickness of Phanerozoic rocks. Contours are in Kilometers. (from Porter et al., 1982, with permission) 28

3.2 Compiled aeromagnetic map for Manitoba and Saskatchewan in Canada and parts of North and South Dakota, Montana and Wyoming in the United States. Dotted lines show the important tectonic boundaries of the geological units. (from Green, et al., 1985, with permission) 32

3.3 Compiled Bouguer gravity anomaly map for Manitoba and Saskatchewan in Canada and parts of North and South Dakota, Montana and Wyoming in the United States. Tectonic boundaries are the same as shown in Figure 3.2. (from Green et al., 1985, with permission) 34

3.4 Location of the conductive body called the North American Central Plains anomaly, shown by the shaded strip. (from Camfield et al., 1977, with permission) 35

3.5 Tectonic map of the study area showing the locations of the shots and receivers used for this study. CC - Churchill craton, CLZ - Cree Lake zone, FF-SL - Flin Flon-Snow Lake belt, FRB - Fox River belt, GL - Glennie Lake domain, KG - Kisseynew belt, LR-LL - La Ronge-Lynn Lake Belt, R-SI - Reindeer-South Indian Lake belt, SC - Superior craton, TF - Thompson boundary fault, TFF - Tabbernor fault/fold zone, TNB - Thompson belt, W-C - Wathaman-Chipaweyan batholith, WC - Wyoming craton. (from Green, Chiu and others, 1984) 37

Figure Page

3.6 A spatial seismic refraction recording array to obtain a three-dimensional structure on the Moho discontinuity. The triangle of receivers has dimensions of 350 km and a receiver spacing of 2.5 km. The lines are surface projections of rays traversing below the Moho. Each source is recorded by all the receivers. 40

3.7 A spatial seismic refraction recording array to obtain a three-dimensional structure of intermediate crustal interfaces. The lines are surface projections of the head waves over one-third of the array shown in Figure 3.6. 41

3.8 Compiled Moho depths in the study area. Dotted lines are magnetic trends from Fig. 3.2. Lines A, B and C define the S^2R^2 profiles for this study. 44

3.9 (a) Plot of raw data, (b) Power spectrum estimate of record (5,5,1). The distance is 273.9 km from the shot. 48

3.10 (a) Plot of raw data, (b) Power spectrum estimate of record (6,9,1). The distance is 272.4 km from the shot. 49

3.11 (a) Power spectrum of noise for record (5,5,1), (b) Power spectrum of noise for record (6,9,1). 51

4.1 Record section of inline refraction line B in southern Saskatchewan (from Macrides, 1983, with permission). 54

Figure Page

4.2 Crustal model of inline refraction profile B (from Macrides, 1983). Shot 3 is the model from the source near Wynyard to the southwest. Shot 4 is from the source near Swift Current to the northeast. 56

4.3 Refracted (solid line) and reflected (dashed line) ray paths and the coordinate system. The direction cosines for the planes are a, b and c, and d is the distance of the normal to the origin. 58

4.4 (a) 3-D test model. The location of the receivers are shown as crosses along a triangular array on the surface. The sources are indicated as stars at the vertices. The three faulted blocks are marked as 1, 2, 3. (b) to (d) are the reduced travel times of the head waves from Moho discontinuity for sources S1 to S3. The dotted line is the computed initial assumption to the least-squares inversion. The dashed line is the first iteration, and the solid is the theoretical value. 59

4.5 (a) to (c) Reduced travel-time diagrams for S1 to S3 versus azimuth for both refracted and wide-angle reflected seismic rays. No noise is included. (i) Initial computed assumption for refracted arrivals; (ii) theoretical curve and final iterations for refraction arrivals; (iii) initial computed assumption for reflected arrivals; (iv) travel time for reflected waves after first iteration; (v) theoretical curve and second iteration for reflected waves. 62

4.6 The same results as in Figure 4.5 but with the introduction of random noise into the theoretical times. The standard deviation for the noise is 0.1 sec. 63

Figure Page

4.7 Surface projections of rays traversing below the Moho in Saskatchewan experiment (1981). 65

4.8 Reduced seismic refraction travel-time plots versus azimuth for the three broadside lines. The first curvilinear line (H) marks the Moho head wave, the other line (R1) marks the wide-angle reflections from the crust, and the third one the wide-angle Moho reflection (R3). 66

4.9 Reduced seismic refraction travel-time plots versus azimuth for the three broadside lines. DT is defined as normal moveout correction. The line (R1) marks the wide-angle reflections from the crust, and the second one the wide-angle Moho reflection (R3). 67

4.10 Map of southern Saskatchewan showing the location of the sources (small stars) and receivers (crosses) for spatial seismic refraction data. Aeromagnetic trends and faults are dashed lines. A, B, and C are refraction profiles. R, Reindeer-South Indian Lake belt; LR, La Ronge-Lynn Lake belt; GL, Glennie Lake domain; T, Tabbernor fault; FF, Flin Flon-Snow Lake belt. Earthquakes are shown as large stars. 69

4.11 Locations of the reflection points. A, B, and C are broadside refraction profiles corresponding to shot numbers 5, 9 and 2. The numbers on the outside triangle are the receiver station numbers; the numbers of the inside triangle are the corresponding projections of reflection mid-points from shots to receivers. Faults are solid lines. 71

Figure Page

4.12 (a) The structure of the reflected branch R1. Travel-time curves for: (b) shot2; (c) shot9; and (d) shot5. The solid line is from the field observations. The dashed line is the final value from the least-squares iteration assuming only two faulted planes. 73

4.13 (a) The structure of the reflected branch R2. Travel-time curves for: (b) shot2; (c) shot9; and (d) shot5. The solid line is from the field observations. The dashed line is the final value from the least-squares iteration assuming only two faulted planes. 75

4.14 (a) The structure of the Moho (R3) using wide-angle reflections only. Travel-time curves for: (b) shot2; (c) shot9; and (d) shot5. The solid line is from the field observations. The dashed line is the final value from the least-squares iteration assuming only two faulted planes. 77

4.15 (a) The structure of the Moho from refraction data. Travel-time curves of the refracted Moho arrivals for: (b) shot2; (c) shot9; and (d) shot5. The solid line is from the field observations. The dashed line is the final value from the least-squares iteration assuming only three faulted planes. 79

4.16 (a) The structure of the Moho from a combination of refraction and reflection data. Travel-time curves for refracted and reflected arrivals for: (b) shot2; (c) shot9; and (d) shot5. The solid line is from the field observations. The dotted line is for refracted arrivals after the fourth iteration. The crosses are the reflected arrivals after the fourth iteration. 81

Figure Page

4.17 (a) The resolution matrix from Saskatchewan spatial seismic refraction data. (b) The corresponding covariance matrix. Both matrices have dimensions of 12*12. The order of the elements from 1 to 12 for the model parameters on blocks 1, 2, and 3 is a_1, b_1, d_1, V_1, a_2, b_2, d_2, V_2, a_3, b_3, d_3, and V_3. 83

5.1 Reflected and transmitted ray paths and the coordinate system used in the ray-tracing algorithm. The solid circle is the shot and the square is the receiver. 90

5.2 Three-dimensional plot of synthetic model and ray paths from shots to receivers. The solid circles are shots and the squares are receivers. 92

5.3 (a) and (b). Shot and receiver configuration used in the synthetic data. The solid circles are shots and the squares are receivers. (c) and (d) are the corresponding isochron maps. 93

5.4 (a) to (f). Residual times between the computed and known model at each iteration step. Times are in milliseconds. 95

5.5 (a) to (f). Residual times between the computed and known model at each iteration step, with the introduction of random noise into the theoretical travel times. The standard deviation of the noise is 20 msec. Times are in milliseconds. 97

Figure Page

5.6 Three-dimensional plot of ray paths and the model obtained from the inversion procedure with the random noise added to the observations. 98

5.7 The expanded map of southern Vancouver Island shows the shot and receiver locations used in this study. Solid squares are sources; squares are receivers; crosses indicate an approximate surface projection of sub-surface reflecting points. 99

5.8 Example of a selected record. Ground length is approximately 10.8 km. Reflecting horizons C and E were used in this study. 101

5.9 Another example of a selected record. Ground length is approximately 10.8 km. Reflecting horizons C and E were used in this study. 102

5.10 The corresponding frequency-domain migrated section in this region. C is the decollement zone and E, the subduction zone. 103

5.11 The structure of the decollement zone obtained from the inversion procedure. 105

5.12 The structure of the subduction zone obtained from the inversion procedure. 107

5.13 The resolution matrices for the subduction zone. The order of model parameters from 1 to 4 is d, b, a, and V. (a) velocity parameter is not included; (b) velocity parameter is included. 108

Figure Page

5.14 The covariance matrices for the subducted plate. The order of model parameters from 1 to 4 is d, b, a, and V. (a) velocity parameter is not included; (b) velocity parameter is included. 110

5.15 Structural map of the decollement zone obtained by simple migration. 112

5.16 Structural map of the subduction zone obtained by simple migration. 113

5.17 Schematic diagram shows the structure of the decollement and subducting slabs. 115

1. INTRODUCTION

The purpose of this thesis is to describe a new tomographic method for obtaining three-dimensional structure and velocity information of the earth's lithosphere. The concept of seismic tomography has become an important tool for seismic modelling. The essence of seismic tomography is to extract information about the earth's structure and physical parameters of the media through which the seismic rays travel. By minimizing the difference between observations and computed travel times obtained by tracing the ray paths through an initial model, the initial model is modified iteratively by inverting a linearized version of a set of least-squares equations. The method handles both the refraction and/or reflection data.

The lithosphere is the colder, stronger, and more rigid outer shell, about 100 km thick, including the earth's crust and upper mantle. The crust is always defined as the region above the Mohorovicic discontinuity (or Moho). This discontinuity is the intervening boundary between the low velocity, very heterogeneous crust, about 5 to 60 km thick and a higher velocity, more homogeneous substratum called the mantle. Furthermore, this discontinuity has been found to be almost universally present beneath continents and oceans where the compressional wave velocity increases rapidly or discontinuously from deep crustal velocities of 6.5 to 7.3 km/s to mantle velocities between 7.7 and 8.4 km/s. Below the lithosphere is the asthenosphere which is usually thought to be a partially molten zone and is identified with a decrease in shear wave velocity, and sometimes, also the mantle compressional velocity. This thesis concentrates only on a determination of the structure of the crust and Moho discontinuity.

A knowledge of the composition and geometrical configuration of the crust and its relationship to features at or near the earth's surface is essential to understanding the geological and tectonic framework of the continent. This knowledge, in turn, is useful in the exploration of buried mineral and fossil fuel resources as well as in formulating on hypotheses on the nature, origin and history of large horizontal and vertical movements that are manifested to-day in earthquakes, mountain building and continental drift.

The bulk of this thesis is divided into four major chapters. Chapter 2 describes the formulation, the numerical aspect of the seismic tomographic technique. Chapter 3 describes in detail the geological and geophysical setting in Saskatchewan region as well as the spatial seismic refraction recording method (S^2R^2).

Chapter 4 and 5 demonstrate the application of seismic tomographic methods to S^2R^2 data acquired in Saskatchewan and to seismic data obtained on Vancouver Island. The results of the application of these methods are also discussed. However, the results in Chapter 4 will be discussed in greater detail because it is the main objective of this thesis. Finally, in Chapter 6 a summary of the major conclusions is presented.

2. FORMULATION OF SEISMIC TOMOGRAPHY

2.1 Introduction

The aim of this chapter is to describe a procedure for obtaining a three-dimensional structural and velocity model from seismic refraction or/and reflection data. It involves a new iterative processing method based on the least-squares inversion technique. A computationally efficient algorithm for tracing rays through a laterally inhomogeneous medium with curved interfaces was developed as part of a tomographic method for inverting travel-time data. This ray-tracing method may be used as a stand-alone tool for forward modelling. The linear inversion is formulated as an iteratively damped least-squares technique (Levenburg, 1944; Marquardt, 1963). The damping factor, which adds to the diagonal parameters of the matrix for stabilizing the solution, is computed automatically for each iteration (Hoerl and Kennard, 1970; Hoerl et al., 1975).

Tomography is a method for obtaining an image of the medium by mathematically combining information from numerous raypaths which travel through the media. Medical tomography has been successfully used to reconstruct an image of organs within the body by X-rays or by ultrasonic waves. Some of the medical studies of tomograph include: the computerized tomography with X-ray emission and ultrasound sources (Kak, 1979); the reconstruction of an image by ultrasonic reflectivity tomography (Norton and Linzer, 1979); the investigation of computerized tomography by direct Fourier inversion and optimum interpolation (Stark and Paul, 1981).

In geophysics the process of "seismic tomography" involves the construction of an image of subsurface structures using seismic waves reflected or critically refracted from several horizons. Seismic tomography has been applied to various geophysical problems. Cutler et al. (1984) presented a discussion of the formulation and methodology of seismic tomography. The least-squares inversion of travel times can also be treated as a "seismic tomography" problem (See e.g. Aki and Lee 1976; Hawley et al., 1981). They inverted the teleseismic travel-time observations to obtain a three-dimensional model of the earth. Some of the studies that are relevant to the present investigation include: the inversion of three-dimensional seismic data (Gjoystdal and Ursin 1981); the reconstruction of a seismic velocity profile from offset vertical seismic profiling and well-to-well boreholes (Devaney, 1984); the discussion of well-determined and poorly-determined features in seismic tomography (Bube and Resnick, 1984). Recently, Lines and Trietel (1984) gave a detailed review of linear least-squares inversion and its applications to geophysical problems.

2.2 The forward modelling

The earth's structure in this study will be modelled by piecewise polynomial surfaces of arbitrary shape. The medium between each successive pair of interfaces is assumed to be homogeneous, isotropic and perfectly elastic. This assumption is only an approximation of the true structure in terms of tractable mathematics. Since the study involves in determining the gross earth's structure with an average seismic wavelength of 1.0 km, it is a good approximation to assume a homogeneous medium between interfaces because of the large seismic wavelength in the crustal study. Thus, at most, two kinds of signals can propagate in the body of such a medium, compressional and shear waves. Their velocities, of course, differ in different media. However, any ray connecting two points within a layer is a straight line. It is found that the ray path between source and receiver pair is traced through by solving a system of nonlinear equations.

A three-dimensional ray-tracing algorithm was developed by Chander(1977) for planar interfaces. It has been generalized in this thesis to allow for curved interfaces as well as intersecting surfaces of planar interfaces. This formulation provides a simple and flexible way of computing reflected and critically refracted waves through a 3-D structure. The critically refracted wave is limited to planar interfaces of arbitrary orientation. Furthermore, this algorithm includes some desirable features in solving seismic problems, the algorithm allows for: (1) shot and receiver locations at any depth, (2) any number of layer interfaces with arbitrary shape, (3) low velocity layers interbedded with higher velocity layers, (4) multiples and converted phases along the ray path, (5) the incorporation of geological constraints, and (6) the lateral variation of velocity in the model.

Let the source location and receiver location be (x_0, y_0, z_0) and (x_n, y_n, z_n) respectively. The travel time, t, along the ray is:

$$t = \sum_{i=1}^{n}[(x_i-x_{i-1})^2+(y_i-y_{i-1})^2+(z_i-z_{i-1})^2]^{1/2}/V_i, \qquad (2.1)$$

where n is the number of ray segments, V_1 and V_n represent the velocities at the source and receiver respectively, and V_i are the constant velocities between interfaces (i-1) and i.

The L interfaces bounding each layer are defined by a polynomial surface of the form

$$z_i = d_i + f_i(x,y), \qquad i = 1, 2, \ldots L, \qquad (2.2)$$

where d_i is the distance of the normal to the origin and $f_i(x,y)$ is a function of x and y.

According to Fermat's principle, partial derivatives of t with respect to x and y yield the ray path having a mininum time. Therefore, we have to solve a system of 2n-2 equations simultaneously for t to be stationary (i.e. the ray path satisfies Snell's law):

$$\begin{aligned}
\partial t/\partial x_i = {} & [x_i - x_{i-1} + \partial z_i/\partial x_i \, (z_i - z_{i-1})] \, /V_i[(x_i - x_{i-1})^2 \\
& + (y_i - y_{i-1})^2 + (z_i - z_{i-1})^2]^{1/2} + [x_i - x_{i+1} + \partial z_i/\partial x_i \, (z_i - z_{i+1})] \\
& /V_{i+1}[(x_i - x_{i+1})^2 + (y_i - y_{i+1})^2 + (z_i - z_{i+1})^2]^{1/2} \\
= {} & 0, \qquad i=1, 2, \ldots\ldots n-1.
\end{aligned}$$

$$\begin{aligned}
\partial t/\partial y_i = {} & [y_i - y_{i-1} + \partial z_i/\partial y_i \, (z_i - z_{i-1})] \, /V_i[(x_i - x_{i-1})^2 \\
& + (y_i - y_{i-1})^2 + (z_i - z_{i-1})^2]^{1/2} + [y_i - y_{i+1} + \partial z_i/\partial y_i \, (z_i - z_{i+1})] \\
& /V_{i+1}[(x_i - x_{i+1})^2 + (y_i - y_{i+1})^2 + (z_i - z_{i+1})^2]^{1/2} \\
= {} & 0, \qquad i=1, 2, \ldots\ldots n-1. \qquad (2.3)
\end{aligned}$$

This system of nonlinear equations can be written in a compacted form as:

$$f_i(\mathbf{x},\mathbf{y}) = f_i(x_1, x_2, \ldots x_{n-1}, y_1, y_2, \ldots\ldots y_{n-1}) = 0,$$

or in an alternative form with 2n-2 variables

$$f_i(\mathbf{x}) = f_i(x_1, x_2, \ldots\ldots x_{2n-2}) = 0, \quad i = 1 \ldots\ldots 2n-2. \qquad (2.4)$$

This system of equations can be solved by Newton's method. In the classical Newton's method a guess, **x**, is made of the solution of the system (2.4), and we calculate the elements of the Jacobian matrix,

$$A_{kj} = \partial f_k(\mathbf{x})/\partial x_j \qquad (2.5)$$

at the guess. Next, we obtain a correction vector, $\Delta\mathbf{x}$, by solving a system of linear equations,

$$\sum_{j=1}^{2n-2} A_{kj}\Delta x_j = -f_k(\mathbf{x}), \qquad k=1,\ 2,\ldots.\ 2n-2, \tag{2.6}$$

and we complete the iteration by replacing the vector $\mathbf{x}$ by the vector $(\mathbf{x}+\Delta\mathbf{x})$. The success of this method is due to the fact that the correction is calculated so that, if the Jacobian is non-singular at the solution and if the functions $f_k(\mathbf{x})$ are twice differentiable, then the Newton's iteration converges rapidly when the guess is a sufficiently good one so that it is near the solution.

It is well known that the classical Newton's iteration often fails when the initial model is not a good estimate of the final solution (Stark, 1970). As in the case of all 3-D problems, it is difficult to obtain a good estimate for the initial model. Hence, we adopted the approach of Powell (1970) to overcome this difficulty. The principle idea in Powell's method is to make a compromise between Newton's method and the steepest descent method by introducing a parameter k into the normal least-squares formulation of (2.6) (Levenberg, 1944; Marquardt, 1963). Equation (2.6) becomes:

$$(\mathbf{A}'\mathbf{A} + k\mathbf{I})\Delta\mathbf{x} = -\mathbf{A}'\mathbf{f}, \tag{2.7}$$

where the parameter k is calculated by a search process which tries to make the estimate $(\mathbf{x}+k\Delta\mathbf{x})$ better than the estimate x so that $F(x+kx)<F(x)$ and $F(x)$ is defined as:

$$F(\mathbf{x}) = \sum_{k=1}^{2n-2} \{f_k(x)\}^2.$$

The essential feature in this algorithm is to guarantee a decrease in the sum of squares of the residual via the steepest descent direction when x is far from a minimum and to switch to the rapid convergence of Newton's method as the minimum is approached. The parameter k is known as a "damping factor" and will be discussed in more detail later.

2.3 Inversion procedure

The travel-time function is a nonlinear function in terms of the coefficients of the layer interfaces and the velocity parameters. We can approximate the travel-time function by a first order Taylor series expansion to form a set of linear equations for the observed data:

$$T_i = t_i(\mathbf{x}^0) + \sum_{j=1}^{m} \partial t_i/\partial x_j \Big|_{x=x^0} (x_j - x_j^0), \qquad (2.8)$$

where,

T_i = observed travel time,

$\mathbf{x}^0$ = initial estimate of model parameters,

$t_i(\mathbf{x}^0)$ = computed travel time from an initial estimate of the model parameters. Then we define,

$$\begin{aligned} \Delta x_j &= x_j - x_j^o & j&=1, \ldots m. \\ A_{ij} &= \partial t_i / \partial x_j, & j&=1, \ldots m. \\ \Delta t_i &= T_i - t_i(x_i^o), & i&=1, \ldots N. \end{aligned} \tag{2.9}$$

N is the total number of observed data and m the total number of model parameters. We rewrite equation (2.8) in vector and matrix notation:

$$\mathbf{\Delta t} = \mathbf{A}\ \mathbf{\Delta x}, \tag{2.10}$$

where $\mathbf{\Delta t}$ is a (N*1) vector, $\mathbf{\Delta x}$ is a (m*1) vector and **A** is a (N*m) matrix containing the partial derivatives.

In general, there are more observations than model parameters. An exact solution is usually not available, thus we may apply a least-squares procedure to minimize the cumulative squared error, $\mathbf{e}'\mathbf{e}$, where $\mathbf{e} = \mathbf{\Delta t} - \mathbf{A}\mathbf{\Delta x}$ with respect to parameter vector $\mathbf{\Delta x}$. The least-squares formulation (Gauss-Newton) is:

$$\mathbf{A}'\mathbf{A}\ \mathbf{\Delta x} = \mathbf{A}'\mathbf{\Delta t}, \tag{2.11}$$

and the solution is,

$$\mathbf{\Delta x} = (\mathbf{A}'\mathbf{A})^{-1}\ \mathbf{A}'\mathbf{\Delta t}. \tag{2.12}$$

Equation (2.12) represents a system of normal equations. The matrix **A'A** is always symmetric and its eigenvalues are not only real but nonnegative. By applying the least-squares method, we have a much better and smaller set of equations to solve.

The Gaussian elimination scheme known as Cholesky's method is simple, fast, and economical for solving the normal equations. Unfortunately, this method for the linear least-squares problem is also known to be numerically unstable (Miller and Wrathall, 1980). The algorithm is based on the following decomposition. If **A'A** is a symmetric, nonnegative definite matrix, it can be decomposed uniquely into LL' where L is a lower triangular matrix with positive diagonal elements (Forsythe and Moles, 1967, p.29).
Let **A'b** = h, and we apply the decomposition in normal equations (2.12), it becomes,

$$LL' \Delta x = h$$

This represents two triangular systems:

$$Ly = h, \text{ and } L'\Delta x = y,$$

which are very easily solved by forward elimination and back substitution for the unknown y and Δx.

As was mentioned earlier, the Gaussian elimination method has the distinct advantage of being the fastest known technique for solving a set of linear equations. The total count of multiplicative operations for Cholesky's method in solving the normal equations is $nm^2/2 + m^3/6$ (Lawson, 1974, P.122), where n and m are the number of equations and unknowns in matrix A, respectively.

One disadvantage of the elimination scheme occurs when the original matrix **A** is ill-conditioned, that is singular or nearly singular. Perhaps even more dangerous is the case of near singularity when the algorithm will converge to a solution, however the solution consists of random numbers unrelated to the original problem. Of course, this does not always happen; it may just happen often enough to make this approach unreliable. Another disadvantage is that highly correlated or nearly linearly dependent basis vectors (columns of **A**) create a failure in this approach.

In many applications it is necessary to determine the rank of a matrix or to determine whether or not the matrix is deficient in rank. Theoretically, one can use Gaussian elimination to reduce the matrix to row echelon form and then count the number of nonzero rows. However, this approach is not practical when working in finite precision arithmetic. If **A** is rank deficient, and **U** is the computed echelon form, then because of the rounding errors in the elimination process, it is unlikely that **U** will have the proper number of nonzero rows. In practise the coefficient matrix **A** usually involves some errors. This may be due to errors in the data or to the finite number system. Thus, it is generally more practical to ask whether **A** is "close" to a rank deficient matrix. However, it may well turn out that **A** is close to being rank deficient and the computed echelon form, U , is not.

2.4 Singular Value Decompostion (SVD)

Another computational scheme known as SVD can be used to determine how close **A** is to a matrix of smaller rank. This method requires more computations (total count of arithematic operations $2nm^2 + 4m^3$), but provides more information on various aspects of the solution. It is especially important in cases where a matrix is ill-conditioned, that is, singular or nearly singular. Much of the fundamental work of this approach was done by Golub and his colleagues (such as Golub and Businger, 1965, and Golub and Reinsch, 1970). Recent books by Stewart (1973) and Forsythe et al.(1977) discussed the computational aspects of SVD as well as many related topics.

The motivation of this method involves factoring **A** into (Golub and Reinsch, 1970):

$$\mathbf{A} = \mathbf{U}\Lambda\mathbf{V}', \tag{2.13}$$

where U is N*N data space array,

Λ is an N*m array of m singular values,

V is a m*m solution space array.

A more detailed description of the SVD method in solving the least-squares problems can be found in the book by Lawson and Hanson (1974), and Aki and Richards (1980).

The following observations are useful when we apply the SVD to solve linear least-squares problems. Let **A** be a N*m matrix with a singular value decomposition:

$$\mathbf{A} = \mathbf{U}\Lambda\mathbf{V}',$$

v_i be the column vectors of **V**, and u_i be the column vectors of **U**.

(1) Since

$$\mathbf{A}'\mathbf{A} = \mathbf{V}\ \Lambda'\Lambda\ \mathbf{V}',$$

and $\Lambda'\Lambda$ is a m*m diagonal matrix containing at most m positive squares of the eigenvalues, λ_i^2 of **A'A**, and since λ_i is a nonnegative square root of the eigenvalues of **A'A**, they are unique and equal to the singular values. However, the orthogonal matrices **U** and **V** may not be unique;

(2) Since **V** diagonalizes **A'A**, it follows that v_j's are eigenvectors of **A'A** and

$$\mathbf{V}'\mathbf{V} = \mathbf{V}\mathbf{V}' = \mathbf{I};$$

(3) Since

$$\mathbf{A}\mathbf{A}' = \mathbf{U}\Lambda\Lambda'\mathbf{U}',$$

it follows that **U** diagonalizes **AA'** and that u_j's are eigenvectors of **AA'** and

$$\mathbf{U}'\mathbf{U} = \mathbf{I};$$

(4) Since multiplying a matrix on either side by a nonsingular matrix does not alter its rank, it follows that **A** and Λ have the same rank. Thus, if $\lambda_1 > \lambda_2 > \ldots . \lambda_s > 0$ and $\lambda_{s+1} \ldots = \lambda_m = 0$, then **A** has rank s, for the rank of a matrix is the number of nonzero singular values;

(5) the least-squares solution in equation (2.12) becomes:

$$\begin{aligned} \Delta \mathbf{x} &= (\mathbf{V}\Lambda\mathbf{U}'\mathbf{U}\Lambda\mathbf{V}')^{-1}\mathbf{V}\Lambda\mathbf{U}'\Delta t \\ &= (\mathbf{V}\Lambda^2\mathbf{V}')^{-1}\,\mathbf{V}\Lambda\mathbf{U}'\Delta t \qquad (2.14) \\ &= \mathbf{V}\Lambda^{-2}\mathbf{V}'\,\mathbf{V}\Lambda\mathbf{U}'\Delta t \\ &= \mathbf{V}\Lambda^{-1}\mathbf{U}'\Delta t. \end{aligned}$$

The solution $\Delta\mathbf{x}$ is the weighted vector product sum as

$$\Delta \mathbf{x} = \sum_{i=1}^{m} \frac{1}{\lambda_i} v_i u_i' \Delta t. \qquad (2.15)$$

If we let $y_i = u_i'\Delta t$ $(i = 1, \ldots m)$ be the magnitude of the projection of the discrepancy vector Δt onto ith observation eigenvector $\mathbf{U}_i$, so

$$\Delta \mathbf{x} = \sum_{i=1}^{m} \frac{y_i}{\lambda_i} v_i .$$

Thus the solution vector is seen to be composed of a sum of weighted eigenvectors of the matrix **A'A** in the model space.

The weights are in turn, composed of the data vector transformed by the eigenvectors of the matrix **A'A** in the data space and multiplied by the inverse of the singular values of the matrix **A**. In particular, if y_i/λ_i is small, the term $(y_i/\lambda_i)v_i$ has little influence on the solution. Furthermore, if λ_i is very small, the term $(y_i/\lambda_i)v_i$ will be large (unless y_i is simultaneously very small) and has the dominant influence on the solution. The solution in general is stable and accurate unless λ_i is so small that we may question its numerical accuracy.

In nonlinear least-squares problems, the solution is a linear approximation to a nonlinear problem, thus the solution must be computed iteratively. The speed of convergence of the normal equations decreases as the relative nonlinearity of the problems increases. If this nonlinearity is too large the method may not converge at all. Another disadvantage is that if the matrix **A** does not have full rank or **A** is ill-conditioned, the performance of the Gauss-Newton method deteriorates badly. The next section will give a discussion on how to stabilize the solution in cases of an ill-conditioned matrix.

2.5 Treating the ranking deficient case

An ill-conditioned matrix manifests itself if small or zero singular values of the matrix exist. If some of the eigenvalues of the matrix **A** are small, random errors in data could cause strong fluctuations in the solution. One way of suppressing the undesirable effect of small eigenvalues is to use the damped least-squares approach or known as the "ridge regression", to modify the small eigenvalues of the system. In order to reduce the difficulties when the matrix **A'A** is nearly singular or singular, a constraint, say k, can be added to the diagonal elements of the matrix **A'A**. The effect of this constraint is to prevent the solution from being out of bounds. This approach was first introduced by Levenberg (1944) and later described in detail by Marquardt (1963).

The constrained normal equations become

$$(\mathbf{A'A} + k\mathbf{I})\Delta\mathbf{x} = \mathbf{A'}\Delta t,$$

and the solution is

$$\Delta\mathbf{x} = (\mathbf{A'A} + k\mathbf{I})^{-1}\mathbf{A'}\Delta t, \qquad (2.16)$$

By adding a constant, k, to the main diagonal of the matrix **A'A**, we have effectively added a DC level to the eigenvalues of the matrix **A'A** so none of the eigenvalues approaches zero. Levenberg (1944) terms the constant k as a 'damping factor', since it prevents the matrix **A'A** becoming singular or nearly singular by damping out the negligibly small eigenvalues. We write (**A'A** + kI) in terms of **U**, Λ, and **V**

$$(\mathbf{A'A} + k\mathbf{I}) = \mathbf{V}\Lambda^2\mathbf{V'} + k\mathbf{I}$$

$$= V(\Lambda^2+kI)V'.$$

The inverse of this matrix is,

$$\begin{aligned}(A'A + kI)^{-1} &= V(\Lambda^2+ kI)^{-1}V' \\ &= V\,\mathrm{diag}\,[1/(\lambda_j^2+k)]V' \qquad (2.17)\end{aligned}$$

We then substitute (2.17) into (2.16)

$$\begin{aligned}\Delta x &= V\,\mathrm{diag}\,[1/(\lambda_j^2+k)]V'V\Lambda U'\Delta t \\ &= V\,\mathrm{diag}\,[\lambda_j/(\lambda_j^2+k)]U'\Delta t. \qquad (2.18)\end{aligned}$$

By comparing the equations (2.14) and (2.18), the eigenvalues in the damped least-squares formulation are replaced by

$$\frac{\Lambda}{\Lambda^2+ kI}, \qquad (2.19)$$

where k is a damping factor. However, a large positive k increases the stability of the solution but decreases the resolution of model parameters. Hence, it is desirable to choose k as small as possible to achieve maximum resolution but large enough to stabilize the solution.

The selection of k for a particular problem is important in controlling the resolution of the inversion. Theobald (1974) showed that there always exists a range of k values for which the damped least squares has smaller variances than the least-squares method. A theoretical condition that will guarantee that the damped least-squares method is better than the least squares is

$$0< k < \sigma^2 / \Delta\mathbf{x}'\Delta\mathbf{x},$$

where σ^2 is the unknown error variance, and $\Delta\mathbf{x}$ is the unknown parameter vector.

Unfortunately, the optimal values of k cannot be determined with certainty because it depends on the unknown parameter vector, $\Delta\mathbf{x}$, and unknown error variance, σ^2. In practise, k must be determined empirically or estimated from the data. Hoerl and Kennard (1970) originally suggested that k can be determined from an inspection of the "ridge trace" (a plot of $\Delta\mathbf{x}(k)$'s versus a range of k). They used certain guidelines involving sign reversals, stability and increase in the residual sum of squares to determine the damping factor k. Hoerl et al. (1975) further developed an algorithm for the automatic selection of k. They proposed the estimate of k as follow:

$$k = m\, \sigma^2{}_d / X'X,$$

where $\sigma_d{}^2$ is the least-squares estimator of the variance in the data, X is the least-squares solution, and m is the number of eigenvalues. The quantity of $\sigma_d{}^2$ is obtained by

$$\sigma_d{}^2 = Ø(0) / (N-m),$$

where N is number of observations and $\emptyset(0)$ is the residual sum of squares for the least-squares estimate and is defined by

$$\emptyset(0) = (\Delta t-AX)'(\Delta t-AX).$$

The ridge-type estimation of k developed by Hoerl el al. (1970,1975) is widely used in statistical applications of data fitting. Lawless and Wang (1976) further concluded that ridge-type estimators were far superior to least-squares methods. Therefore, I adopted Hoerl's technique to compute the damping factor, k, automatically.

In addition to the damping factor, scaling can be used to speed the convergence when solving the normal equations and also to avoid "ill conditioning" caused by different scales in which the model parameters are expressed. Each column of the matrix **A** is scaled by a root mean sum of squared values d_j, and d_j is defined as follows:

$$d_j = \left(\sum_{i=1}^{N} A_{ij}^2 \right)^{1/2},$$

$$A_{ij} = A_{ij} / d_j. \tag{2.20}$$

The effect of the scaling is to reduce numerical inaccuracies such that all the model parameters will be scaled alike. The estimates of the parameters from the scaled matrix are then transformed back to original parameters by:

$$\Delta \mathbf{x} = \Delta x_j/d_j, \qquad j = 1, \ldots m. \qquad (2.21)$$

2.6 Resolution and covariance matrices

The solution of the damped least-squares problem is ambiguous without the description of its uniqueness and reliability. In this section we investigate what constitutes a good solution, realizing that there are uncertainties in both the model and data. The uniqueness and reliability have been thoroughly discussed in the geophysical literature (Backus and Gilbert, 1968, 1970; Jackson, 1972, 1979; and Aki and Richards, 1980). The treatment here follows an approach given by Aki and Richards (1980, p. 675-699). We first derive the resolution and covariance matrices from the normal equations and then modify the eigenvalues to get the resolution and covariance matrices of the constrained normal equations.

The normal equations from (2.11) are:

$$\mathbf{A}'\mathbf{A}\ \Delta\mathbf{x} = \mathbf{A}'\Delta\mathbf{t}, \qquad (2.22)$$

where $\Delta\mathbf{x}$ is a (1*m) vector in the model space,

Δt is a (1*N) vector in data space,

$\mathbf{A}$ is a (N*m) matrix.

By singular value decomposition, we obtain

$$\mathbf{A} = \mathbf{U}_m \Lambda_m \mathbf{V}_m', \qquad (2.23)$$

where Λ has a complete set of m nonzero singular values and $\mathbf{U}_m$ and $\mathbf{V}_m$ are made up from the eigenvectors with m nonzero eigenvalues of Λ_m. Substituting equation (2.23) into the normal equations, we obtain the least-squares solution (or generalized inverse)

$$\begin{aligned} \Delta\mathbf{x}_g &= (\mathbf{A}^t\mathbf{A})^{-1}\mathbf{A}^t\Delta\mathbf{t}, \\ &= \mathbf{V}_m\Lambda_m^{-2}\mathbf{V}_m^t\ \mathbf{V}_m\Lambda_m\mathbf{U}_m^t\Delta\mathbf{t}, \\ &= \mathbf{V}_m\Lambda_m^{-1}\mathbf{U}_m^t\Delta\mathbf{t}, \\ &= \mathbf{A}_g^{-1}\Delta\mathbf{t}. \end{aligned} \tag{2.24}$$

$\Delta\mathbf{x}_g$ is the generalized least-squares solution, and $\mathbf{A}_g$ is called the generalized inverse operator. The equation (2.24) can be written as:

$$\Delta\mathbf{x}_g = \mathbf{A}_g^{-1}\mathbf{A}\Delta\mathbf{x},$$

using equation (2.23), the equation above becomes,

$$\begin{aligned} \Delta\mathbf{x}_g &= \mathbf{V}_m\Lambda_m^{-1}\mathbf{U}_m^t\ \mathbf{U}_m\Lambda_m\mathbf{V}_m^t\Delta\mathbf{x}, \\ &= \mathbf{V}_m\mathbf{V}_m^t\Delta\mathbf{x}. \end{aligned} \tag{2.25}$$

The matrix $\mathbf{V}_m\mathbf{V}_m^t$ is called the resolution matrix $\mathbf{R}$. If $\mathbf{V}_m\mathbf{V}_m^t$ is the identity matrix $\mathbf{I}$, resolution is perfect and the generalized inverse is equal to the true solution. If the row vectors of $\mathbf{V}_m\mathbf{V}_m^t$ have components spread around the diagonal (with low values elsewhere), the generalized inverse represents a smoothed solution over the spread, and is expressed as a weighted average by summing weighting coefficients of the row vectors of the resolution matrix. Therefore, the diagonal elements of the resolution matrix can be used as a rough measure of the resolution in model space.

Since we introduce the damping factor into the solution, the resolution matrix **R** becomes (Aki and Richards 1980, p.698):

$$\mathbf{R} = V_m \frac{\Lambda_m^2}{\Lambda_m^2 + kI} V_m^t . \tag{2.26}$$

The contributions of eigenvectors with eigenvalues smaller than k are suppressed in the damped least-squares solution; thus, the introduction of the damping factor, k, will degrade resolution but stabilize the covariance.

The reliability of the solution can be measured by its covariance matrix. The covariance matrix C is:

$$< \Delta\mathbf{x}_s \Delta\mathbf{x}_s^t > = \mathbf{A}_s^{-1} < \Delta t \Delta t^t > (\mathbf{A}_s^t)^{-1} .$$

Assuming that all the components of the data vectors are statistically independent and share the same variance σ_d^2, we have

$$< \Delta\mathbf{x}_s \Delta\mathbf{x}_s^t > = \sigma_d^2 \mathbf{A}_s^{-1} (\mathbf{A}_s^t)^{-1},$$

putting $\mathbf{A}_s^{-1} = (\mathbf{A}_s^t \mathbf{A}_s)^{-1} \mathbf{A}_s^t$ we have,

$$<\Delta x_s \Delta x_s^t> = \sigma_d^2 (A_s^t A_s)^{-1} \tag{2.27}$$

This is the variance of the solution for the least-squares solution. In general, putting $A_s^{-1} = V_m \Lambda_m^{-1} U_m^t$ gives

$$\begin{aligned} C &= \sigma_d^2 V_m \Lambda_m^{-1} U_m^t \, U_m \Lambda_m^{-1} V_m^t, \\ &= \sigma_d^2 V_m \Lambda_m^{-2} V_m^t. \end{aligned}$$

Obviously, the covariance of the solution becomes large when some of the eigenvalues are small. Since the diagonal element of the covariance matrix is proportional to the square of the standard error of the corresponding element of the solution vector, large standard errors are an indicator of an ill-conditioned matrix. The introduction of the damping factor, k, into the solution will degrade the resolution in both model and data spaces, but also decrease the covariance by damping out the small eigenvalues.

The covariance matrix is:

$$C = \sigma_d^2 V_m \frac{\Lambda_m^2}{(\Lambda_m^2 + kI)^2} V_m^t. \tag{2.28}$$

Again, from the equations (2.26) and (2.28) the use of a damping factor, k, introduces a tradeoff between resolution and covariance. As the resolution is degraded it acts to dampen the inverse matrix $(A^t A + kI)^{-1}$ and thus improve the covariance matrix.

2.7 Conclusions

The singular value decomposition has advantages over the Gaussian elimination for solving the normal equations. If the matrix is well-conditioned, Gaussian elimination is fast and efficient in solving the normal equations. However, the matrix of the normal equations is not well-conditioned in most geophysical problems, the singular value decomposition provides more insight into the stability and uniqueness of the least-squares solution. Therefore, the singular value decomposition approach is used to solve for the least-squares problems.

Two computer programs were written to implement the theory of seismic tomography (see Appendix). The first computer program mainly deals with spatial seismic refraction data. It allows head waves and wide-angle reflections to propagate through normally faulted planes. The damped least-squares formulation inverts the travel-time data from head waves and/or wide-angle reflections to reconstruct a crustal model, with the constraint of several normal faults. The interfaces in this computer program are limited to plane layers, but interfaces can intersect each other. The second computer program mainly deals with zero-offset and nonzero-offset reflection data. It traces the rays from sources to receivers through a number of polynomial surfaces. The damped least-squares formulation inverts the reflection data to reconstruct interval velocities as well as polynomial surfaces of the reflectors.

3. REGIONAL SETTING, DATA ACQUISITION AND PROCESSING IN THE SASKATCHEWAN REGION

3.1 Geology of the Williston Basin

The Williston Basin is a major intracratonic feature on the North American continent. The term "Williston Basin" is variously applied to much of the sedimentary succession in Saskatchewan and Manitoba, but in a structural context, it denotes the circular depression on the Precambrian crystalline basement centered in North Dakota as drawn in Fig. 3.1. Its shape and size is not well defined. Rocks deposited during most periods of Phanerozoic times are present in the basin. The stratigraphy consists of early Paleozoic clastic rocks (marine sandstones and shales), followed by mainly Paleozoic carbonates and evaporites, and finally by Mesozoic and Cenezoic clastics. Glacial drift covers much of the nearly horizontal bedrock in this region. The thickness of the sedimentary basin, in general, increases towards the southern part of the basin and thins towards the exposed Canadian Shield in northern Saskatchewan. The thickest section in the sedimentary basin, at about 4,875m, is located in southeastern North Dakota (Gerhard, 1982). The variations of basin thickness probably represent different regional sedimentation, erosion and subsidence of the basin at various times throughout Phanerozoric time. However, the basin has undergone relatively mild tectonic distortion during Phanerozoic time.

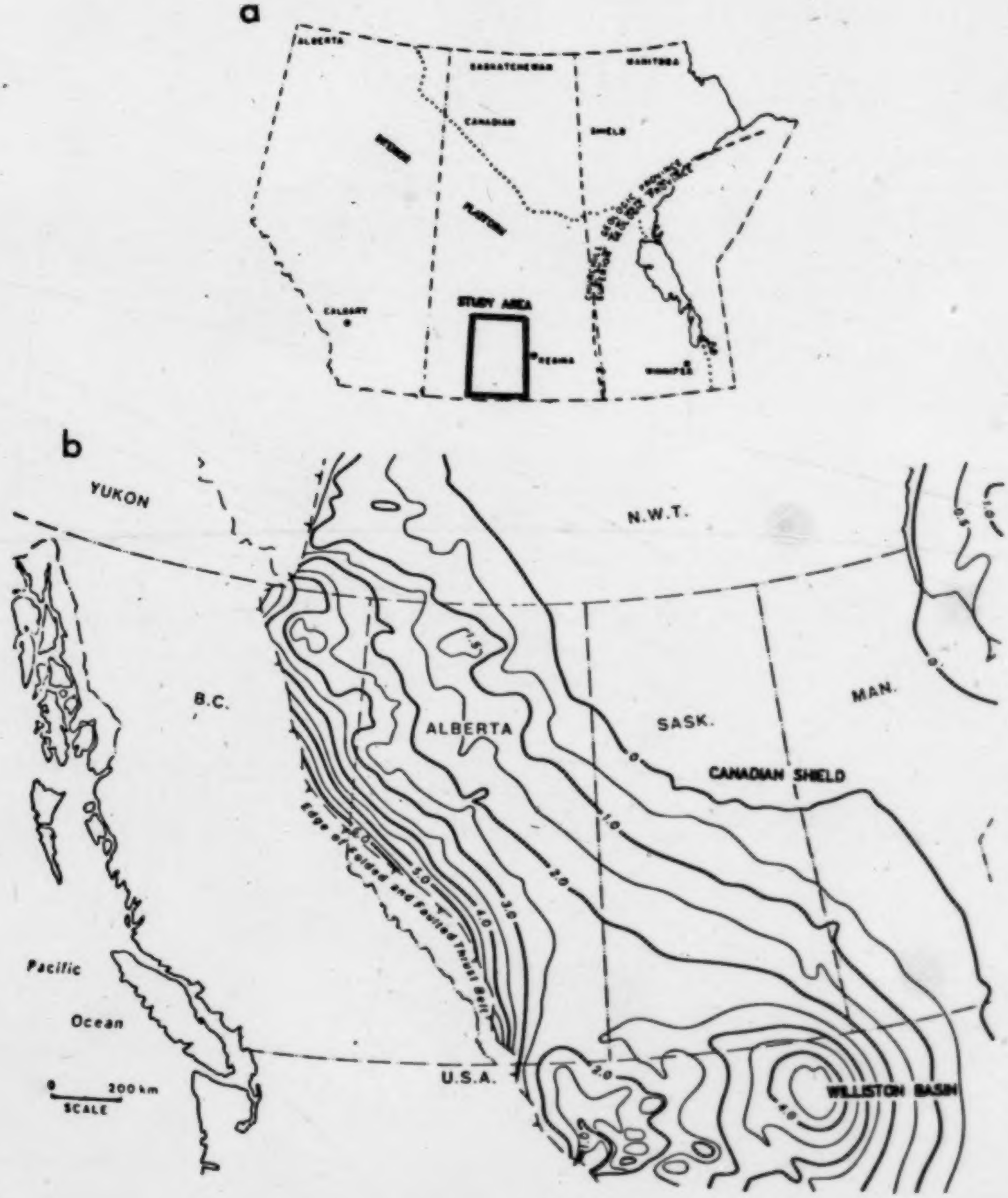
a
ALBERTA
SASKATCHEWAN
MANITOBA
CANADIAN
SHIELD
PLATFORM
STUDY AREA
CALGARY
REGINA
WINNIPEG
b
YUKON
N.W.T.
B.C.
ALBERTA
SASK.
MAN.
CANADIAN SHIELD
Edge of Folded and Faulted Thrust Belt
Pacific
Ocean
U.S.A.
WILLISTON BASIN
0
1.0
1.5
2.0
3.0
4.0
5.0
6.0
0 200 km
SCALE

Figure 3.1 (a) Principal physiographic divisions in Western Canada and the study area (rectangle). (b) The Western Canada sedimentary basin. Total preserved thickness of Phanerozoic rocks. Contours are in Kilometers. (from Porter et al., 1982, with permission)

The distortion is largely related to movement of Precambrian basement rocks. Furthermore, Porter (1982) has provided a detailed study of the evolution of the Williston Basin.

3.2 Deep structures

Beneath the sedimentary sequences of the Williston Basin is the Precambrian crystalline basement, a covered portion of the Canadian Shield. The Shield is a relatively stable portion of the continent and forms the basement of the western part of the North American craton. It has been relatively undisturbed since Precambrian time, except for gentle warping. The rock units are characterized by granitic and high-grade metamorphic rocks, as well as highly deformed and metamorphosed sediments and volcanic rocks, which implies a series of intense mountain making episodes in the Precambrian Era. The Shield also includes some very old sediments that were hardly touched by deformation and metamorphism. Most geological information on the Precambrian rocks comes from studies of the exposed Shield together with a few core samples. Some studies included Bell (1971), Price and Douglas (1972), Burwash et al. (1973, 1976), Lewry et al. (1978, 1981, 1983), Ermanovics et al. (1978, 1983). From the pattern of geologic rock types, fault zones, gravity and magnetic anomalies, and from radiometric age determinations, the Canadian Precambrian Shield is subdivided into a number of provinces. Each province has its own distinct geological and geophysical characteristics.

However, only one major tectonic province, the Churchill province, is significantly involved in this study area, so discussions focus mainly on this tectonic province. The Superior province is just to the west of the study area and will be mentioned briefly.

The Churchill province is a vast region of the Canadian Shield underlain predominantly by gneissic and grantitoid rocks of great structural and petrological complexity. It contains linear or curved belts of variably deformed and metamorphosed (lower Proterozoic) supracrustal rocks. Remnants of plutonic rocks of Archean age, recognized in a few places within the province, have been involved in two major orogenies, the Kenoran and Hudsonian. The predominant Hudsonian structural grain trends northeast to north in the western part of the province and changes gradually through east to southeast in the eastern part. Large masses of weakly foliated granitic rocks are common. Radiometric age determinations suggest that the Hudsonian orogeny, the structures of which define the province, occurred mainly between 1,850 and 1,550 m.y. ago.

The Superior Province is by far the largest and oldest crustal unit of Archean rocks with ages clustering about 2,500 m.y., corresponding to an orogeny called Kenoran. It contains an usually broad range of plutonic and supracrustal rocks ranging from granulite complexes of uncertain origin through migmatite to zeolite-bearing lava flows and sediments. The distinctive characteristics of the Superior province are: (1) predominance of crystalline rocks in the form of migmatite and plutons relative to supracrustal rocks; (2) supracrustal rocks of low to medium metamorphic rank; (3) complex and varied structural styles dominated by steep isoclinal folds and extensive wrench faulting; (4) prevailing east-trending structure; (5) numerous, highly mineralized, volcanic-rich greenstone belts.

3.3 Geophysical characteristics

A good correlation generally exists between surface geology and Bouguer gravity and magnetic anomalies. Relatively positive Bouguer anomalies occur over greenstone belts, granulites, and mafic to ultramafic intrusions; negative anomalies characterize granitic rocks. The more intensive, linear magnetic anomalies coincide with volcanic sedimentary belts and granulites; low intensity anomalies correspond to non-ferromagnetic granites and some sedimentary and volcanic rocks. Thus, both gravity and magnetic anomalies provide reliable information for delineating major geological units where outcrops are not available. As a result of extensive regional gravity and aeromagnetic surveys, Green et al. (1985) compiled all available aeromagnetic and gravity data in this region. The aeromagnetic map (Figure 3.2) shows one distinctive magnetic feature: the remarkable parallelism between the margin of the Superior craton, the margin of the Churchill craton and the boundaries of intervening terrains. The magnetic

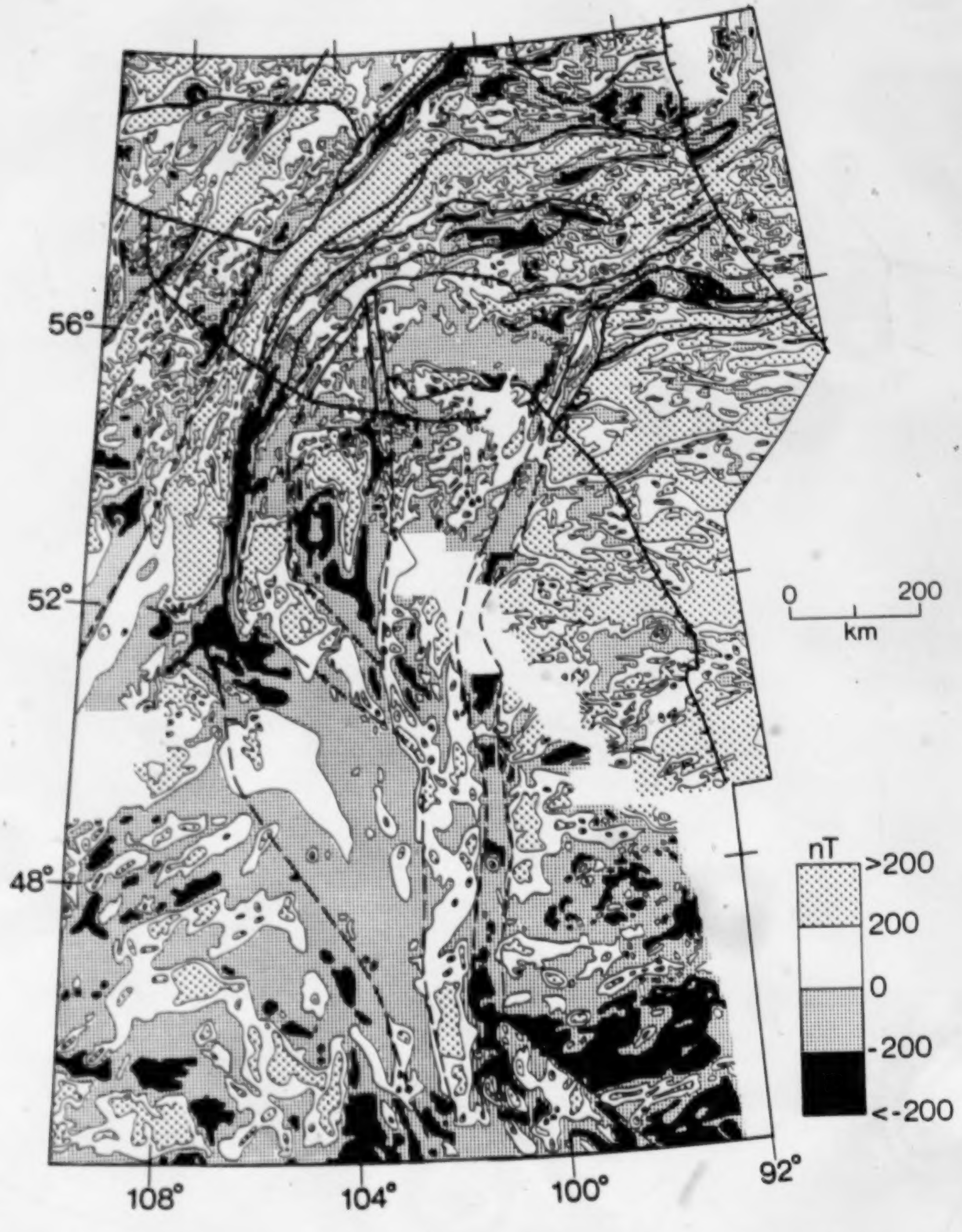
56°
52°
48°
108°
104°
100°
92°
0
200
km
nT
>200
200
0
-200
<-200

Figure 3.2 Compiled aeromagnetic map for Manitoba and Saskatchewan in Canada and parts of North and South Dakota, Montana and Wyoming in the United States. Dotted lines show the important tectonic boundaries of the geological units. (from Green, et al., 1985, with permission)

anomalies dominate mostly in N-S trends in the southern portion and in a NE-SW direction in the northern portion of the map. Across most terrains the gravity contours (Fig. 3.3) are also parallel to both regional geological units and the dominant magnetic trends. The most prominent positive gravity anomaly associated with the transition zone from the Churchill to the Superior Province is known as the Nelson Front. It extends from the Hudson Bay Basin in the northeast across a large part of the Shield to a position beneath the Williston Basin in south-central Manitoba. Geomagnetic depth sounding methods also provide further insights on the deep crustal structure. A highly conductive zone, known as the North American Central Plains anomaly (NACP) extends from the northern part in Montana to the exposed Shield in Saskatchewan (Fig. 3.4) (Camfield and Gough, 1977). This long narrow low resistivity zone has been traced at a longitude of about 105°W. This anomaly might be related either to a zone of conductive mineralization of graphite or to saline water migrating through a fault zone in the basement.

3.4 Extension of Canadian Shield beneath the Williston Basin

The westward extension of the Canadian Shield beneath the Phanerozoic covered rocks of the Interior Platform provides the basic tectonic framework of the Williston Basin. The geological knowledge of the northern exposed Shield has improved substantially over the past decade (eg.

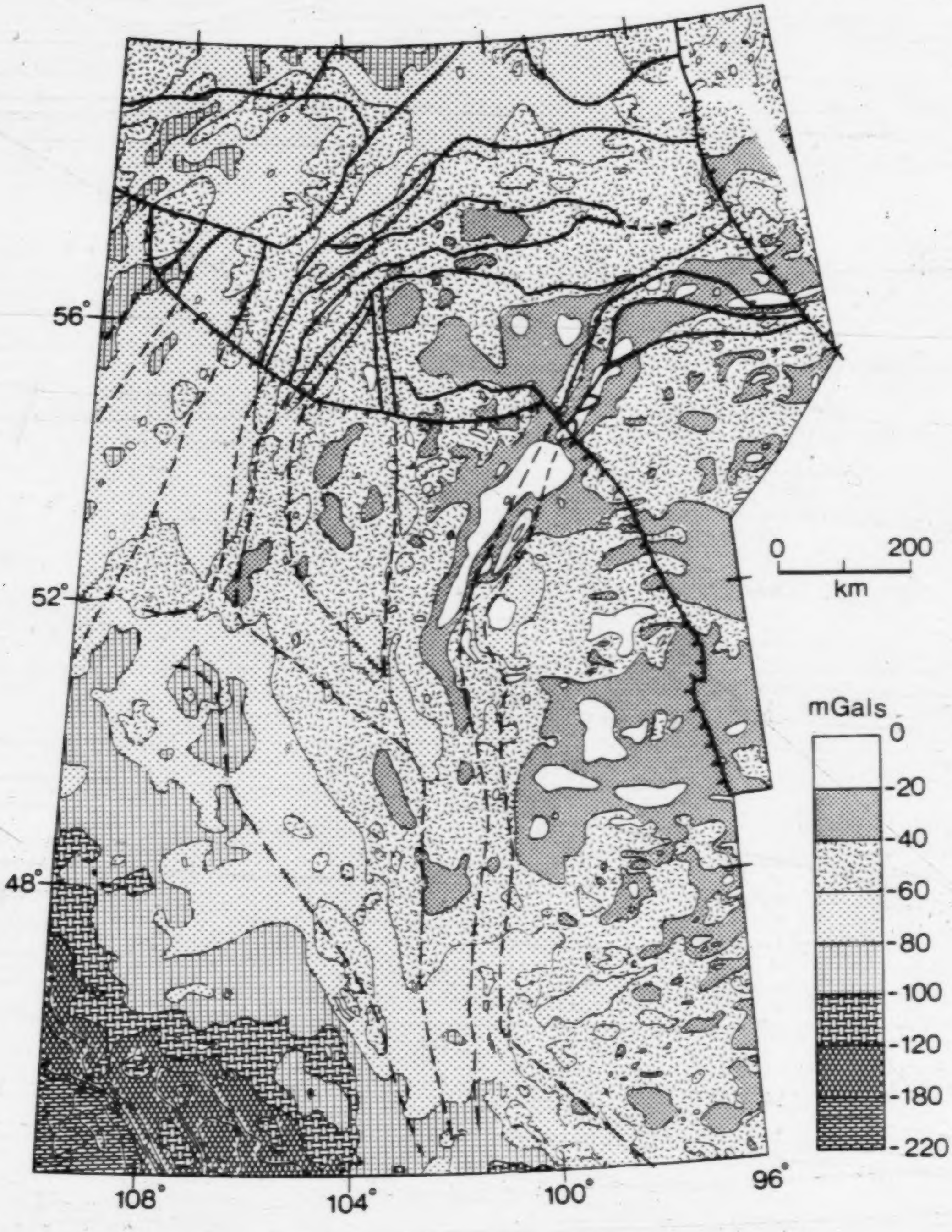
56°
52°
48°
108°
104°
100°
96°
0
200
km
mGals
0
-20
-40
-60
-80
-100
-120
-180
-220

Figure 3.3 Compiled Bouguer gravity anomaly map for Manitoba and Saskatchewan in Canada and parts of North and South Dakota, Montana and Wyoming in the United States. Tectonic boundaries are the same as shown in Figure 3.2. (from Green et al., 1985, with permission)

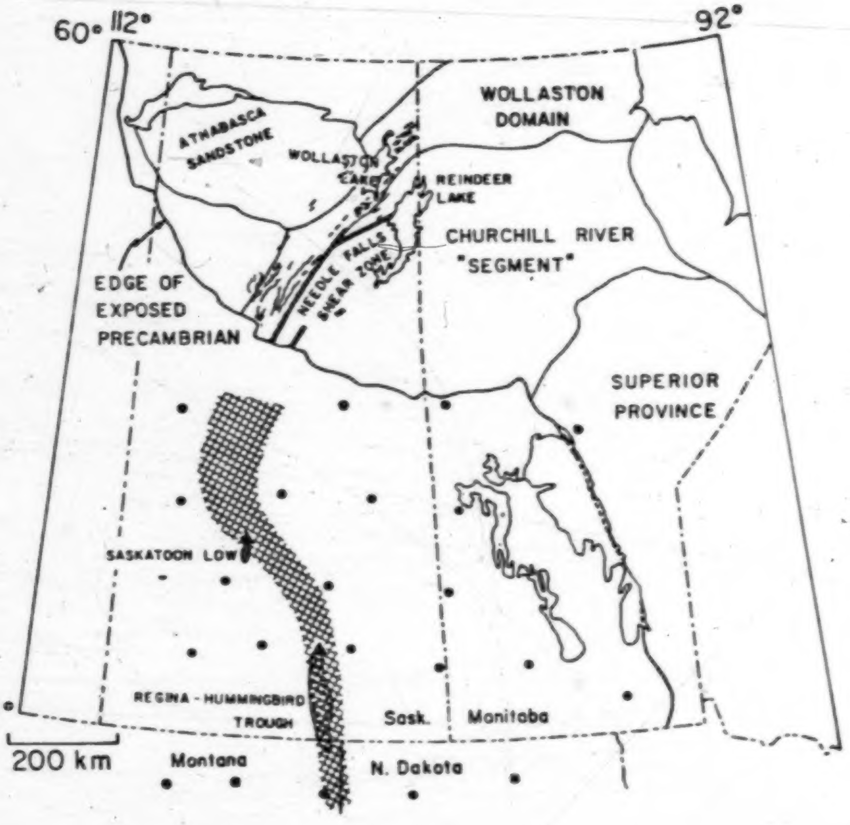
60°
112°
92°
WOLLASTON DOMAIN
ATHABASCA SANDSTONE
WOLLASTON LAKE
REINDEER LAKE
CHURCHILL RIVER "SEGMENT"
NEEDLE FALLS SHEAR ZONE
EDGE OF EXPOSED PRECAMBRIAN
SUPERIOR PROVINCE
SASKATOON LOW
REGINA - HUMMINGBIRD TROUGH
49°
200 km
Sask.
Manitoba
Montana
N. Dakota

Figure 3.4 Location of the conductive body called the North American Central Plains anomaly, shown by the shaded strip. (from Camfield et al., 1977, with permission)

Lewry and Sibbald, 1977; Lewry et al., 1978 and 1983; and Bailes and McRitchie, 1978), but there is little tectonic information of the southern region of the Canadian Shield. Based on the regional geophysical information, including aeromagnetic, gravity, seismic, electromagnetic induction data, Green et al. (1984) extended the Canadian Shield beneath the Phanerozoic Williston Basin of south-central Canada to the north-central United States (Fig. 3.5).

The seismic refraction profiles in this study are labelled as A, B, and C. These three profiles are underlain by the geological units of Wyoming craton, the Reindeer-South Indian belt and the La-Ronge-Lynn Lake belt.

The La-Ronge-Lynn Lake belt is a granite/greenstone belt of Proterozoic age. It consists of four main lithological sequences, the Amisk group of metavolcanic rocks and associated metasediments, the late-to post-Amisk intrusive rocks, the Missi-group of alluvial deposits and post-Missi intrusive rocks. In addition to the characteristic lithologies it also displays rare earth trace elements similar to those observed in modern volcanic island arcs. Multiphase deformation and metamorphism are also present. However, internal structures are mostly parallel to the trend of the belt, being E-W to the north of the Kisseynew belt and changing to NE-SW along its southwestern region.

The Reindeer-South Indian Lakes belt is wedged between the north and the northwestern margins of the La-Ronge-Lynn

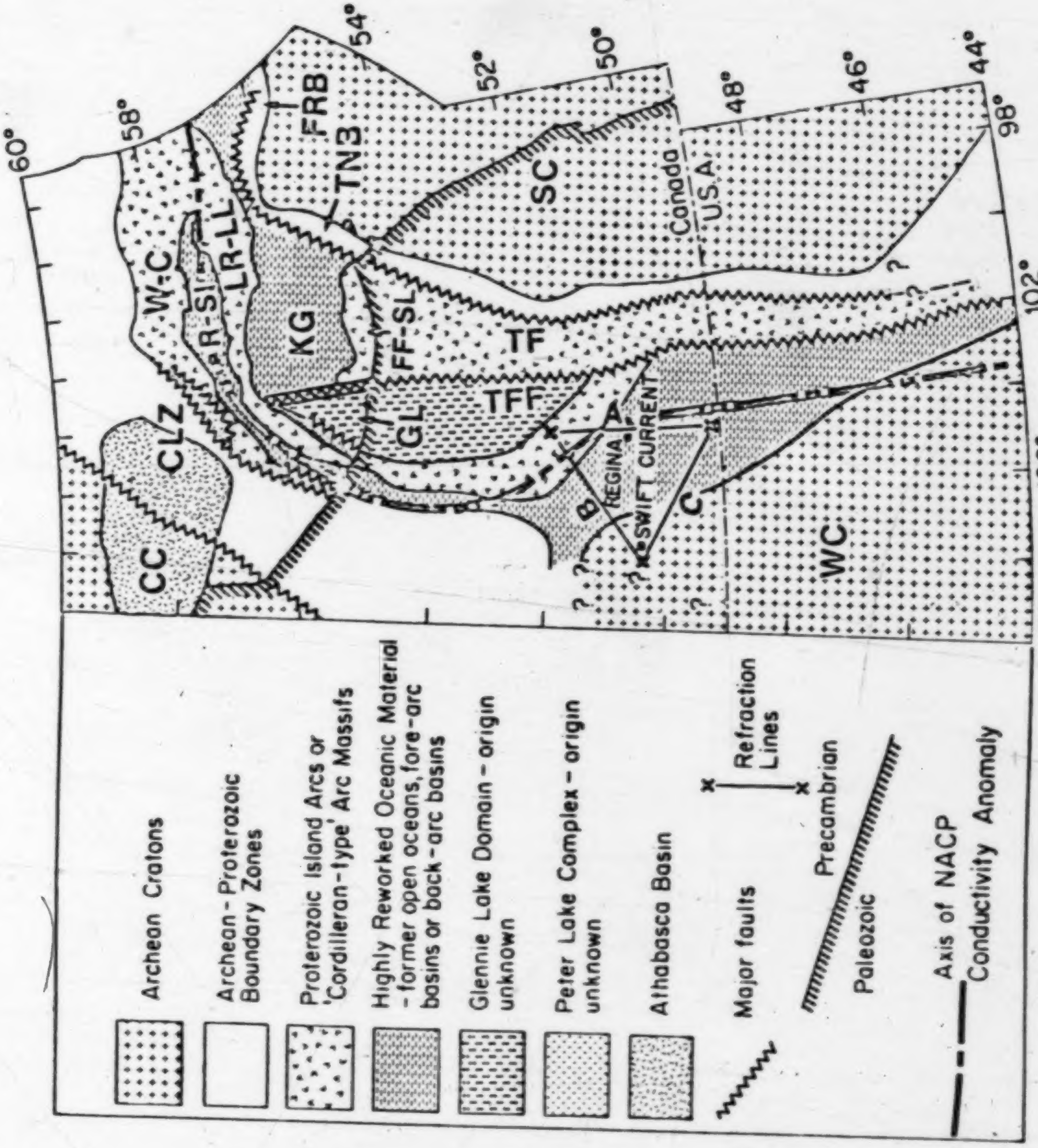
Archean Cratons
Archean-Proterozoic Boundary Zones
Proterozoic Island Arcs or 'Cordilleran-type' Arc Massifs
Highly Reworked Oceanic Material - former open oceans, fore-arc basins or back-arc basins
Glennie Lake Domain - origin unknown
Peter Lake Complex - origin unknown
Athabasca Basin
Major faults
Refraction Lines
Precambrian
Paleozoic
Axis of NACP Conductivity Anomaly
60°
58°
54°
52°
50°
48°
46°
44°
98°
102°
106°
110°
CC
CLZ
W-C
R-SI
LR-LL
KG
FRB
TN3
SC
FF-SL
TF
TFF
GL
A
B
C
REGINA
SWIFT CURRENT
Canada
U.S.A.
WC

Figure 3.5 Tectonic map of the study area showing the locations of the shots and receivers used for this study. CC - Churchill craton, CLZ - Cree Lake zone, FF-SL - Flin Flon-Snow Lake belt, FRB - Fox River belt, GL - Glennie Lake domain, KG - Kisseynew belt, LR-LL - La Ronge-Lynn Lake Belt, R-SI - Reindeer-South Indian Lake belt, SC - Superior craton, TF - Thompson boundary fault, TFF - Tabbernor fault/fold zone, TNB - Thompson belt, W-C - Wathaman-Chipaweyan batholith, WC - Wyoming craton. (from Green, Chiu and others, 1984)

Lake belt and the Wathaman-Chipewyan batholith. Its rock units are mainly graywackes, siltstones and mudstones that have been subjected to high grades of metamorphism to form paragneisses and migmatite. These rocks originated as volcanic detritus from the nearby island arcs; they were deposited contemporaneously with volcanic activity. Quartz diorite to granodiorite intrusions are relatively common in this terrain. Internal structures generally follow the trend of the belt similiar to that described for the La-Ronge-Lynn Lake belt.

Finally, the Wyoming Province underlies the Western United States and Canada and is exposed mainly in the cores of young mountain ranges in Wyoming and Montana. Because of inadequate exposure the boundaries of the province are poorly known. It is comprised principally of gneisses, migmatite, and granitic plutons. The greenstone belts are not well preserved and their remnants make up most of the remainder of the province. The structure of Wyoming Province is very complex and no overall structural trend characterizes the province. The metamorphic grade ranges from the upper greenschist to the lower granulite facies.

3.5 Ideal theoretical refraction recordings (S^3R^3)

The ideal seismic refraction experiment is one that yields accurate, high resolution, three-dimensional structure with a minimum number of sources. An effective method for obtaining the three-dimensional crustal structure was suggested by E. R. Kanasewich at a COCRUST meeting in 1979. This three-dimensional recording method is called Spatial Seismic Recording Refraction (S^2R^2) in this thesis. Elastic wave sources are placed at the vertices and mid-points of an equilateral triangle of receivers and each source is recorded simultaneously by all the receivers around and interior to the triangle (Figure 3.6). In an actual field experiment, the deployment of receivers and sources would be constrained by the availability of access routes. However, the method is very robust and major variations in the geometry do not complicate the inversion process. The reversed in-line refraction data gives a control on the velocities while the broadside refraction and wide-angle reflection data yield the detailed structure over the area of interest. In continental crustal refraction experiments the deepest horizon of interest (Moho) may vary in depth from 30 to 60 km. Therefore, source to receiver distances may need to extend to a maximum of 300 to 400 km. However, intermediate layers at depths of 10 to 25 km are also of great interest to tie together near vertical incidence reflection surveys and geological outcrops. This objective may be met with sources at the midpoints of the triangle of receivers. The projection of the head wave portion of the ray path for one third of the area is shown in Figure 3.7. In marine refraction surveys, the role of source and receiver is often reversed. A limited number of ocean bottom seismometers is used together with a mobile

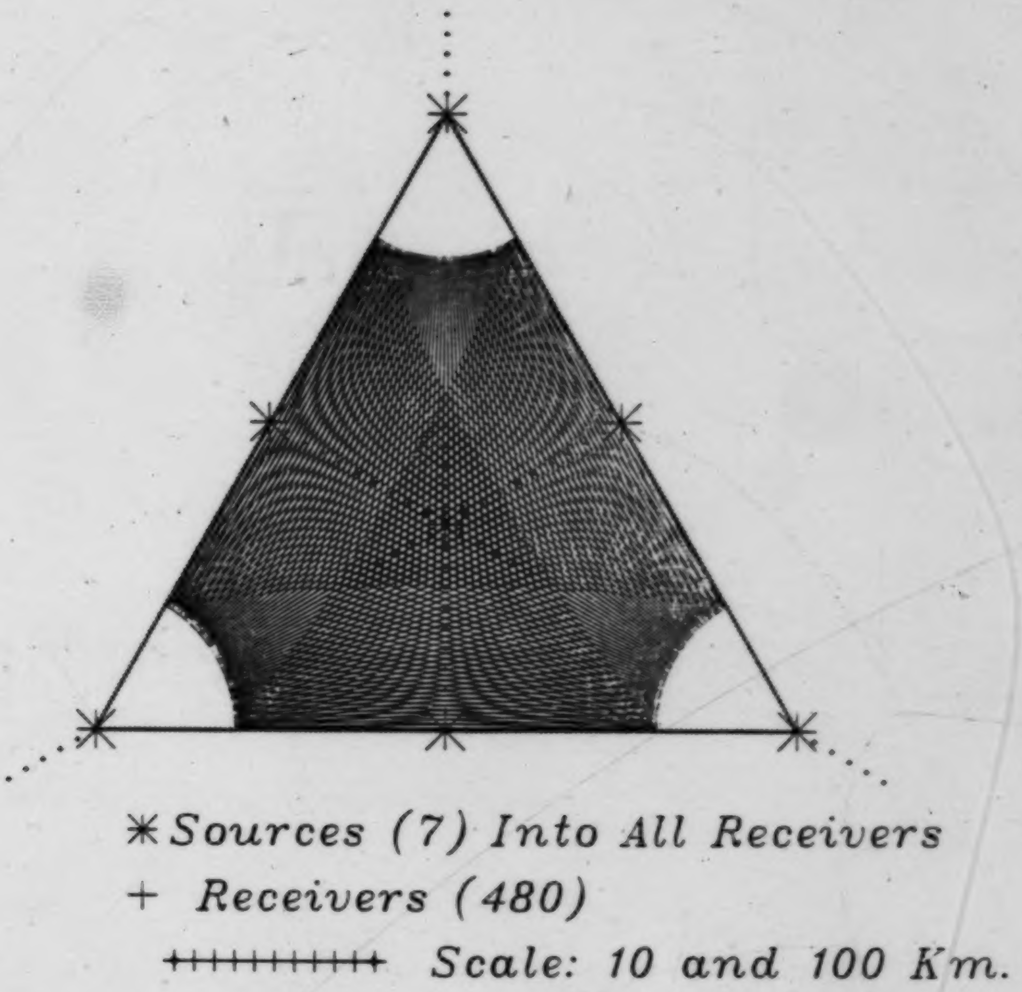
✳ Sources (7) Into All Receivers
+ Receivers (480)
++++++++++ Scale: 10 and 100 Km.

Figure 3.6 A spatial seismic refraction recording array to obtain a three-dimensional structure on the Moho discontinuity. The triangle of receivers has dimensions of 350 km and a receiver spacing of 2.5 km. The lines are surface projections of rays traversing below the Moho. Each source is recorded by all the receivers.

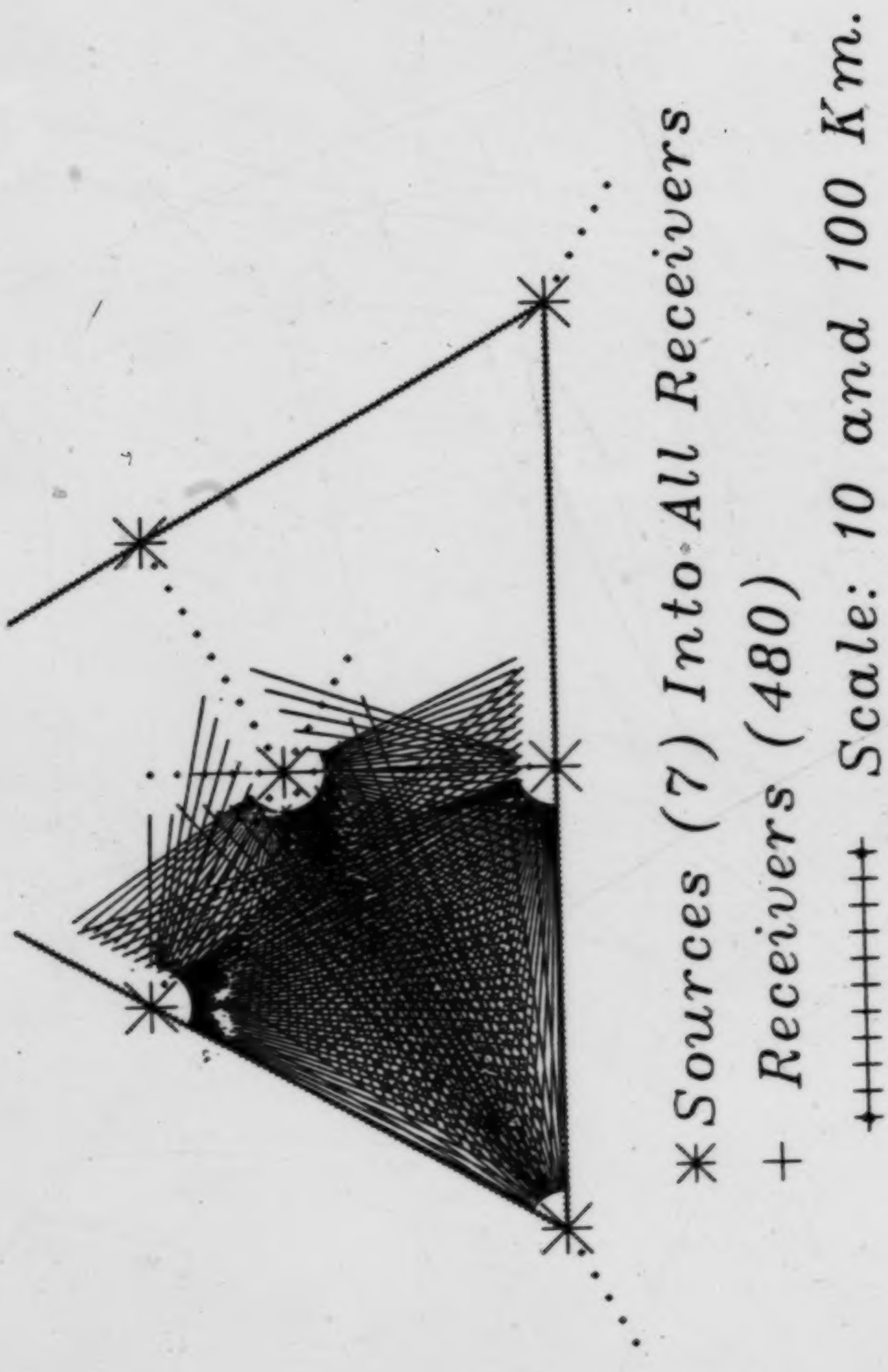
✳ Sources (7) Into All Receivers
+ Receivers (480)
Scale: 10 and 100 Km.

Figure 3.7 A spatial seismic refraction recording array to obtain a three-dimensional structure of intermediate crustal interfaces. The lines are surface projections of the head waves over one-third of the array shown in Figure 3.6.

(air gun) source moving along the triangular path. On land a large number of identical independent event recording instruments are desirable to reduce the enviromental and monetary cost of chemical sources. There is also a scientific advantage to having only one or two explosions at each source location since this reduces the complication of making many difficult source corrections. For good phase correlation, the spacing of receivers for crustal studies should be less than 0.5 km and certainly less than 3 km, because the average seismic wavelength is about 1.0 km in the deep crustal seismic study. For a 350-km equilateral triangle and 1 km spacing, about 1100 recorders are required. This is about five times the capability of any national seismic resource base at the present time. Present plans in Canada call for the acquisition of 240 identical digital recording seismic refraction instruments for PROJECT LITHOPROBE. Scientists in the United States are recommending that 1000 such instruments be made available (Report to the National Academy of Sciences, the Panel on Seismological Studies of the Continental Lithosphere, Committee on Seismology, George Thompson, Chairman). In Figures 3.6 and 3.7, an example of the deployment of 480 (2x240) such instruments is shown with a receiver spacing of 2.5 km. Duplicate shot sources are required at seven locations to perform the experiment with each source being recorded by 240 recorders.

3.6 Previous seismic studies

Previous seismic studies reveal that the crust in this region ranges from a minimum of 37 to a maximum of 55 km in Montana. Fig. 3.8 shows the compilation of Moho depths in this region. The early analyses of seismic data to obtain crustal structures were from Maureau (1964) and Chandra and Cumming (1972). They provided some crustal depths mainly west of Swift Current. In addition, McCamy and Meyer (1964) obtained thick, multi-layered crust from 50 to 55 km in Montana. Recent seismic studies include Sereda (1978), Green et al. (1980, 1981), Delandro and Moon (1982), Shahriar (1982), Macrides (1983), Hajnal et al. (1984), and Kanasewich and Chiu (1985). Some of the important results can be summarized as follows: (a) the upper crust is laterally heterogeneous with P-wave velocities ranging from 5.9 to 6.5 km/s; (b) characteristic low velocity zones may occur in the upper to mid-crustal regions (Shahriar, 1982 and Macrides, 1983); (c) mid-crustal velocities are relatively uniform, ranging from 6.5 to 7 km/s; (d) the P-wave velocities of the Moho ranges from a minimum of 7.8 to a maximum of 8.5 km/s.

The combined refraction and reflection interpretations also indicate the existence of a major crustal fault within the Churchill province (Green et al., 1979, and Kazmierczak, 1980), at a longitude of 103°. The fault is easily delineated by the magnetic data and the change of crustal thickness across the fault is a least 5 km. Another

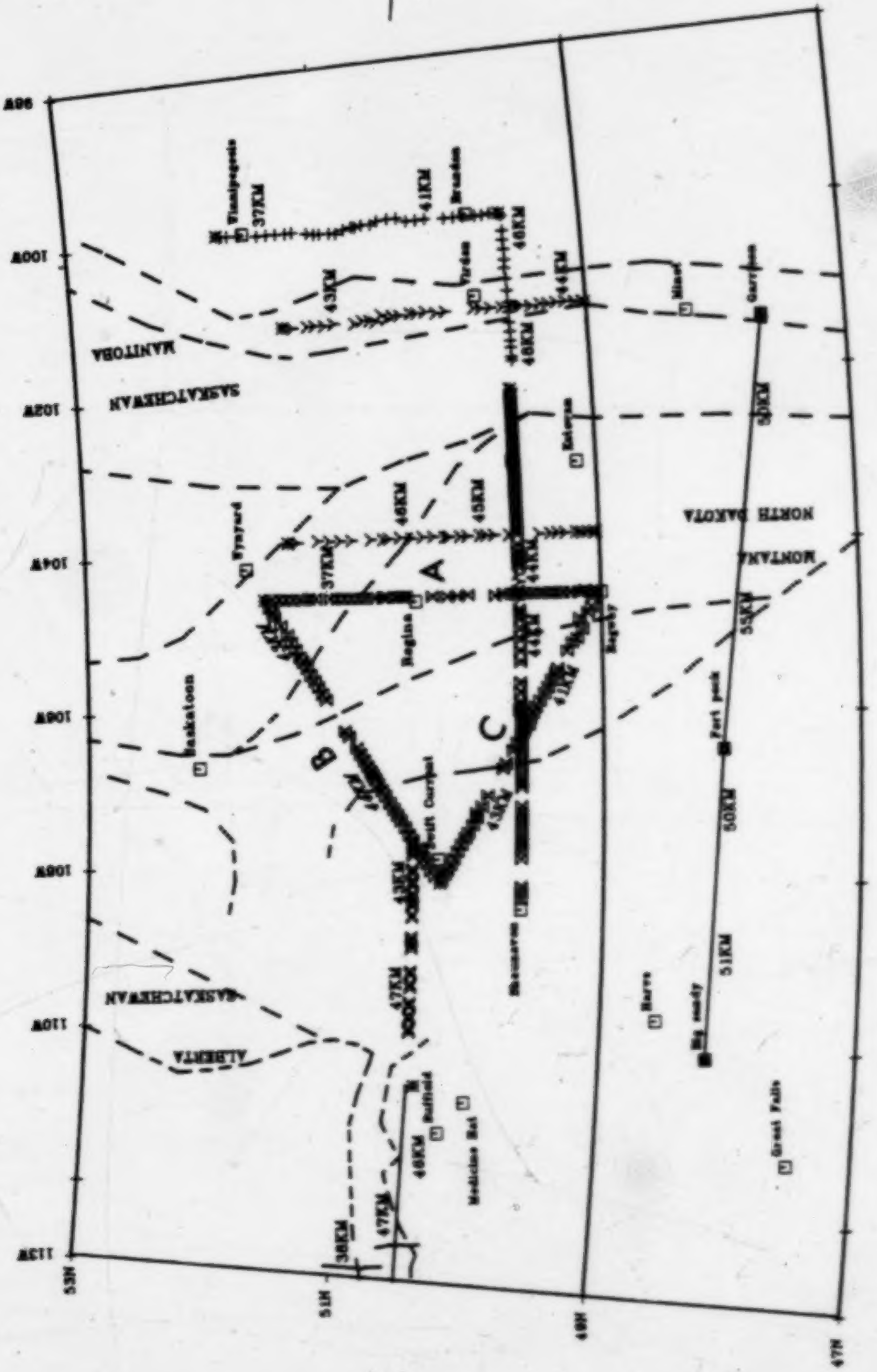
96W
100W
102W
104W
106W
108W
110W
113W
53N
51N
49N
47N
MANITOBA
SASKATCHEWAN
ALBERTA
NORTH DAKOTA
MONTANA
Winnipegosis
Brandon
Virden
Minot
Garrison
Estevan
Wynyard
Regina
Saskatoon
Swift Current
Shaunavon
Fort peck
Big sandy
Havre
Great Falls
Suffield
Medicine Hat
A
B
C
37KM
41KM
46KM
43KM
44KM
46KM
50KM
46KM
45KM
37KM
43KM
55KM
50KM
51KM
43KM
47KM
46KM
47KM
36KM

Figure 3.8 Compiled Moho depths in the study area. Dotted lines are magnetic trends from Fig. 3.2. Lines A, B and C define the S^3R^3 profiles for this study.

lineament of some tectonic significance possibly extending into the study area from the west is a major crustal rift discovered by Kanasewich et al. (1969). It trends approximately east-west through southern Alberta between latitudes 50°N and 51°N. The Moho depths of the crustal rift are similar to those in Saskatchewan. It is postulated that this crustal rift may extend into the Saskatchewan region.

3.7 Data acquisition

In August 1981 the CO-CRUST group conducted a field program in Saskatchewan to evaluate the Spatial Seismic Refraction Recording (S^3R^3). The COCRUST group included scientists from Universities of Alberta, Saskatchewan, British Columbia, Manitoba, Western Ontario, Toronto, and the Department of Energy, Mines and Resources, Ottawa. The field experiment consisted of three reversed refraction profiles and three broadside refraction profiles in a configuration of a triangle (Fig. 3.8). The three refraction profiles were labelled as A, B and C and each had total lengths of 287.9 km, 288.6 km, 288.4 km respectively. Only 45 stations were avalaible for one profile at a time, thus three shots were required for each line, two inline shots plus a broadside shot. All recording sites were selected along available roads and no location deviates more than 1 km from the straight lines defining the equilateral triangle. The average separation between recording sites was 6.5 km, because the number of receiver stations was limited to 45 stations in this field experment. Elevations, latitudes and longitudes of all recording sites, and shot locations were taken from a 1:50,000 topographic map. Time of shots, receiver coordinates and elevations as well as instrumentation and shot point information were compiled by Dr. Hajnal of the Geological Department from the University of Saskatchewan.

All field data were recorded on magnetic tape and were redigitized at a rate of 60 Hz because of different recording systems used in the field experiment. Each record contains 7200 samples (about 120 sec.), and the first three data words provide information concerning receiver number, shot number, and orientation of the seismometer. The data were written in format (5E16.6) with a block length of 1200 samples (4800 bytes). Thus each event consists of 6 blocks of data on magnetic tape.

3.8 Spectral analysis

A seismic trace is a time representation of ground velocity following the explosion of the source. The application of a Fourier transform converts the time-domain measurements of the seismic trace into frequency domain measurements and thus the amplitude of each frequency components can be evaluated. A power spectrum is a smoothed measure of the square of the amplitude for each frequency. Knowledge of frequency, amplitude, and phase characteristics are extremely important in designing digital processing techniques to improve seismic data.

The finite length of seismic data represents the truncation of the infinite data by a rectangular function. The discontinuity between the beginning and the end of the data creates undesirable side-lobe effects in the frequency domain, thus the power spectrum of the truncated data may be negative at some frequencies. A Daniel window, which represents the closest inverse of a rectangular window in the frequency domain, is useful to apply on data to eliminate the undesirable effect of the truncated data and to reduce the variance of the power estimate. Kanasewich (1981, P. 121-124) presented a detailed discussion of the theory and the computation procedure of Daniel power estimates and he recommended the use of the Daniel spectral estimate when the data set had 100 to 4000 samples.

A computer program written by Baxter and Kanasewich (1984, personal communication) was used to compute the Daniel power spectrum in this study. The parameter, m, which determines the resolution was taken to be 4. If the number of samples is not equal to a power of 2, zeros are padded at the tail to make the time series a power of 2. Fig. 3.9 and Fig. 3.10 show the applications of a Daniel window on records (5,5,1) and (6,9,1) of the broadside data. Most of the seismic energy is concentrated between the frequencies 4 and 15 Hz. Since the receivers of the broadside data were all approximately the same distance from the shots, we concluded that the frequency content of 'useful' signal

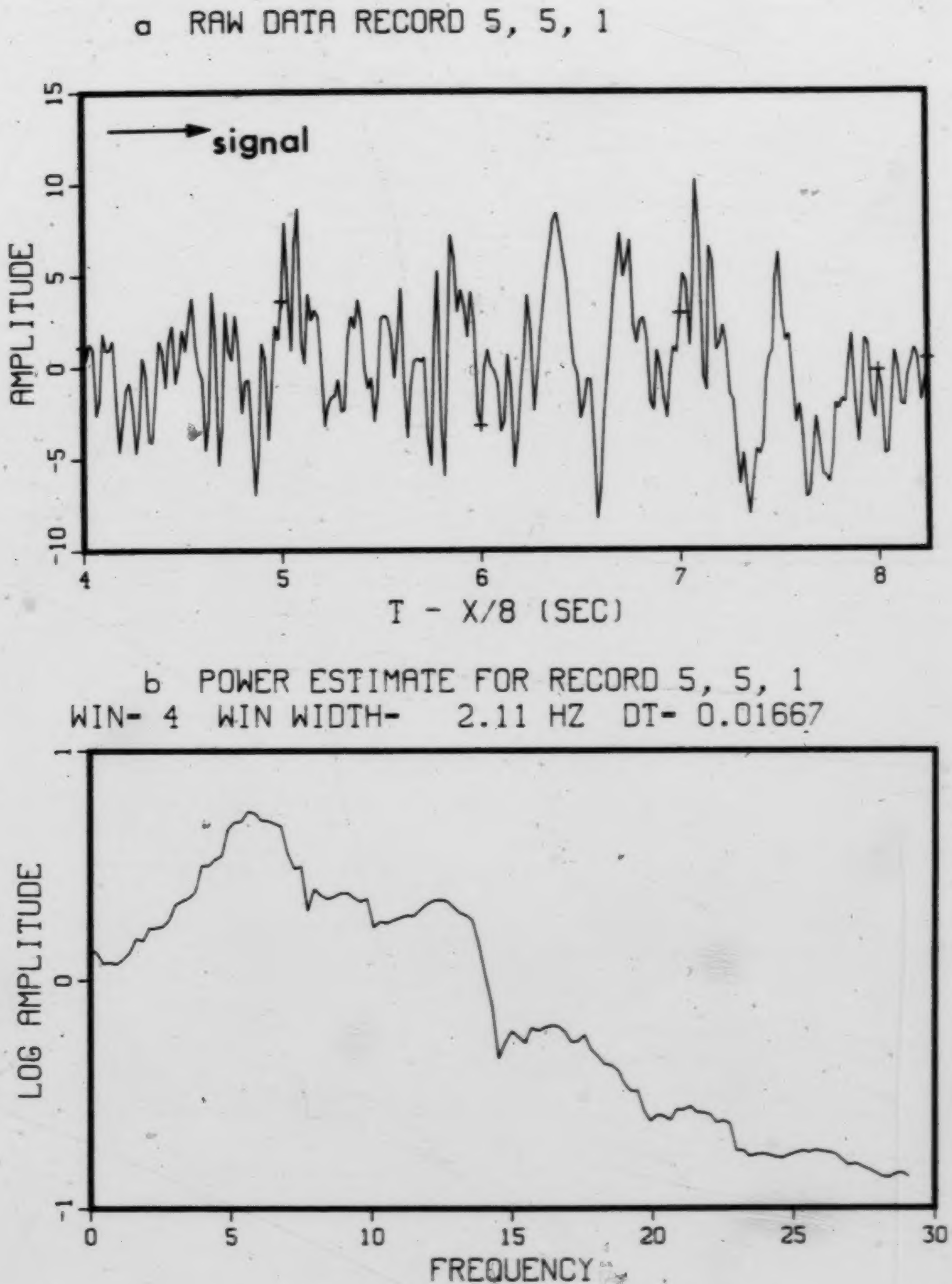

Figure 3.9 (a) Plot of raw data, (b) Power spectrum estimate of record (5,5,1). The distance is 273.9 km from the shot.

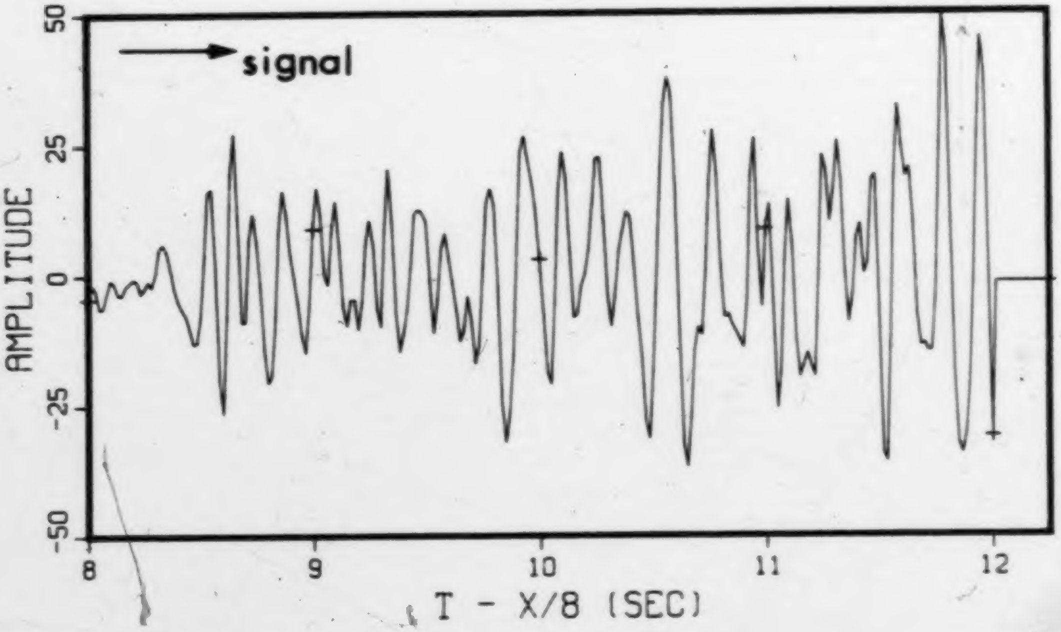

a RAW DATA RECORD 6, 9, 1

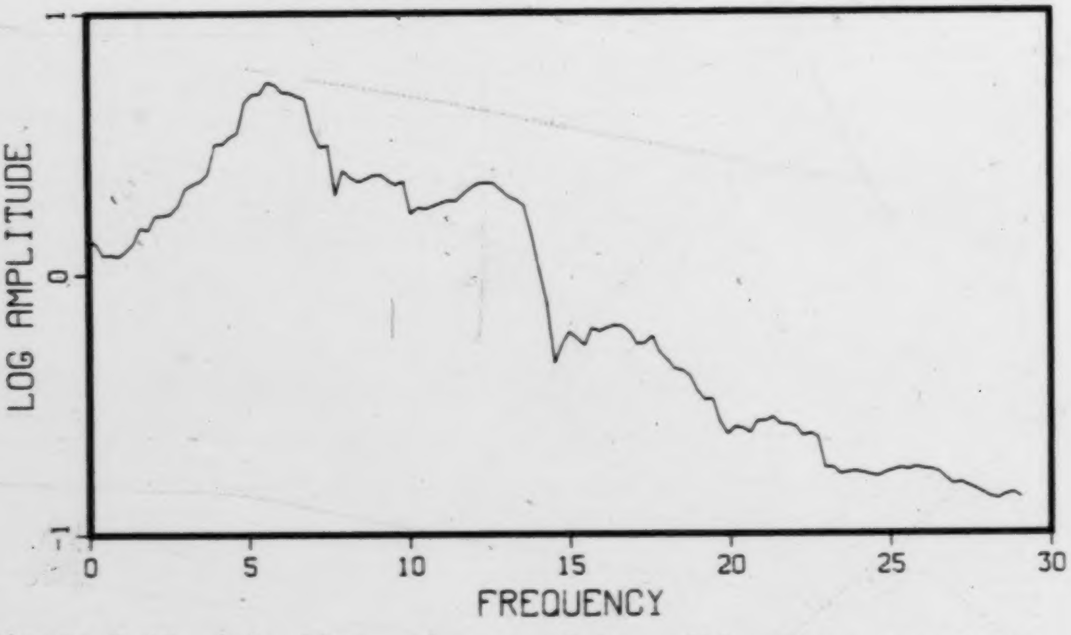

b POWER ESTIMATE FOR RECORD 6, 9, 1
WIN- 4 WIN WIDTH- 2.11 HZ DT- 0.01667

Figure 3.10 (a) Plot of raw data, (b) Power spectrum estimate of record (6,9,1). The distance is 272.4 km from the shot.

energy was restricted to a range of 4 to 15 Hz.

Furthermore, the power spectrum of the background noise will be useful for the filtering of the records. The power spectra of several records were computed; Fig. 3.11 shows two typical examples of such spectral estimates. The energy of the background noise concentrates mainly in the frequencies 0 to 5 Hz and gradually decreases beyond 17 Hz. The above conclusion suggests that it is appropriate to apply a bandpass filter of 5 to 15 Hz on all records.

3.9 Bandpass filtering

A bandpass filter is a frequency filter designed to pass signal frequencies in a particular band and to attenuate all other frequencies. The purpose of applying a bandpass filter to seismic signals is to extract useful signals from a noise background. The operation of filtering is especially effective in cases where signal and noise spectra do not overlap over a wide frequency band. Digital recursive filters allow the greatest flexibility in frequency smoothing, thus a recursive zero-phase bandpass Butterworth filter is used in this study. A detailed analysis of the eightpole bandpass Butterworth filter can be found in Kanasewich (1981, p. 237-277). Finally, a bandpass filter of 5-15 Hz was applied to all records following the conclusions of the power spectral analysis discussed in the previous section.

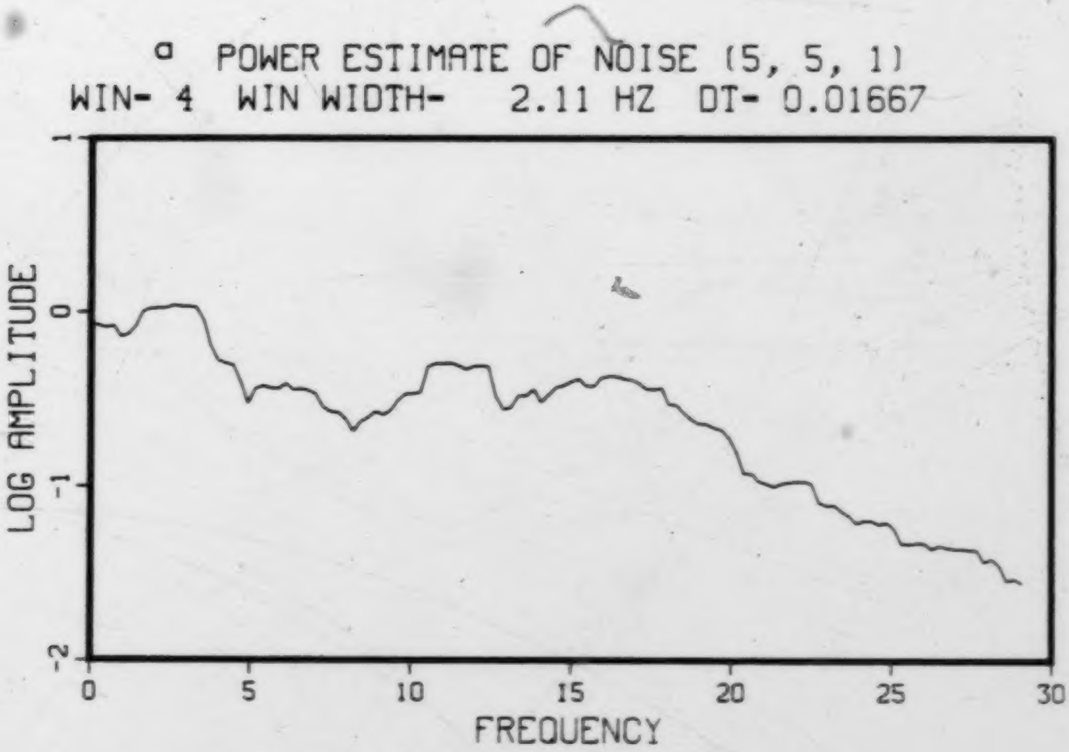

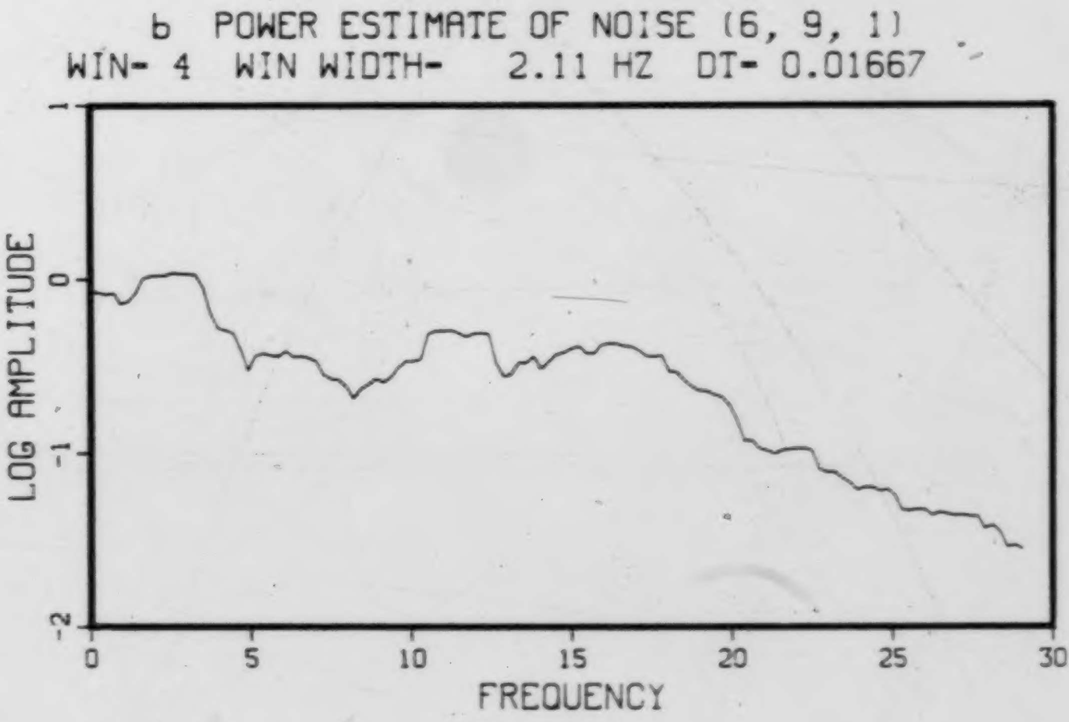

Figure 3.11 (a) Power spectrum of noise for record (5,5,1), (b) Power spectrum of noise for record (6,9,1).

4. INVERSION OF SASKATCHEWAN SPATIAL REFRACTION DATA

4.1 Comments on refracted waves from the crust

Based on travel-time analysis, three dominant seismic waves are observed from the surface down to the upper mantle:

1. Pg is usually considered to be a refracted wave in the upper crust, which has a typical velocity of 5.5 to 6.1 km/s. The Pg phase is usually observed up to a distance of 60-100 km. In general, the amplitude of the Pg phase decays inversely as the square of the distance from the source; beyond 100 km its amplitude becomes very small, and sometimes is not even observable.
2. The next prominent phase, which travels in the lower crust, is designated as P*. However, this prominent phase is only observed in some regions (Berry, 1973). The absence of the P* phase is probably due to lateral heterogeneities in lower crustal layer. The typical velocity is between 6.8 to 7.1 km/s.
3. Pn is generally considered to be a head wave which travels directly beneath the Moho discontinuity. In general, the Pn phase is observed to be a first arrival at distances beyond 200 km. Because of the attenuation and absorption of elastic waves through the earth the amplitude of a pure head wave decays rapidly beyond the critical distance. The typical Pn phase velocity in this study area is between 7.8 to 8.5 km/s.

In the region just beyond the critical angle the reflected wave and head wave interfere resulting in large amplitude arrivals (Cerveny, 1966). The head wave separates from the reflected wave at the end of an interference zone, and its amplitude is usually about one-order of magnitude weaker than the amplitude of the reflected wave. However, the amplitudes of the head waves observed in field data are often larger than the theoretical value. Waves interpreted as head waves are, in most cases, likely reflected refractions which have travel-time characteristics very near pure head waves but with much larger amplitudes. The appreciable amplitude of "head waves" imply positive velocity gradients or curvature of the refracting interface (Cerveny, 1966, and 1971). Thus, an interpretation based solely on the kinematic characteristics of the waves may not be unique in cases of n-layered media; the dynamic parameters of the waves, such as the amplitudes and the shape of the waves, may help to reduce the ambiguity of the solution obtained from the kinematic property only. Since this study involves only the inversion of travel-time data, it is assumed that the first arrivals observed on field records are pure head waves.

4.2 Summary of inline refraction data

The interpretation of inline refraction profiles from Macrides (1983) reveals a very complex structure in the crust below South-Central Saskatchewan. Figure 4.1 shows a

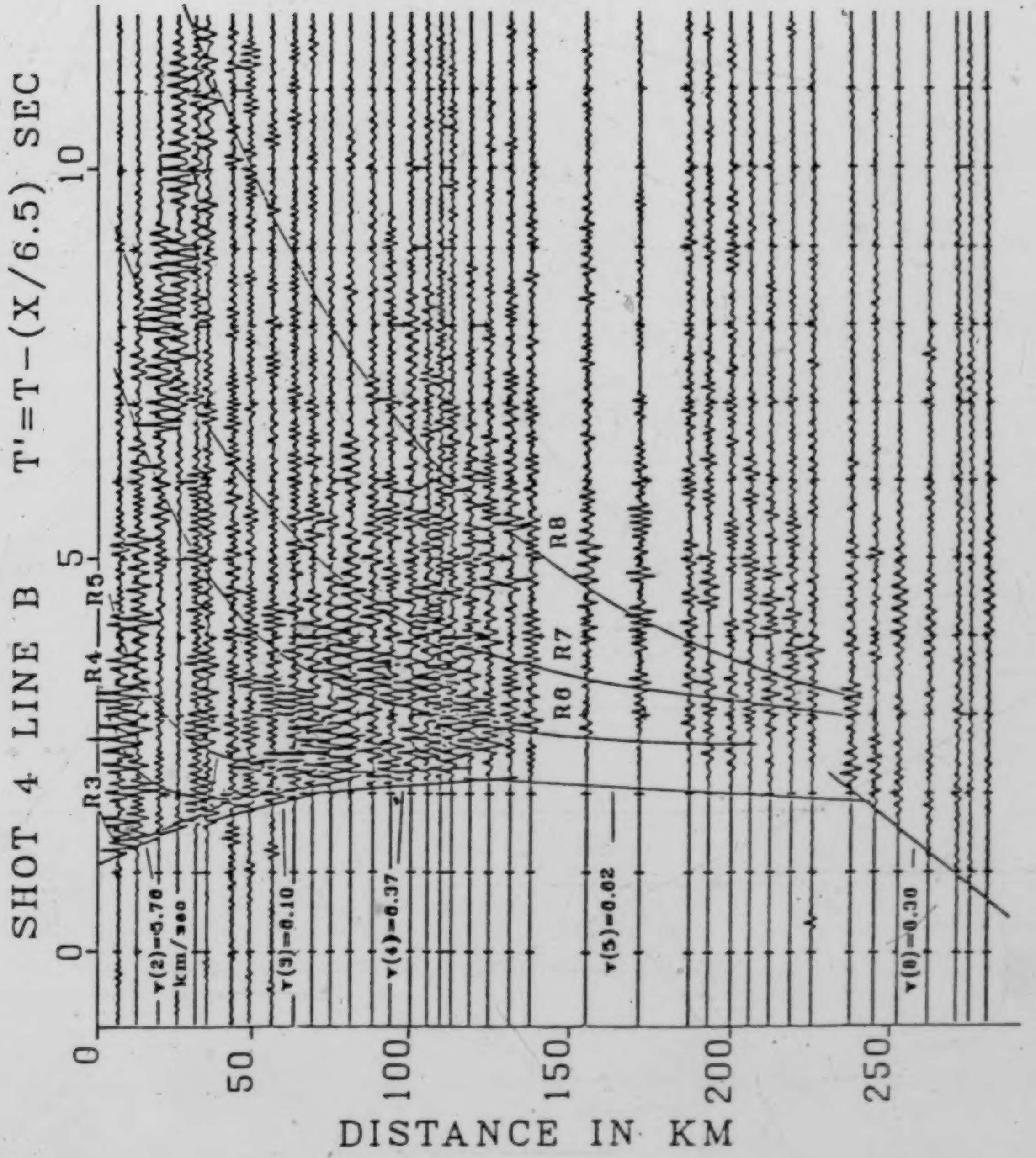

Figure 4.1 Record section of inline refraction line B in southern Saskatchewan (from Macrides, 1983, with permission).

section of the refraction profiles from shot 4 of line B. There are several prominent reflections (R3 to R8) are observed in this record section. In general, a very low noise level and clear first breaks are observed on most record sections. In addition to the analysis of head waves, the secondary arrivals can be correlated and analysed to obtain additional information on crustal structure. R3 is the reflection from the basement; R4 and R5, the reflections from the upper crust; R6 and R7, the reflections from the top and bottom of a low velocity zone situated in the middle crust; R8, the reflection from the Moho. Figure 4.2 shows the corresponding model of shot 4. The results of interpreting (Macrides, 1983) inline refraction profiles indicate: (1) low velocity layers occur below the profile A; (2) there is no evidence of substantial variation in the Pn velocity which is close to 8.13 km/s; (3) the existence of crustal faulting underlies B and C; (4) crustal thickness below the study area varies from 37 km to 47 km. In general, the crustal structure in this study area is rather complex with significant crustal faulting as well as the existence of one or two low velocity zones.

4.3 Test model

The data processing and analysis of the field observations are as important as the initial acquisition if the structural model is to be relatively unambiguous. We assume that we have both observations of reflected and

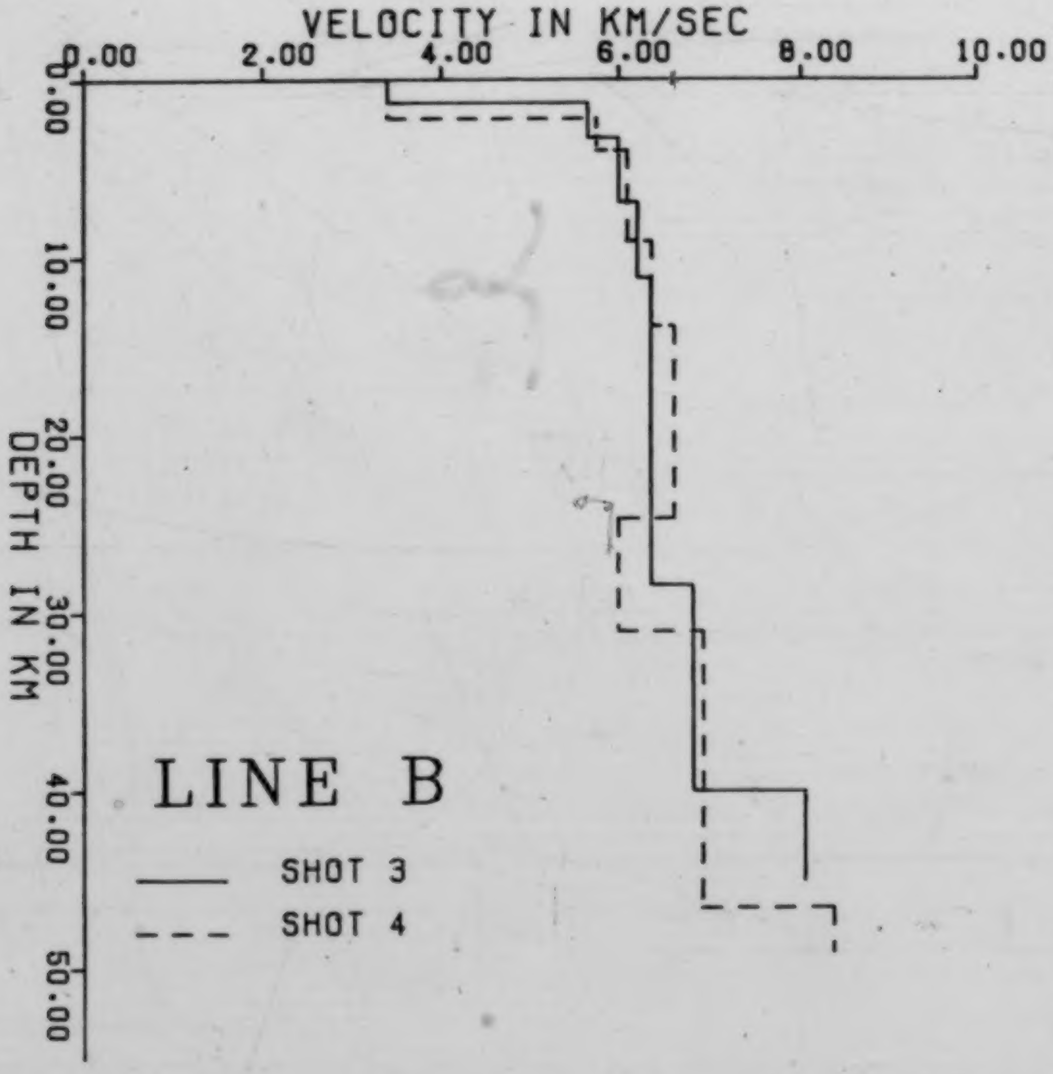

Figure 4.2 Crustal model of inline refraction profile B (from Macrides, 1983). Shot 3 is the model from the source near Wynyard to the southwest. Shot 4 is from the source near Swift Current to the northeast.

critically refracted waves (Figure 4.3). The objective is to test the tomographic method on a synthetic model which consists of a number of plane interfaces.

The L plane interfaces bounding each layer are defined by

$$a_i x_i + b_i y_i + c_i z_i + d_i = 0, \qquad i=1, \ldots m,$$

where a_i, b_i, c_i are direction cosines and d_i is the distance of the normal to the origin. The strike is given by α_i where $\tan\alpha_i = a_i/b_i$ and the dip is β where $\cos\beta_i = c_i$.

A three-dimensional test model with block faulting is shown in Figure 4.4a. It is presumed that the crustal velocities have been determined previously, and the model is a horst type of structure, with Moho head wave velocities of 8.2, 8.0 and 8.3 km/sec, respectively, beneath the three-faulted planes. The spatial seismic refraction recording was arranged in a 380-km equilateral triangle, and each source was only at one of the vertices. A sparse receiver network with only 33 stations was modelled as shown on the surface (Figure 4.4a) to simulate a sub-optimal recording pattern unlike that illustrated in Figure 3.6. Therefore, in the test model, a sparse network is sufficient because there are no errors in the correlation of phases. Three refraction profiles are arranged in a triangluar form and each is shot broadside. In the investigation of the Moho structure, we use only the critically refracted and wide-angle reflected waves in the damped least squares

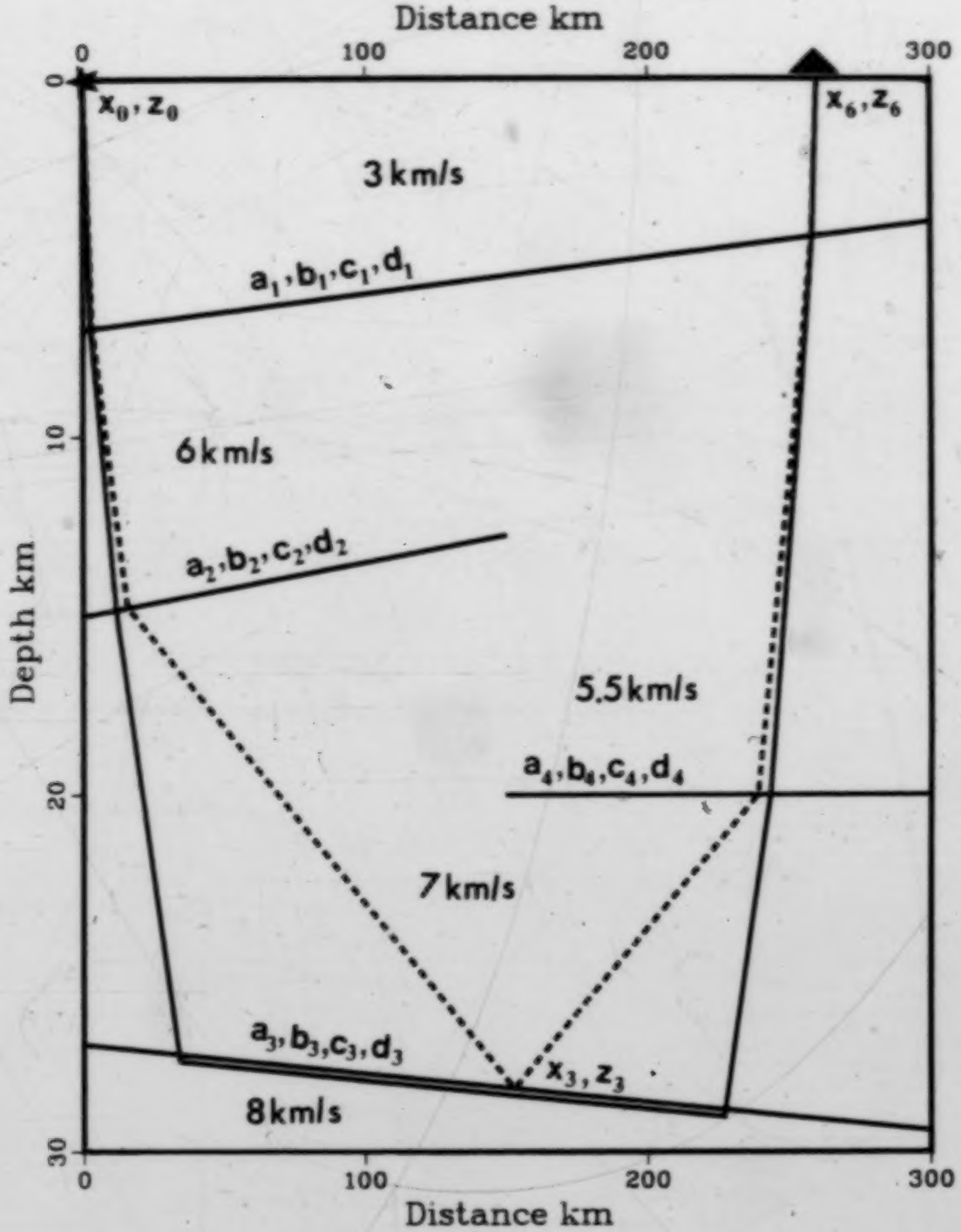
Distance km
0
100
200
300
x0, z0
x6, z6
3 km/s
a1, b1, c1, d1
6 km/s
a2, b2, c2, d2
5.5 km/s
a4, b4, c4, d4
7 km/s
a3, b3, c3, d3
x3, z3
8 km/s
Depth km
0
10
20
30
0
100
200
300
Distance km

Figure 4.3 Refracted (solid line) and reflected (dashed line) ray paths and the coordinate system. The direction cosines for the planes are a, b and c, and d is the distance of the normal to the origin.

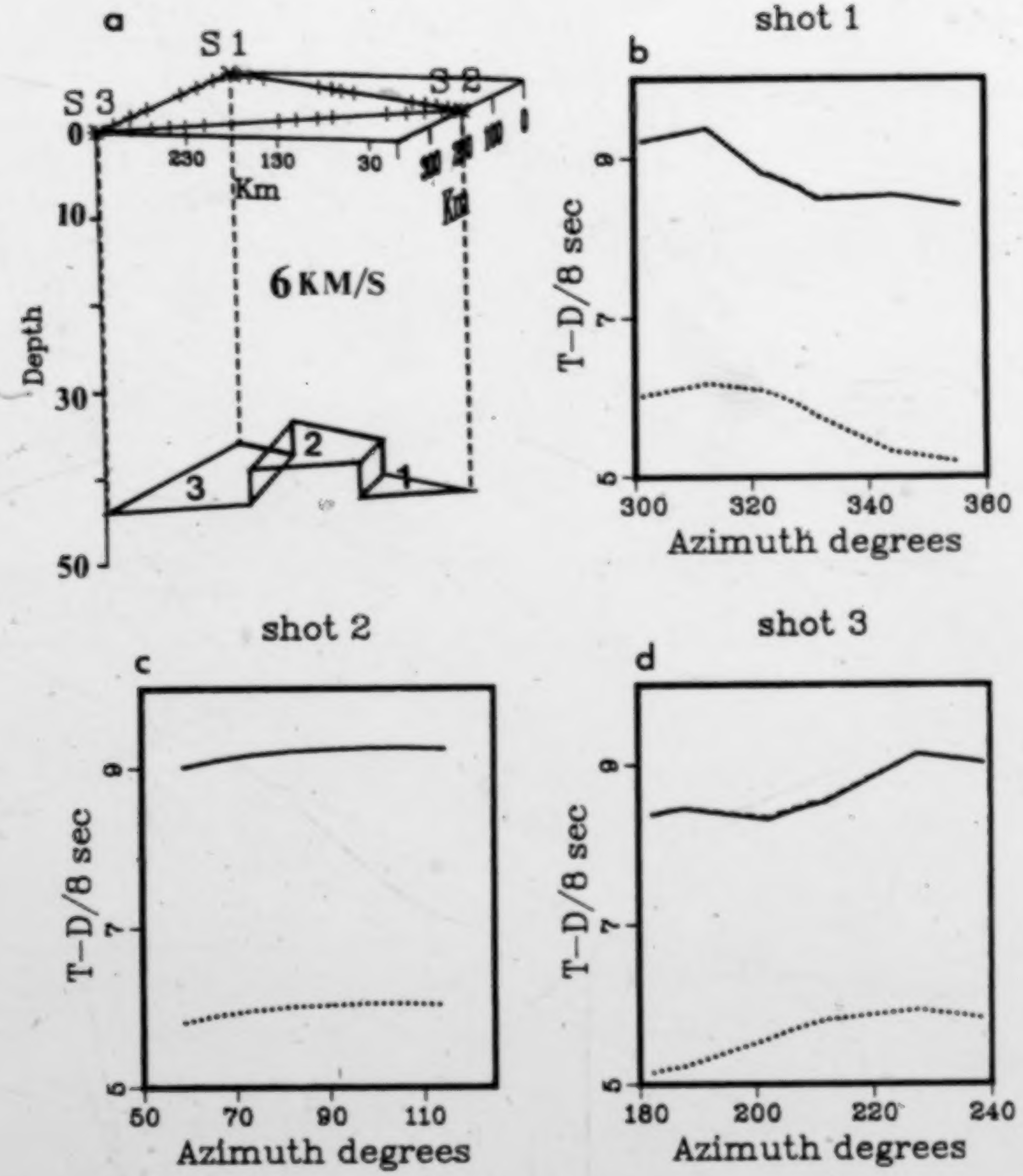

Figure 4.4 (a) 3-D test model. The location of the receivers are shown as crosses along a triangular array on the surface. The sources are indicated as stars at the vertices. The three faulted blocks are marked as 1, 2, 3. (b) to (d) are the reduced travel times of the head waves from Moho discontinuity for sources S1 to S3. The dotted line is the computed initial assumption to the least-squares inversion. The dashed line is the first iteration, and the solid is the theoretical value.

inversion.

The initial model comprises three horizontal planes at a depth of 30 km. The maximum difference of depth between the initial model and the theoretical model is 14 km. We consider three cases: (1) the inversion of critical refraction data only with no error in the data; (2) the inversion of both critical refraction and wide-angle reflection data; (3) the inversion of both refraction and reflection data with noise which has a standard deviation of 100 msec from the theoretical time.

Figure 4.4b shows the arrival times of head waves from source S1. The results from the other two sources are very similar (Figures 4.4c and 4.4d). In two iterations the model response times converge within a standard error of 1.5 msec from the theoretical times. This accuracy is considered to be excellent in crustal seismology. The wide-angle reflection data constrains the model parameters in addition to the head waves. In this particular model, all the wide-angle reflections are confined to planes 2 and 3. Therefore, the model parameters associated with planes 2 and 3 can be determined more accurately because of the additional reflection data. Conversely, the model parameters for plane 1 become less accurate because of the relative decrease of observations. In two iterations, the standard error from the theoretical times is 8.8 msec which is higher than the one from refraction data only. However, the iterated model converges to the theoretical model after eight iterations. Figure 4.5, a to c shows the arrival times for both head and reflected waves for source S1, S2 and S3, respectively. After two iterations, the theoretical curves from each source are matched by the damped least-squares inversion procedure so that it is difficult to display the differences graphically.

Furthermore, we tested the damped least-squares inversion for noisy data. Random numbers having a standard deviation of 100 msec were added to the data. In two iterations, the standard error of the data was 94 msec and it remains approximately the same up to the fifth iteration. The model is acceptable after the second iteration since the standard error is lower than the noise level of 100 msec. Similar results are obtained if the standard deviation of the noise is increased by a factor of 5. The iterated model parameters are reasonably close to the theoretical parameters. Figure 4.6, a to c shows the travel-time curves for source S1, S2 and S3, respectively. At the second iteration, the damped least-squares model curves start matching closely the theoretical curves. In general, the damped least-squares inversion produces robust parameter estimates for the model, and the damping factor controls the stability and resolution of the solution.

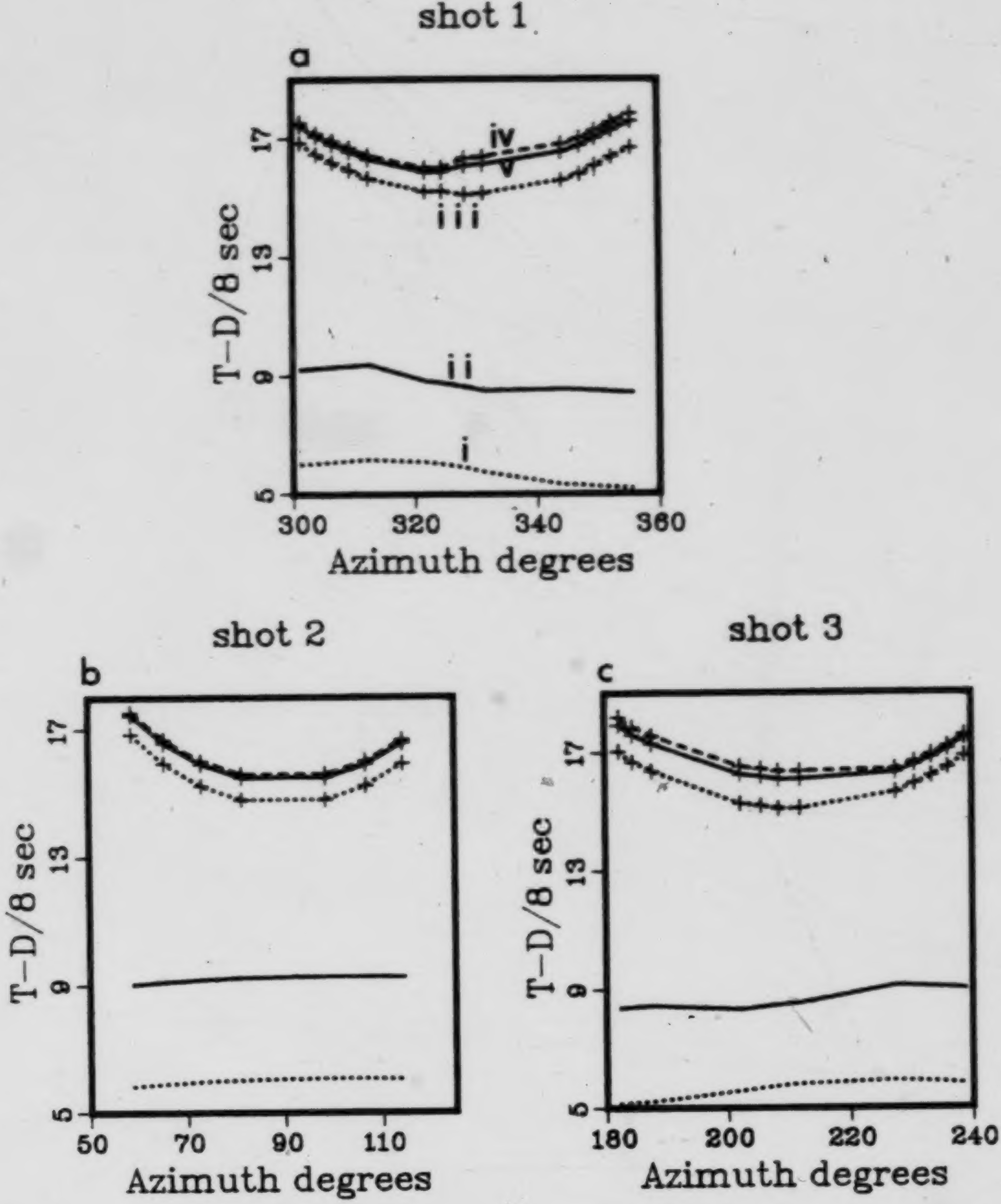

Figure 4.5 (a) to (c) Reduced travel-time diagrams for S1 to S3 versus azimuth for both refracted and wide-angle reflected seismic rays. No noise is included. (i) Initial computed assumption for refracted arrivals; (ii) theoretical curve and final iterations for refraction arrivals; (iii) initial computed assumption for reflected arrivals; (iv) travel time for reflected waves after first iteration; (v) theoretical curve and second iteration for reflected waves.

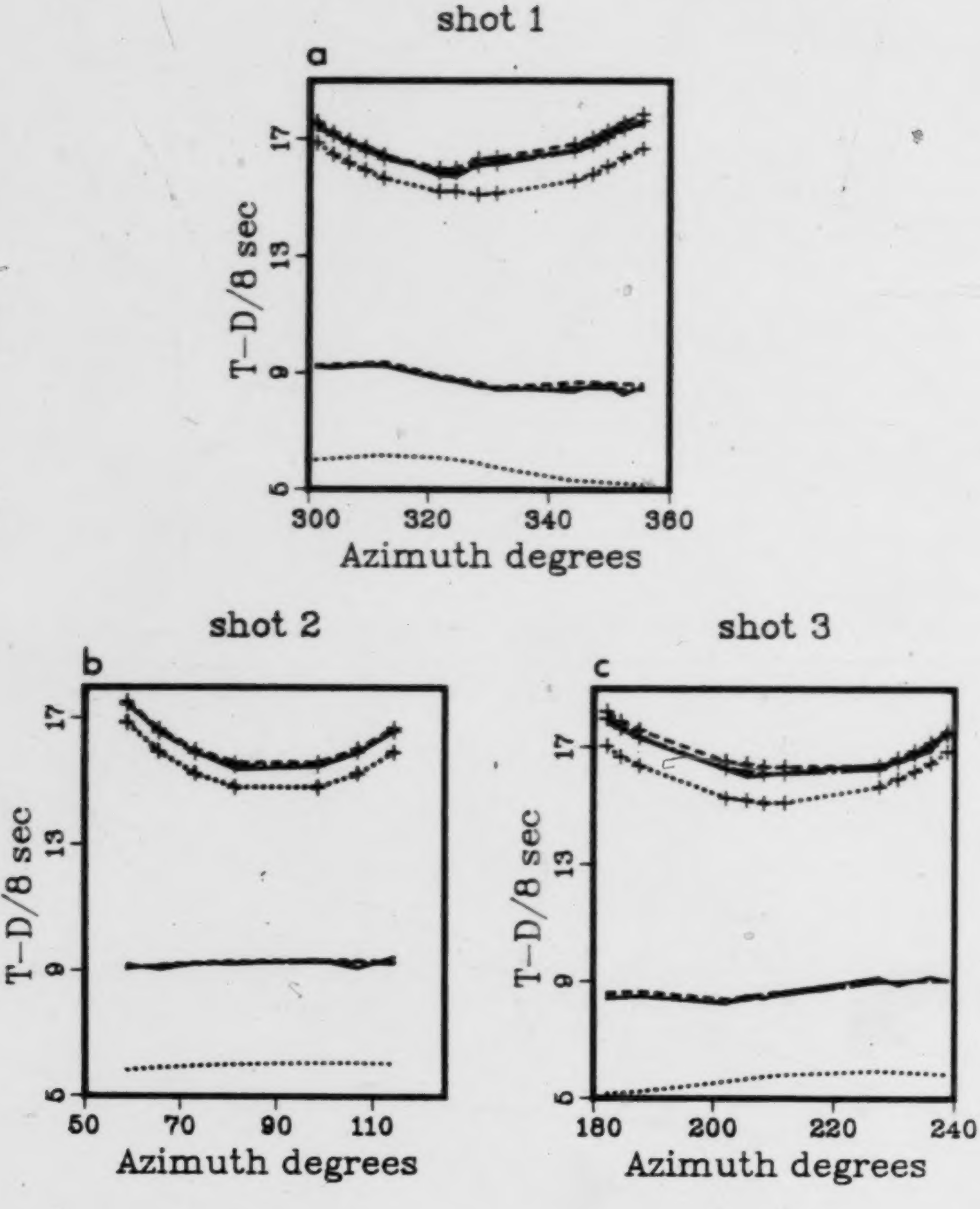

Figure 4.6 The same results as in Figure 4.5 but with the introduction of random noise into the theoretical times. The standard deviation for the noise is 0.1 sec.

4.4 Presentation and comments on spatial refraction data

The spatial seismic refraction recording method was tested in a sub-optimal experiment over the Williston Basin in Saskatchewan (1981). Since only 45 recording instruments were available in an equilateral triangle 288 km on each side, there were some notable gaps due to topography or instrumental difficulties. Figure 4.7 illustrates the surface projections of rays traversing below the Moho in this experiment. This technique produces a high concentration of common rays intersecting at the centre, as well as the area adjacent to the centre. From the redundant information of both head waves and wide-angle reflections we expect to yield a detailed structure at the target horizon.

Two methods have been deployed to display the broadside refraction profiles. The first approach is to plot amplitudes of first arrivals as a function of reduced travel time versus azimuth (Figure 4.8). The profiles have the time axis increasing to the bottom to simulate a "weighted refraction crustal section" of the Moho horizon. This form of presentation simulates a structural section if the head wave and average crustal velocities do not vary greatly along the three broadside profiles. It is very successful in identifying travel-time discontinuities and probable faults on the target horizon.

The second approach is to plot amplitudes of wide-angle reflection as a function of reduced travel time versus azimuth (Figure 4.9). If normal moveout corrections are

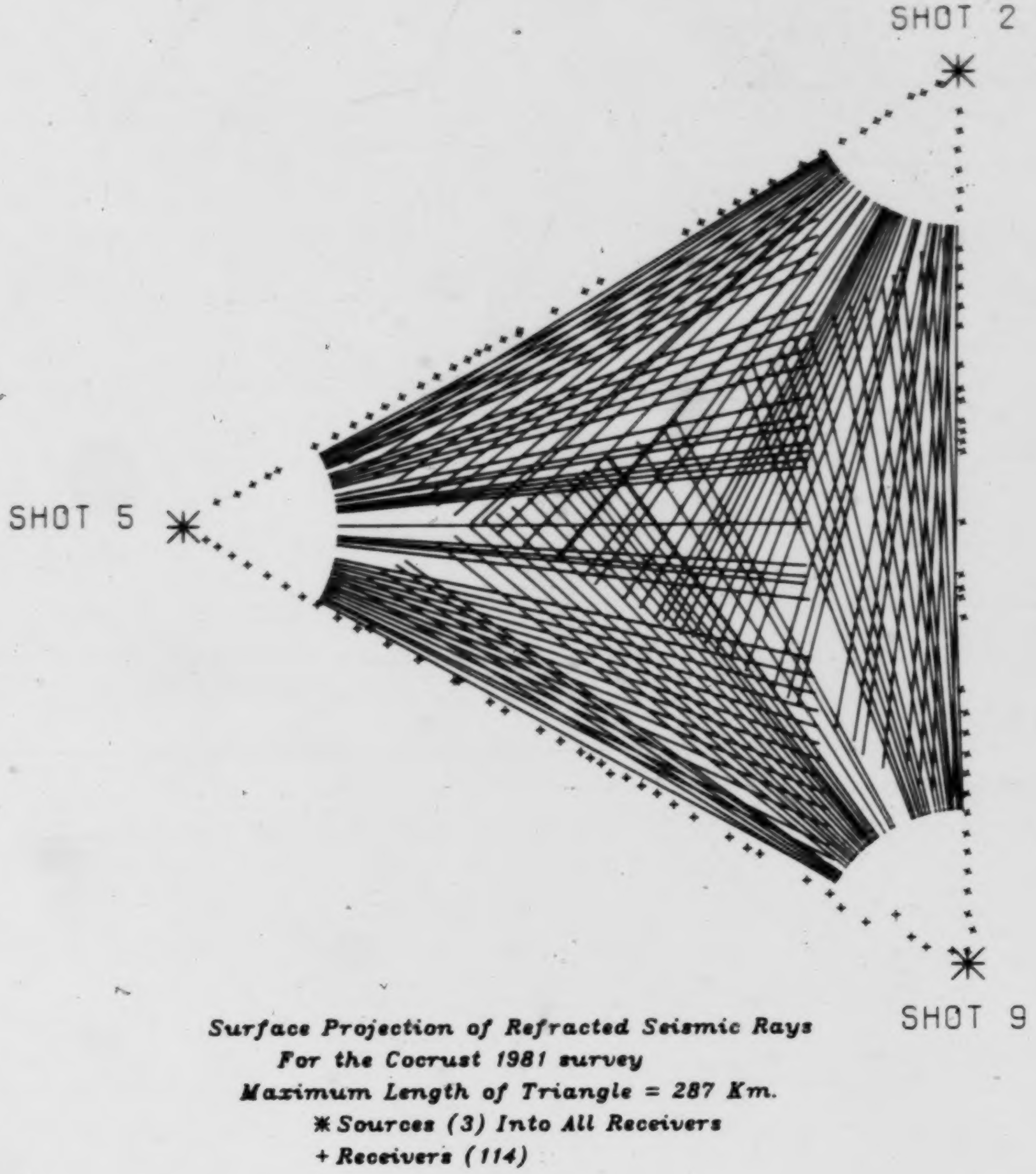
SHOT 2
SHOT 5
SHOT 9
Surface Projection of Refracted Seismic Rays
For the Cocrust 1981 survey
Maximum Length of Triangle = 287 Km.
✱ Sources (3) Into All Receivers
+ Receivers (114)

Figure 4.7 Surface projections of rays traversing below the Moho in Saskatchewan experiment (1981).

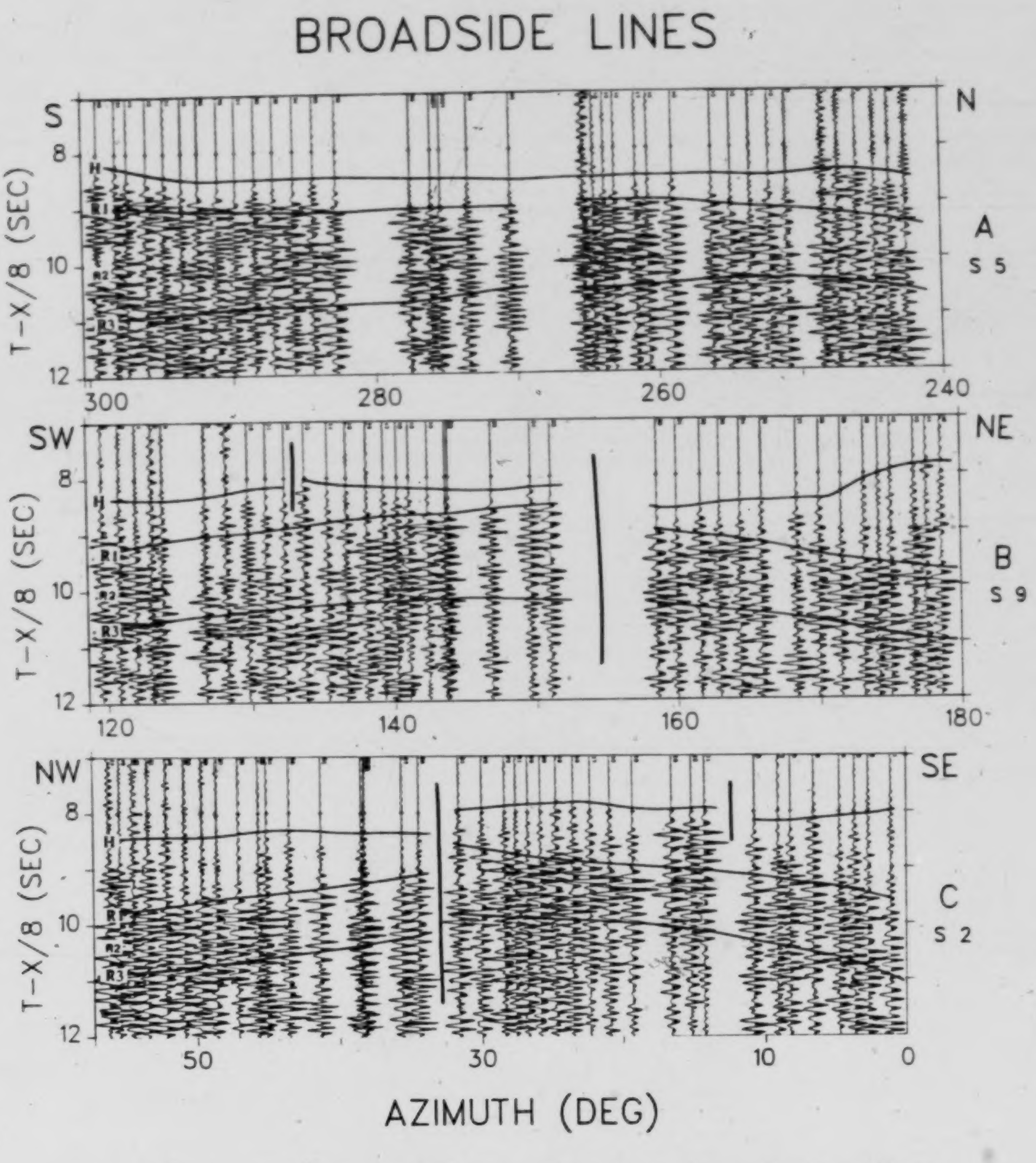

Figure 4.8 Reduced seismic refraction travel-time plots versus azimuth for the three broadside lines. The first curvilinear line (H) marks the Moho head wave, the other line (R1) marks the wide-angle reflections from the crust, and the third one the wide-angle Moho reflection (R3).

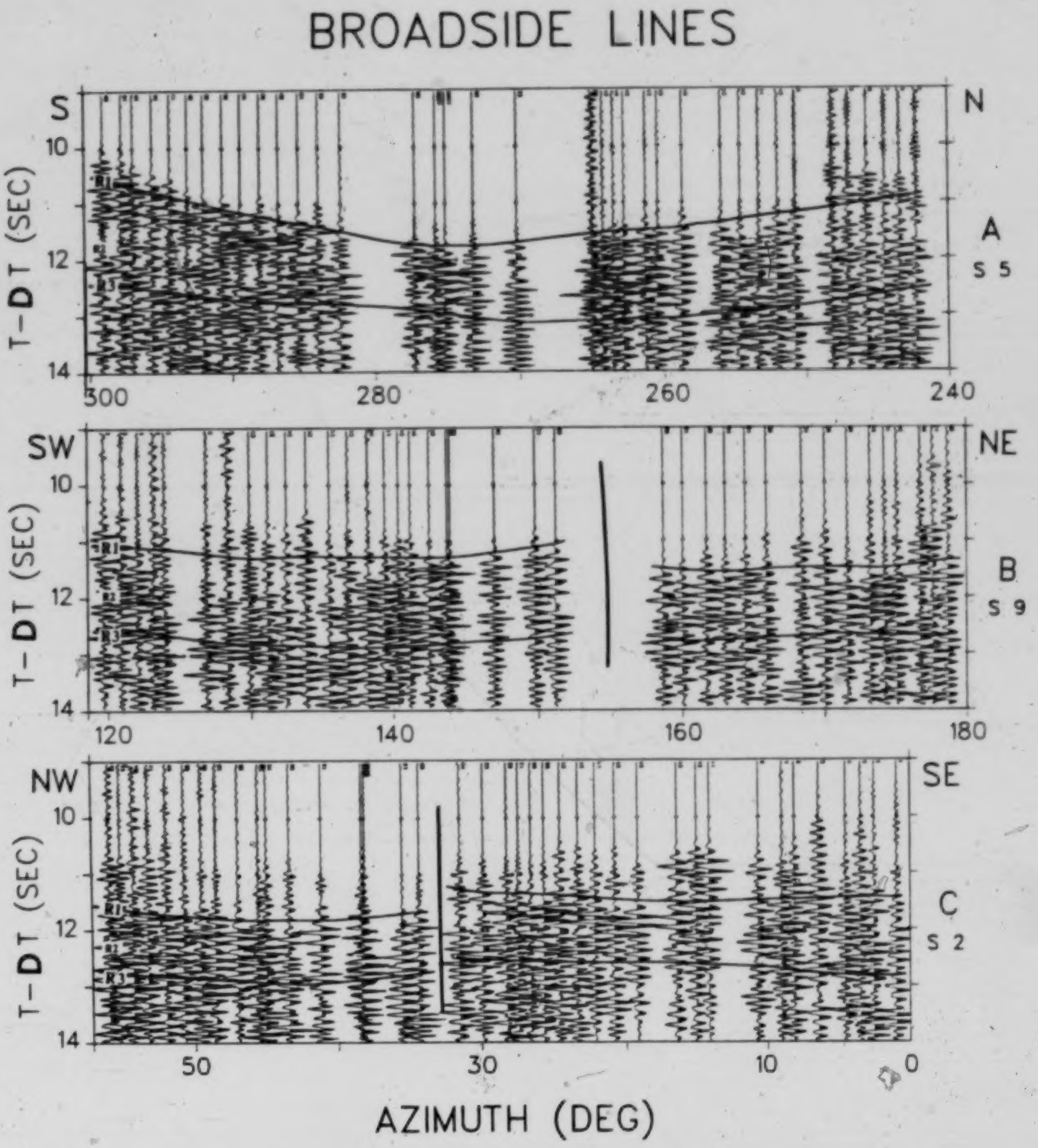

Figure 4.9 Reduced seismic refraction travel-time plots versus azimuth for the three broadside lines. DT is defined as normal moveout correction. The line (R1) marks the wide-angle reflections from the crust, and the second one the wide-angle Moho reflection (R3).

subtracted from the observed reflection times, the time-shifted signals for a reflected branch tend to lineup horizontally. This form of presentation is also successful in identifying travel-time discontinuities from wide-angle reflection data. Both presentations compliment each other to identify possible fault locations. Furthermore, the locations of travel-time discontinuities correspond to major trends of gravity and magnetic anomalies and this may confirm the possible fault locations in the study area. Figure 4.10 shows the location of the sources and receivers, local gravity and aeromagnetic trends, and the fault locations which are defined by the discontinuities of travel-time data.

Three secondary arrivals have been identified in Figures 4.8 and 4.9 as R1, R2, and R3. Only R1 and R3 correlate through all sections. In general, R1 is interpreted as a reflected wave from the middle crust. R2 is the reflected wave from the lower crust, and R3 is the wide-angle reflection from the Moho. Detailed analysis of the secondary arrivals will be discussed in the next section.

4.5 Analyses of wide-angle reflections

From the discontinuities in the broadside data and the trends of anomalies on gravity and aeromagnetic maps, we divided the region beneath the study area into three normally faulted planes. Figure 4.11 is the expanded map

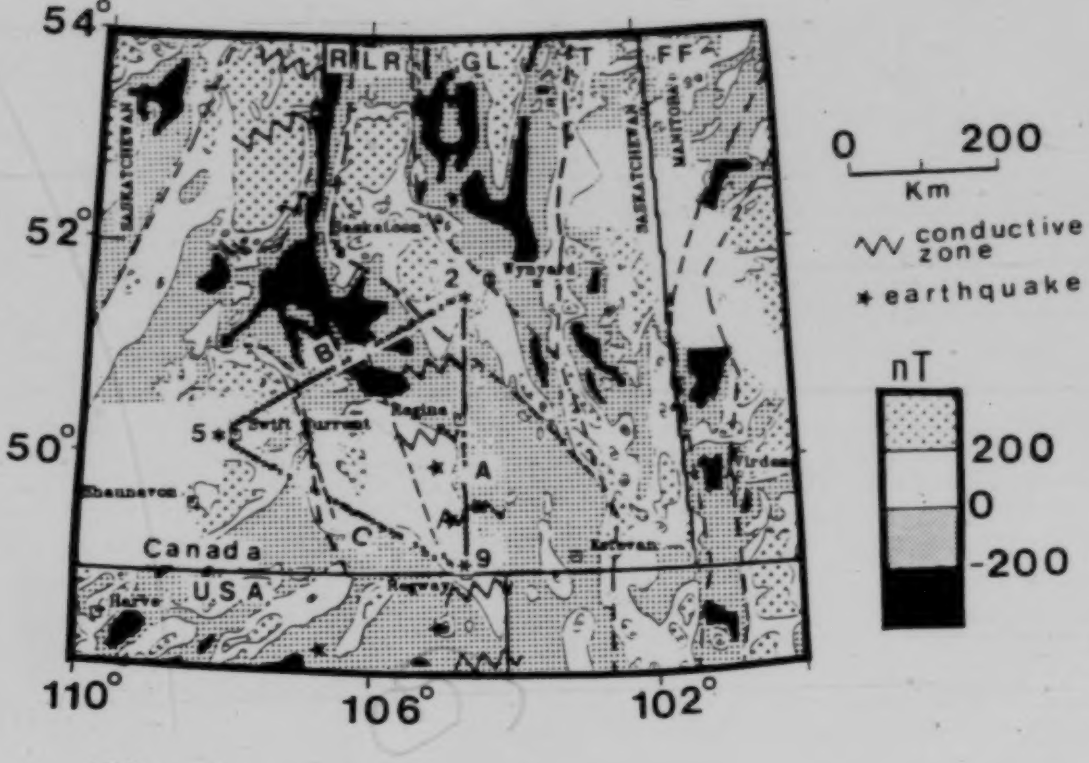
54°
52°
50°
110°
106°
102°
R
LR
GL
T
FF
SASKATCHEWAN
MANITOBA
Saskatoon
Wynyard
2
B
5
Swift Current
Regina
A
C
9
Shaunavon
Estevan
Canada
USA
Havre
0
200
Km
conductive zone
earthquake
nT
200
0
-200

Figure 4.10 Map of southern Saskatchewan showing the location of the sources (small stars) and receivers (crosses) for spatial seismic refraction data. Aeromagnetic trends and faults are dashed lines. A, B, and C are refraction profiles. R, Reindeer-South Indian Lake belt; LR, La Ronge-Lynn Lake belt; GL, Glennie Lake domain; T, Tabbernor fault; FF, Flin Flon-Snow Lake belt. Earthquakes are shown as large stars.

showing the locations of receivers and reflection mid-points as well as fault locations. Obviously, there is no reflection data coming from plane 1; most of the reflection data concentrates on plane 2; and only a reasonable amount of reflection data comes from plane 3. Therefore, the wide-angle reflections can be used to determine the interval velocity and structure of planes 2 and 3. However, the damped least-squares solution of plane 2 is expected to be better and more reliable than plane 3 because of having more observations.

The objective is to invert the travel times of reflection branches R1, R2, and R3 by the damped least-squares algorithm discussed previously to establish the structure of the crust and its interval velocities. The inversion procedure first solves for the upper layers and then freezes the model parameters of the upper layers in order to solve for the lower layers. This approach is often termed a "layer stripping" method, and it provides speed and stability in the inversion procedure. Although freezing is not essential, it is useful in avoiding some model ambiguities by using fewer variables when inverting travel times for deeper layers.

From the analysis of well logs as well as first-break arrivals, the two sedimentary layers have the depths of 3.1 and 4.1 km and velocities are 3.4 and 5.72 km/s, respectively. These upper two sedimentary layers correspond to the base of the Mesozoic clastic sequence and the top of

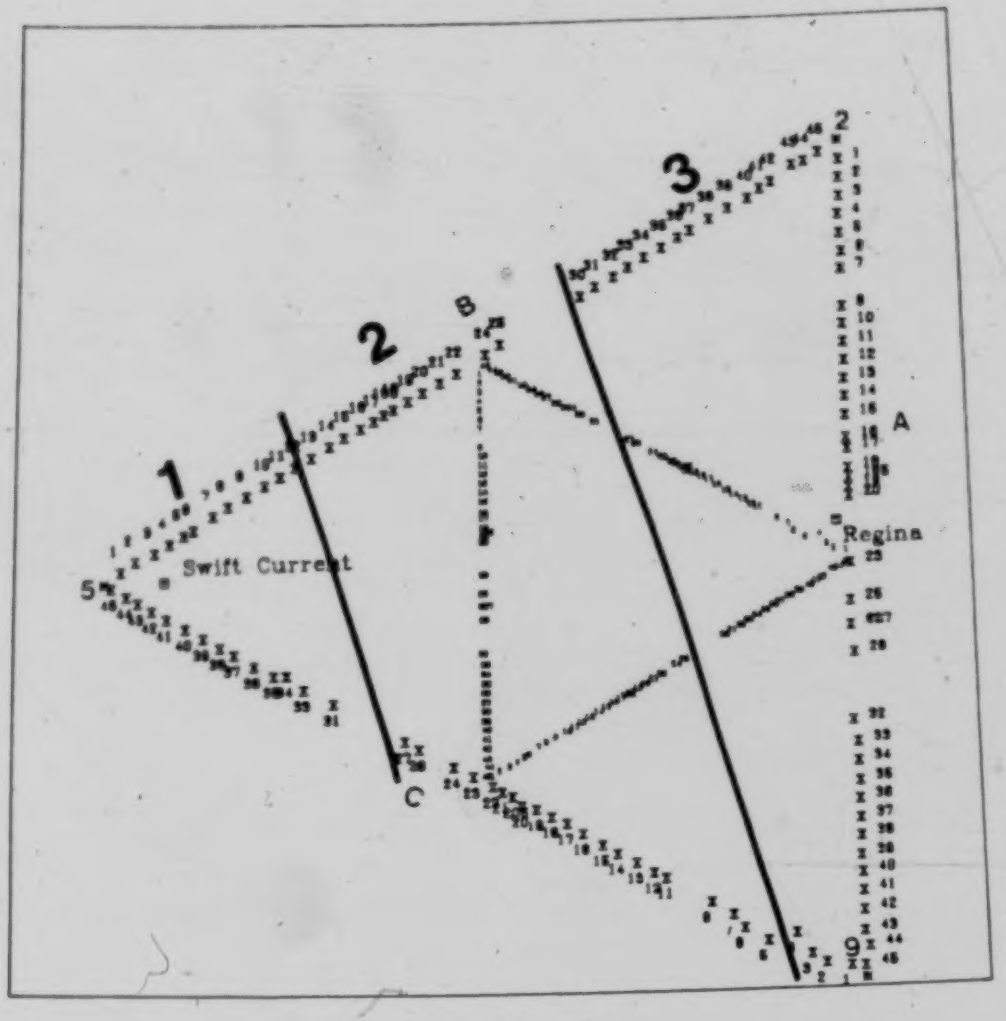

Figure 4.11 Locations of the reflection points. A, B, and C are broadside refraction profiles corresponding to shot numbers 5, 9 and 2. The numbers on the outside triangle are the receiver station numbers; the numbers of the inside triangle are the corresponding projections of reflection mid-points from shots to receivers. Faults are solid lines.

the crystalline basement. Since the interval velocities and depths have been determined, the parameters of the two sedimentary layers remain constant in solving for lower layers.

Quite prominent amplitudes of the reflected branch R1 were observed in all three broadside refraction profiles (Fig 4.9). In most cases, this horizon can be correlated through all sections and the discontinuities of wide-angle reflections are clearly visible on profiles B and C. Since no wide-angle reflections reach plane 1, only coefficients of plane 2 and plane 3 are determined by the damped least-squares inversion. Travel-time data were then picked from bandpass-filtered broadside sections as well as a selected portion from inline data. The frequency interval of the bandpass used is between 5 and 15 Hz.

The initial model consists of three layers: two upper sedimentary layers and a third horizontal layer. The parameters of the two sedimentary layers are assumed to be constant for the inversion. The third layer is the initial guess for the reflection branch R1. Its initial interval velocity and depth are 6.5 km/s and 16 km, respectively. The least-squares inversion procedure was then used to determine the orientation, the depth, and interval velocity of the plane. Figure 4.12a displays the structure of the middle crust as a result of the inversion of reflected branch R1. The contours (km) show the depths from the surface to the interface of R1. The travel-time data fitted quite well with

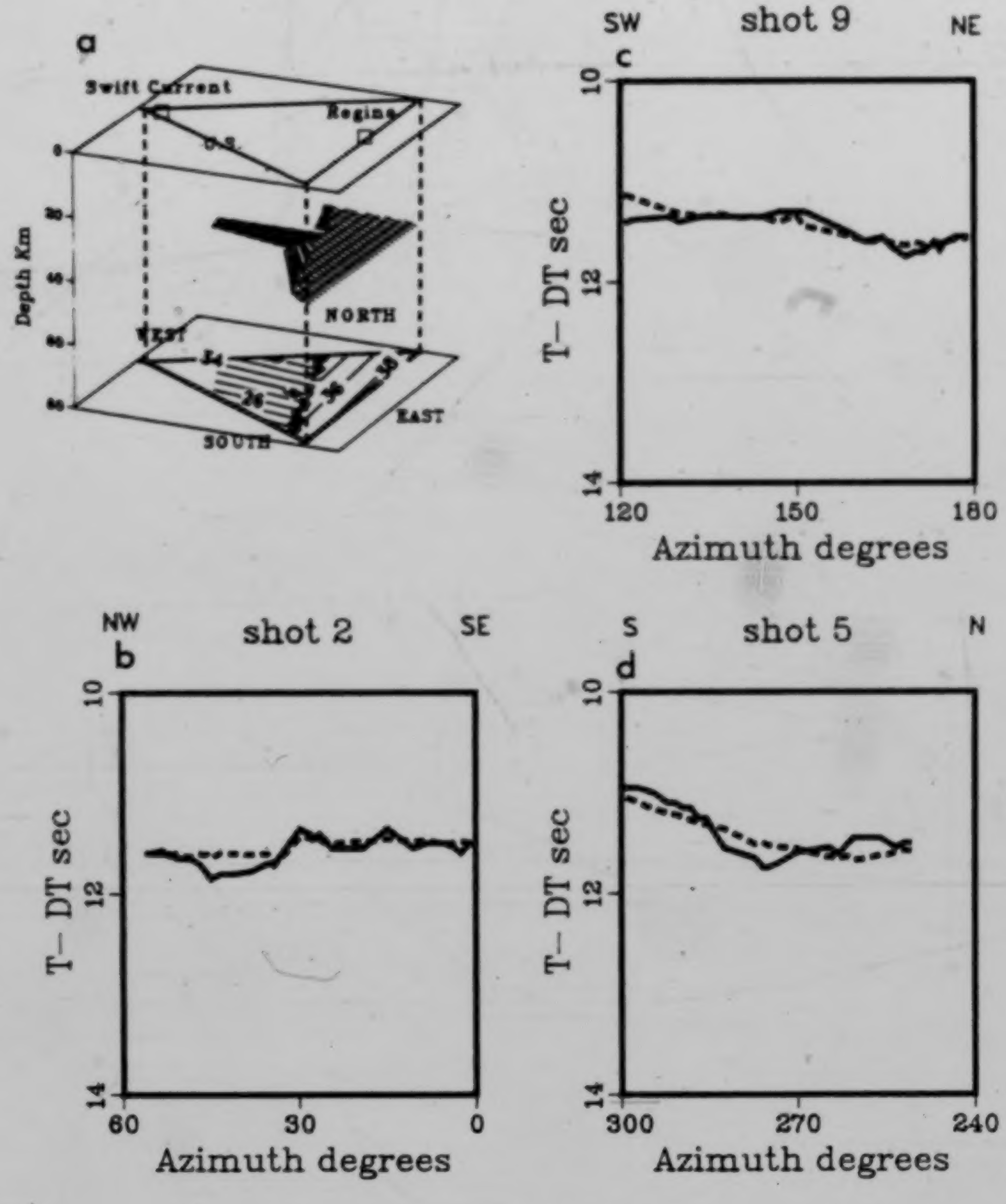

Figure 4.12 (a) The structure of the reflected branch R1. Travel-time curves for: (b) shot2; (c) shot9; and (d) shot5. The solid line is from the field observations. The dashed line is the final value from the least-squares iteration assuming only two faulted planes.

the observations (Figure 4.12, b to d). It shows a normal fault with down thrown side on plane 3. After four iterations, the standard error is 110 msec. This accuracy is quite good considering the uncertainty in picking the wide-angle reflections. Furthermore, the standard error remains approximately the same at the fifth iteration. This implies that the damping factor stabilizes the solution but it may not improve the residuals. This is usually the tradeoff between resolution and stability. The interval velocities on both plane 2 and plane 3 are 6.64 km/s and 6.67 km/s, respectively. This indicates that the formations on both faulted planes may have similar lithological units. Plane 2 dips about 5.7° to the north and plane 3 dips about 4.4° to the northeast.

The inversion procedure continues to model the travel-time data towards greater depth. The inversion of reflected branch R2 is achieved by freezing the model parameters of the upper three layers. The amplitudes of R2 are quite prominent. In general, the correlation of this horizon is relatively reliable through the sections, and the discontinuities of travel-times are also clearly visible at line B and C (Fig 4.9). After five iterations, the standard error is also 110 msec. Figure 4.13a shows the structure of the reflected branch R2. The contours (km) show the depths from the surface to the interface of R2. The travel-time curves computed from the iterated model matched the observations quite well (Figure 4.13, b to d). The interval

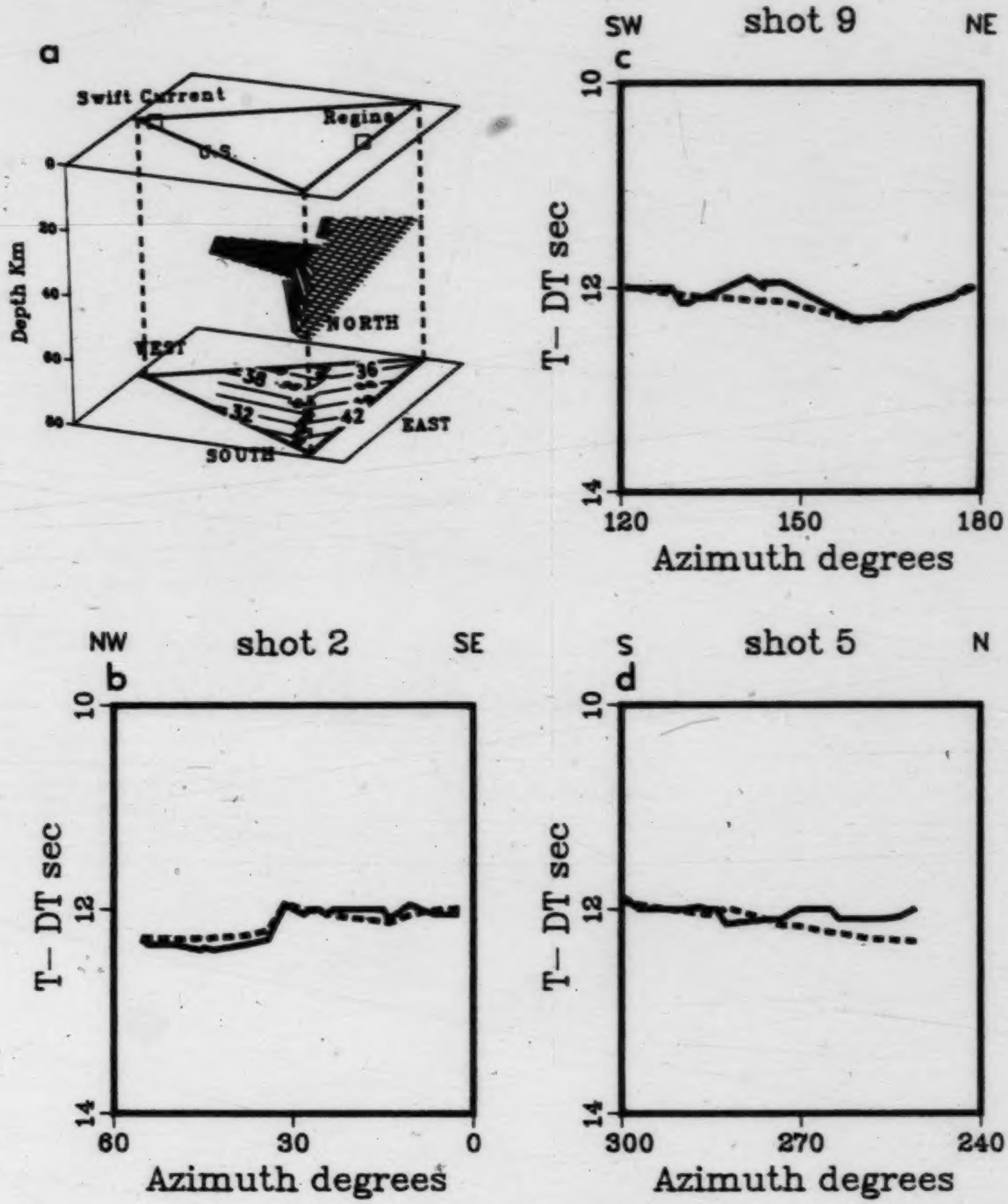

Figure 4.13 (a) The structure of the reflected branch R2. Travel-time curves for: (b) shot2; (c) shot9; and (d) shot5. The solid line is from the field observations. The dashed line is the final value from the least-squares iteration assuming only two faulted planes.

velocities on both plane 2 and plane 3 are 5.92 km/s and 6.1 km/s, respectively. The existence of low velocity zones is also reflected in the inline interpretation by Macrides (1983) in which he found the existence of the low velocity zones on both profiles A, B, and C.

Finally, we carried the inversion procedure further to model the deepest layer of the Moho. Although the supercritical Pn arrivals have quite prominent amplitudes, the correlation of Pn arrivals is difficult in some cases. The locations for the Pn on both ends of each broadside profile are guided by the Pn arrivals of the inline data. After four iterations, the standard error is 120 msec. Figure 4.14a shows the structure of the Moho determined by the damped least-squares inversion using wide-angle reflections only. The contours (km) show the depths from the surface to the interface of R3. Next we will analyse the Moho structure in more detail by including the head wave arrivals. The objective here is to determine the interval velocities above the Moho discontinuity. The travel-time curves computed from the iterated model matches the observations reasonably well (Figure 4.14, c to d) despite the difficulties and uncertainty in picking the Pn arrivals. The interval velocities for plane 2 and plane 3 are 6.72 km/s and 6.85 km/s, respectively. Plane 2 dips 1.5° gently to the north and plane 3 also dips approximately 1.2° to the north.

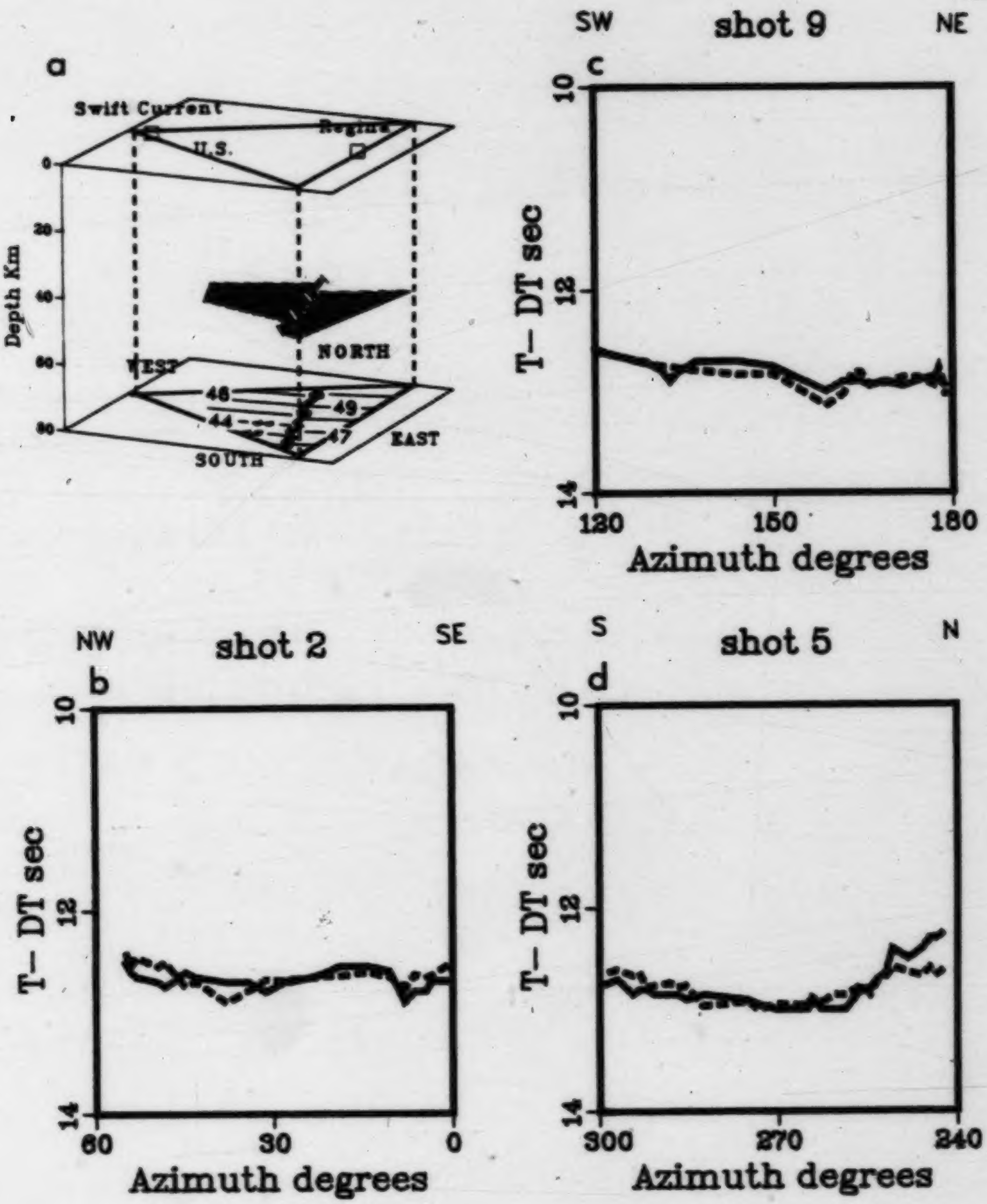

Figure 4.14 (a) The structure of the Moho (R3) using wide-angle reflections only. Travel-time curves for: (b) shot2; (c) shot9; and (d) shot5. The solid line is from the field observations. The dashed line is the final value from the least-squares iteration assuming only two faulted planes.

4.6 Determination of structure of the Moho

The main objective of this experiment is to attempt to delineate the structure of the Moho. The concentration of common rays intersecting at the centre as well as the adjacent areas provides seismic information to construct a three-dimensional structure of the Moho discontinuity. The first-break arrivals from the Moho are relatively clear. In most cases, the observed amplitudes are large enough to permit reasonably good estimates of the first-break energy. The discontinuities of travel-times are clearly visible on profiles B and C (Figure 4.8). Head wave arrivals from broadside data as well as a selected portion of inline data were picked from the original records. As before, the Moho discontinuity in this study area has been divided into three normally faulted planes.

The head waves (first-break arrivals) were first used in the damped least-squares inversion process. The initial model consisted of two upper sedimentary layers and two intermediate crustal interfaces as discussed previously in addition to the Moho discontinuity. The damped least-squares inversion procedure was used to determine the orientation, the depth, and velocity of the Moho discontinuity for the three faulted blocks.

Figure 4.15a shows the structure of the Moho obtained from the damped least-squares inversion of the refraction data. The contours (km) show the depths from the surface to the interfaces of the Moho discontinuity. Figure 4.15, b to

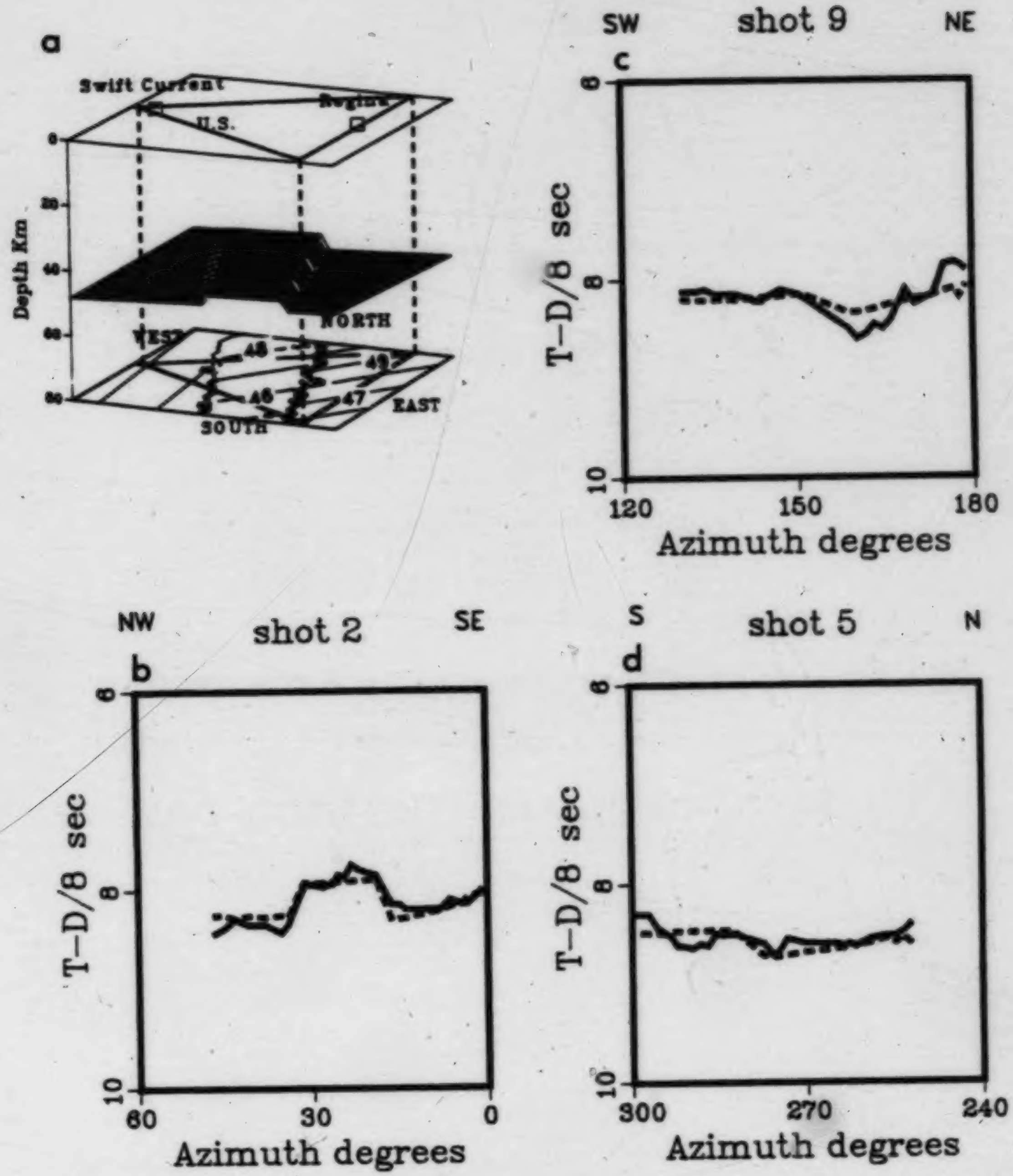

Figure 4.15 (a) The structure of the Moho from refraction data. Travel-time curves of the refracted Moho arrivals for: (b) shot2; (c) shot9; and (d) shot5. The solid line is from the field observations. The dashed line is the final value from the least-squares iteration assuming only three faulted planes.

d, shows the travel-time curves from each shot. In general, the computed travel-time curves match with the observations quite well. In four iterations, the standard error is 110 msec and it stays approximately the same up to the fifth iteration. As before, this implies that the damping factor stablizes the solution but it may not improve the residuals. This is usually the tradeoff between the resolution and stability. The wide-angle Moho reflection data may be included with the first-arrival head wave data. This opens the possibility of miscorrelation as it is performed as a second stage in the inversion procedure, because a clear and unique identification of wide-angle reflections is mostly doubtful, due to the geological complexity. Figure 4.16a shows the Moho structure from both reflection and refraction data. The contours (km) show the depths from the surface to the interfaces of the Moho discontinuity. This model is similar to Figure 4.15a. Figure 4.16, b to d, shows the travel-time curves from each shot. The computed reflection and critical refraction curves match quite well with the observations. The standard error after four iterations is 130 msec. On the whole, despite noisy data and uncertainty in picking arrival times, the damped least-squares inversion performs reasonably well and produces a stable solution. The locations of the reflection mid-points are shown in Figure 4.11 to indicate where the reflection data is controlling the structure. The velocities beneath the faulted blocks 1, 2, and 3 are 8.20, 8.28, and 8.31 km/s,

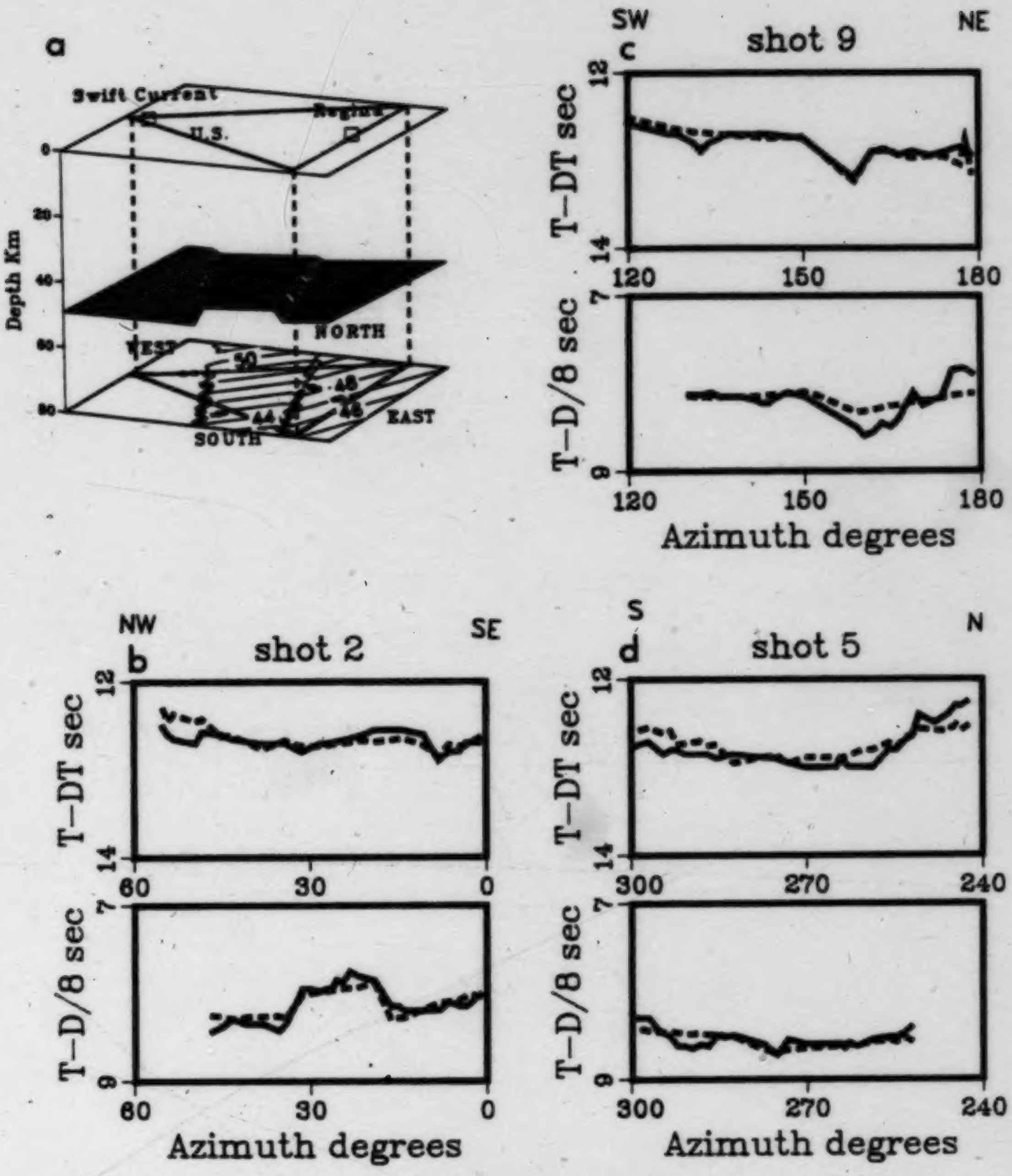

Figure 4.16 (a) The structure of the Moho from a combination of refraction and reflection data. Travel-time curves for refracted and reflected arrivals for: (b) shot2; (c) shot9; and (d) shot5. The solid line is from the field observations. The dotted line is for refracted arrivals after the fourth iteration. The crosses are the reflected arrivals after the fourth iteration.

respectively. In general, all three fault planes dip slightly to the north to northwest with dips of 0.25°, 1.6°, and 1.58° respectively.

The reliability of the damped least-squares solution can be measured by its resolution and covariance matrices. Aki and Richards (1980, p. 675-699) gave an informative description of the uniquess and reliability of the least-squares solution. The diagonal elements of the resolution matrix are useful measures of resolution. If the diagonal elements of the resolution matrix are unity, all model parameters are uniquely determined. Otherwise, the estimates of the model parameters are expressed as a weighted average of true values. Figure 4.17a is the resolution matrix for the Saskatchewan model from both head waves and wide-angle reflections. The peaks represent the magnitude of the diagonal elements. Most of the seismic observations are concentrated on the central block, and their associated parameters are well determined since the magnitude of the diagonal elements for the resolution are fairly close to 1. Plane 3 has a reasonable amount of seismic observations, and its solution is relatively stable. The estimates of resolution for a_3 and d_3 have values of 0.52 and 0.48. This implies that these two model parameters cannot be determined as accurately as the other two which are 0.88 and 0.95. Their estimates are the weighted average of the true values. Plane 1 has only a few partial rays passing under it, and its solution tends to be unstable. The a resolution matrix

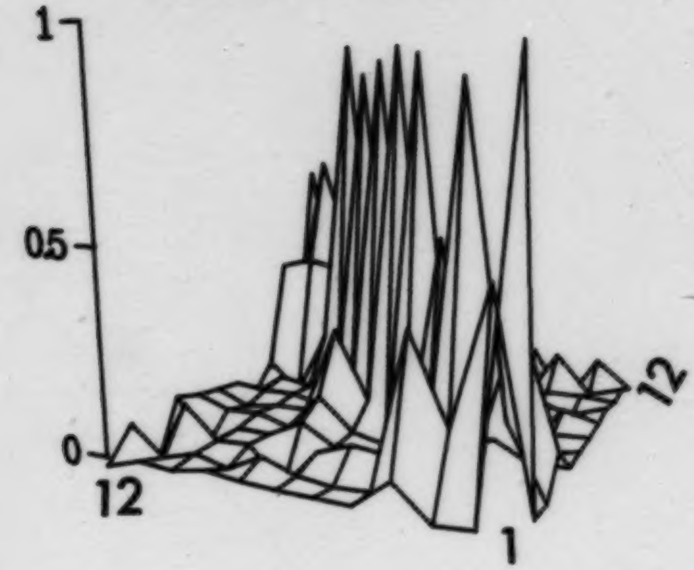

b covariance matrix

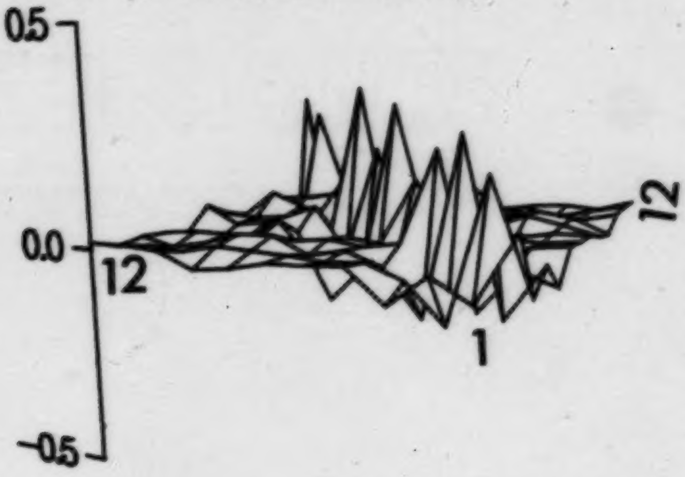

Figure 4.17 (a) The resolution matrix from Saskatchewan spatial seismic refraction data. (b) The corresponding covariance matrix. Both matrices have dimensions of 12*12. The order of the elements from 1 to 12 for the model parameters on blocks 1, 2, and 3 is a_1, b_1, d_1, V_1, a_2, b_2, d_2, V_2, a_3, b_3, d_3, and V_3.

model parameters, corresponding to the depth and velocity for plane 3, fluctuate significantly with each iteration. Because of this instability, the ridge regression tends to produce a relatively large common damping factor to stablilize the solutions for all three planes. This decreases the resolution and variances of the solution. This is also reflected in the covariance matrix (Figure 4.17b)

In summary, the variance of the solutions are relatively small, the maximum being only 0.33, and we concluded that the computed model was fairly reliable. Because of the sparse data bank and the uncertainties in the upper structure, we have opted to accept this model as an approximation to the real structure.

4.7 Discussion of the results

The three-dimensional crustal structure obtained by the damped least-squares inversion generally agrees with the crustal model from the inline refraction model (Macrides, 1983). Since we have only a small set of wide-angle reflection data for determining the structure of the crust, the crustal interfaces in Figures 4.12a and 4.13a are considered to form a tentative model. The depths to the middle crust and to the low velocity zone show a slight discrepancy between this study and the inline refraction interpretation (Macrides, 1983). The discrepancy is possibly due to a relatively high interval velocity of the reflection branch R1 obtained by the damped least-squares inversion in this study. The average interval velocity on both plane 2 and 3 is about 6.65 km/s. This relatively high interval velocity causes the interface to be placed at a greater depth. On the whole, despite the nature of the refraction data and different interpretation techniques between the two studies, the crustal structure obtained by this study shows a similar structure as the inline crustal model (Macrides, 1983).

The orientation, and depth of the Moho can be expected to be variable from one location to another. The Moho discontinuity (Figure 4.16a) has depths ranging from 43 km to a maximum of 49 km in this study area. By comparing the Moho depths from the inline refraction model, the Moho depths in this study are generally consistent with the inline interpretation, despite the nature of the refraction data and different modelling techniques used between the two studies. However, the Moho depth at the north end of profile A shows a significant difference. The depth obtained by Macrides (1983) was 37 km as compared with the depth between 47 to 48 km in this study. This discrepancy is possibly due to the poor signal-to-noise ratio of the head waves obtained from the inline profile A. Hajnal et al. (1984) analysed another refraction profile just east of profile A by synthetic modellings. He concluded that the Moho depth was between 45 to 46 km (Figure 3.8). This confirms that the minimum depth of the Moho at the north end of profile A is likely over 45 km as opposing to 37 km obtained by Macrides

(1983).

Furthermore, the horst type structure of the Moho discontinuity correlates with the geological and geophysical features underlying this portion of central North America. The study area is an area with many prominent features showing significant activity from the earliest Archaen to the present time. During the Phanerozoic Era the Williston Basin evolved as one of the largest circular basins on any continent with a deposition of nearly 5 km of sediments. It is bisected by a north-south zone of small earthquakes (Figure 4.10) which are coincident with the fault between blocks 2 and 3 in Figures 4.15 and 4.16. Many of the features on gravity and aeromagnetic maps can be traced from outcrops in northern Saskatchewan or in Wyoming so it is possible to extrapolate the Precambrain terrain to this area. The fault between blocks 2 and 3 lies along the extension of the boundary between the La Ronge-Lynn Lake greenstone belt of Proterozoic age and the Reindeer-South Indian Belt of highly metamorphosed gneisses and migmatites. It also marks the North American Central plains electrical conductivity zone (Camfield and Gough, 1977). The fault, between blocks 1 and 2, may mark the northern edge of the Wyoming Archaen Crator (Green et al., 1984) or the eastern limit of the Southern Alberta Rift (Kanasewich et al., 1969).

4.8 Conclusions

The method of spatial seismic refraction recording has been shown to be very promising in yielding three-dimensional structure. This has been demonstrated by a sub-optimal field experiment over the Williston Basin in Saskatchewan. The discontinuities of travel-time data correlate quite well to the major boundaries of gravity and aeromagnetic anomalies which in turn identify the possible fault locations.

The derived crustal structure for the study area reveals significant crustal faulting as well as the existence of a low velocity zone. The upthrown block of the fault is located at the central plane. Faulting in the upper mantle may be related to the faults in the crust. The Moho discontinuity was found to consist of three faulted planes. The Pn velocities beneath the three faulted planes suggest that the upper mantle density varies as a result of different lithological blocks of the Moho discontinuity.

The above results have illustrated the usefulness of this new spatial seismic refraction recording as well as the tomographic method to determine a complex crustal structure. The algorithm is fast and efficient in terms of iterations in producing a stable and plausible model in both test data and real field observations.

5. 3-D IMAGING OF VANCOUVER ISLAND REFLECTION DATA

5.1 Introduction

The aim of this chapter is to demonstrate a seismic tomographic technique for obtaining simultaneously compressional velocities and three-dimensional structure from elastic waves reflected at angles of incidence below the critical one. The medium consists of piecewise, homogeneous, and arbitrary three-dimensionally curved interfaces of different elastic properties. The interface is defined by a polynomial surface. The seismic waves are assumed to be transmitted through or reflected by curved interfaces in which the ray paths satisfy Snell's law. The ray tracing for each source-receiver pair is determined by solving a system of non-linear equations and may be used as a stand-alone tool for forward modelling. This method of three-dimensional tracing is fast, accurate and efficient in computing a large group of seismic rays including converted phases and multiples. A damped least-squares inversion scheme is formulated to construct interval velocities and a three-dimensional structure of the reflector by minimizing the difference between the observations and computed travel times. This inversion algorithm can handle both nonzero offset and/or zero offset travel-time observations.

5.2 Synthetic model

The synthetic model in this study will be constructed from piecewise polynomial surfaces of arbitrary shape. Since the medium between each successive pair of interfaces is assumed to be homogeneous, isotropic and perfectly elastic, any ray connecting two points within a layer is a straight line (Figure 5.1). The L interfaces bounding each layer are defined by polynomial surfaces of the form

$$z_i = d_i + f_i(x,y), \qquad i = 1, 2, \ldots L.$$

where d_i is the distance of the normal to the origin, and $f_i(x,y)$ is a function of x and y.

To demonstrate how the method works in practice, we have included one synthetic model example. For a given geologic model, we generated the theoretical arrival times by three-dimensional seismic ray tracing and then applied these data to the inversion procedure. Our technique has involved solving the model parameters associated with a polynomial interface and interval velocity between two interfaces by minimizing the difference between the observations and computed travel times. The computed model can be compared to the original and furthermore the performance of the method can be evaluated by introducing known random noise to the observations.

For the purpose of this study, only reflected P waves are considered; the converted phases and multiples can be

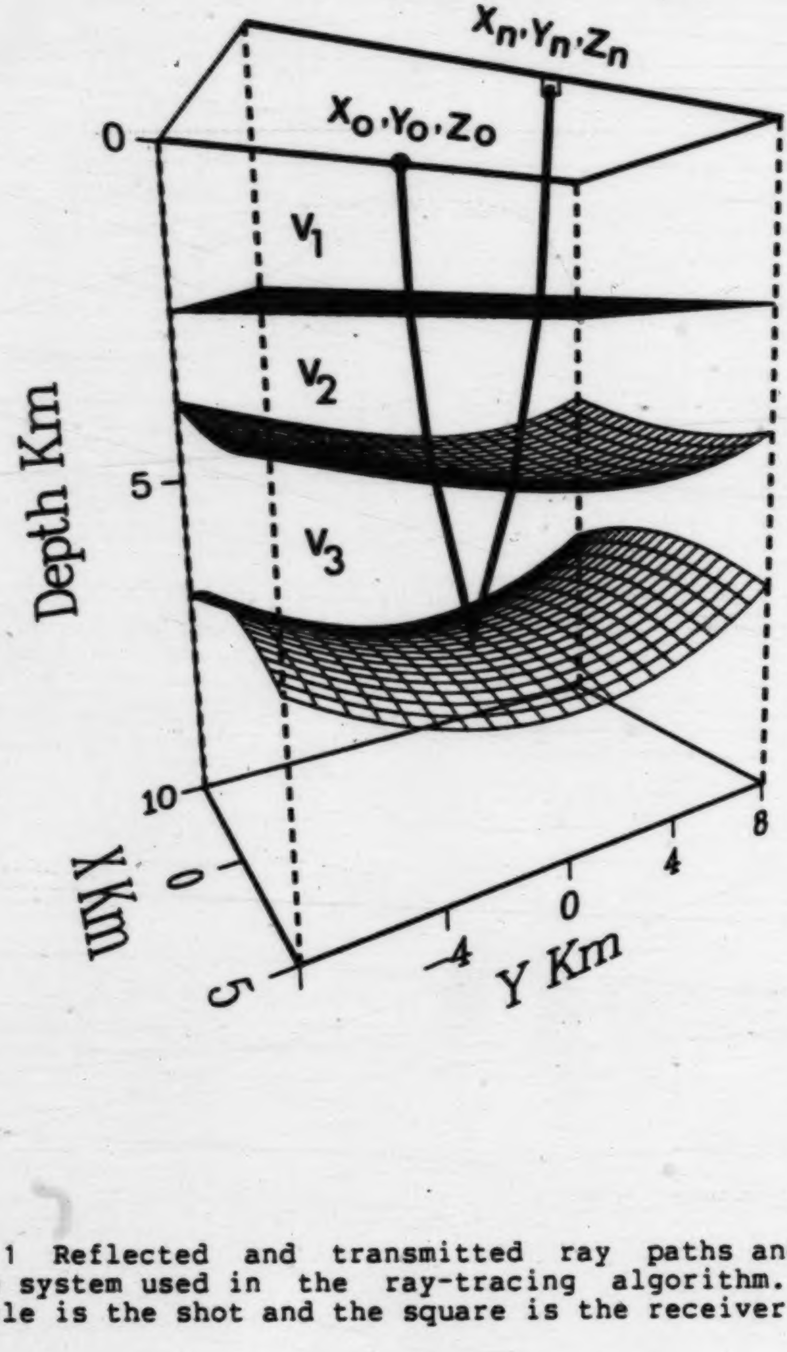

Figure 5.1 Reflected and transmitted ray paths and the coordinate system used in the ray-tracing algorithm. The solid circle is the shot and the square is the receiver.

included with a slight modification of the algorithm. The three-dimensional synthetic model and ray paths from shots to receivers are shown in Figure 5.2. The model consists of three reflectors: (1) a dipping plane, (2) a cubic-order polynomial surface, and (3) a second-order polynomial surface, and also the medium is assumed to be homogeneous and isotropic. The interval velocities between interfaces are 2.0, 3.5 and 4.5 km/s, respectively. Figures 5.3a and 5.3b are the expanded maps showing the shot and receiver configurations in this synthetic model for shots locate at y and x direction respectively. Figure 5.3a shows that the shots locate at the centre of the profiles and each shot generates five observations in the x direction, including observations of zero offset and nonzero offset reflection data. Similarly, each shot generates only seven observations in the y direction (Figure 5.3b). As an example of the efficiency of the ray tracing algorithm it takes 6.2 seconds (CPU time on the Amdahl 470/v6) to trace 70 source and receiver pairs in this synthetic model.

The inversion procedure first solves for the upper layers and then freezes the model parameters of the upper layers in order to solve for the lower layers. For example, in the test model the target horizon is the third interface. Thus the upper two reflectors are assumed to have been determined, and the coefficients of the upper two interfaces remain constant in the inversion procedure. The travel-time data reflected from the third interface are generated by

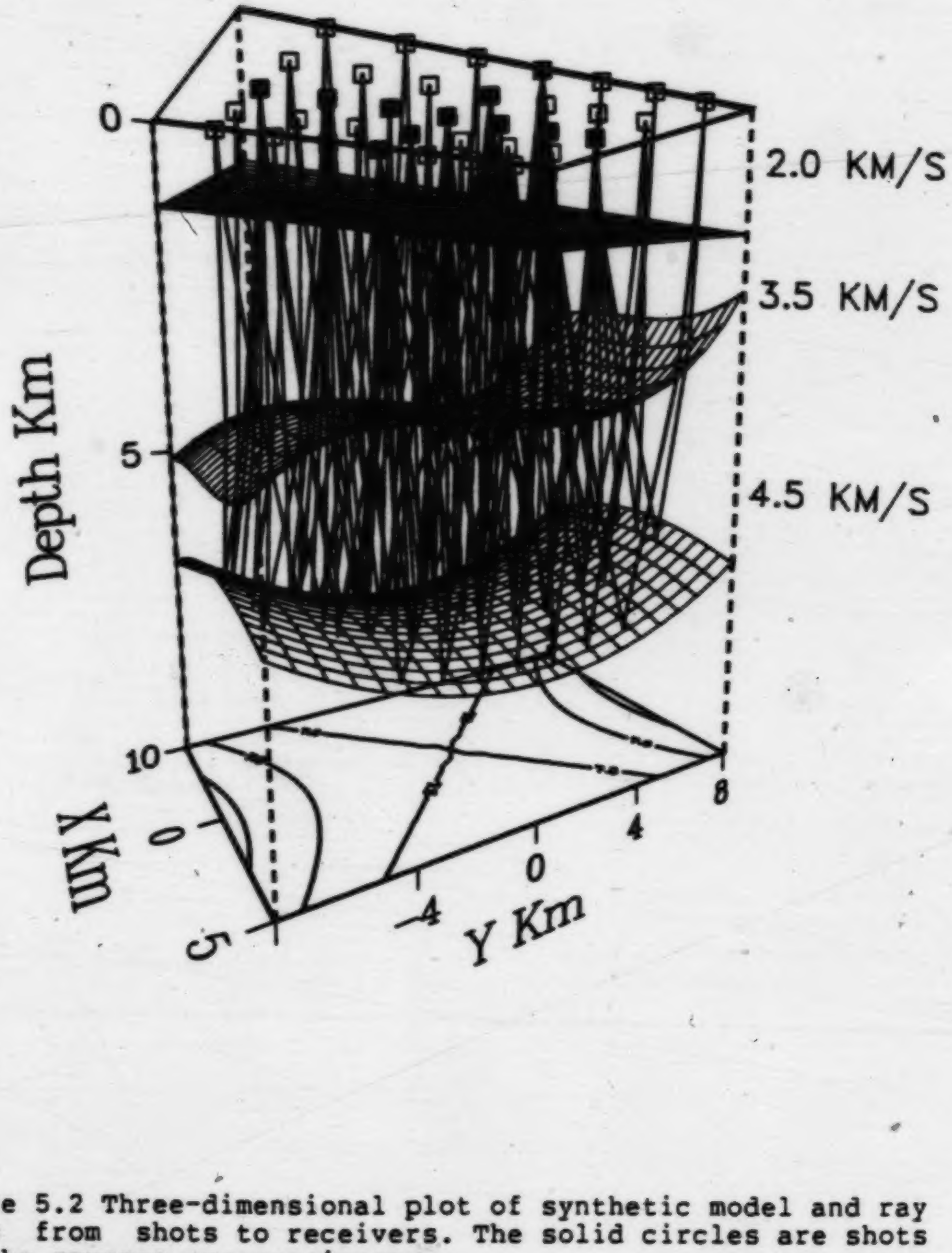
0
5
10
Depth Km
2.0 KM/S
3.5 KM/S
4.5 KM/S
X Km
0
5
-4
0
4
8
Y Km

Figure 5.2 Three-dimensional plot of synthetic model and ray paths from shots to receivers. The solid circles are shots and the squares are receivers.

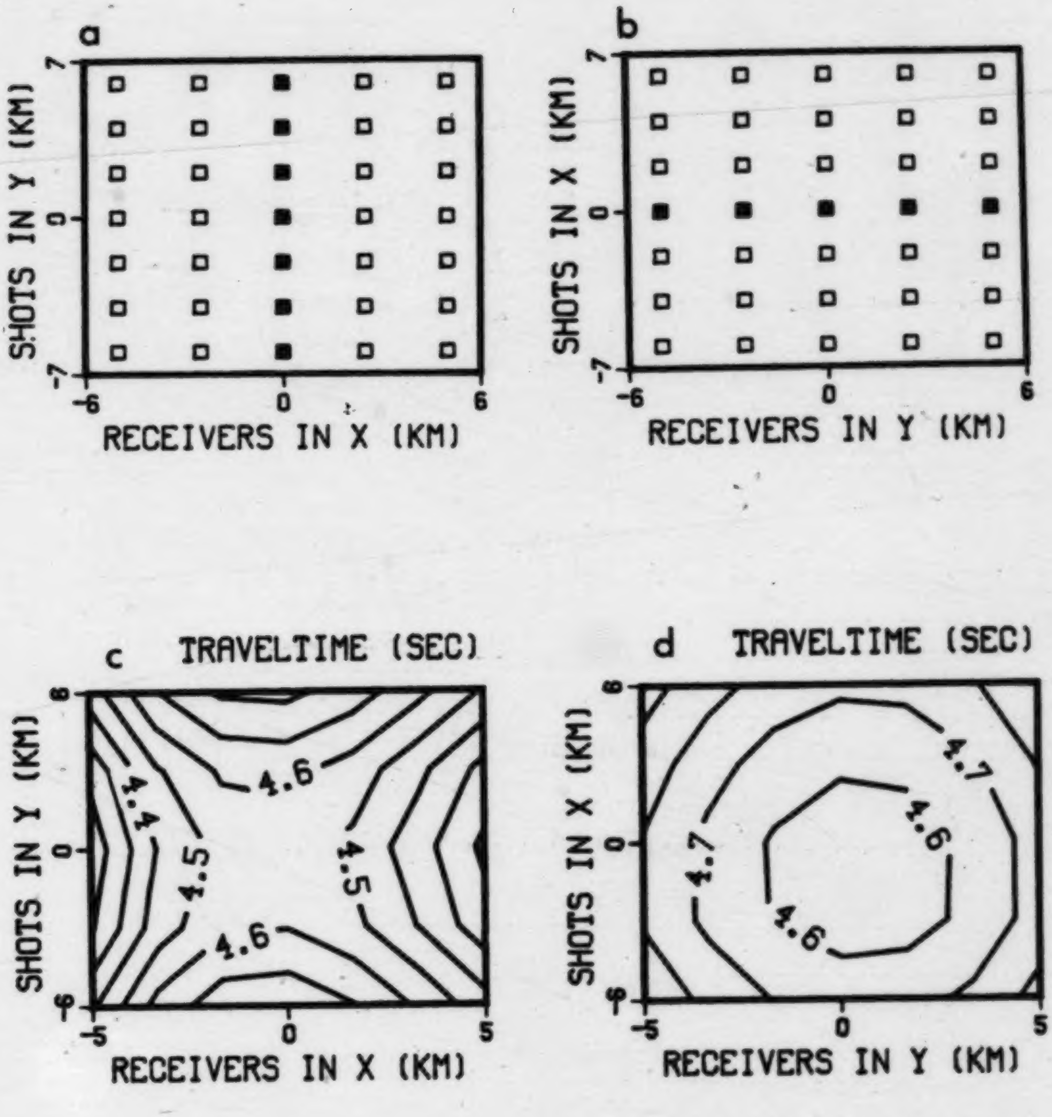

Figure 5.3 (a) and (b). Shot and receiver configuration used in the synthetic data. The solid circles are shots and the squares are receivers. (c) and (d) are the corresponding isochron maps.

tracing the rays from shots to receivers through the known model. Figures 5.3c and 5.3d display the isochron maps corresponding to shot and receiver configuration for shots in y and x direction respectively. The travel-time data are then applied to the inversion algorithm. We first assume the initial model of the third interface to be a third-order polynomial surface. The objective is to reconstruct the interval velocity and second-order polynomial surface of the third interface starting from an initial third-order polynomial surface. In other words, we try to invert the travel-time data by the damped least-squares formulation to reconstruct the interval velocity and structure of the third interface starting from an initial guess. The computed model should approach the theoretical model as the number of iterations increases. Figures 5.4a to 5.4f show how the residual times between the computed and known model change after each iteration. The residual times decrease rapidly in the first three iterations, and gradually reduces approximately to zero at the sixth iteration. The resulting model converges exactly to the known model. It requires 13.5 seconds (CPU time on the Amdahl 470/v6) to perform six iterations in this synthetic model.

Furthermore, we tested the effect of random noise on the damped least-squares inversion. Random numbers having a standard deviation of 20 msec were added to the data generated from the known model. In four iterations, the standard error of the data was 19 msec, and it remained

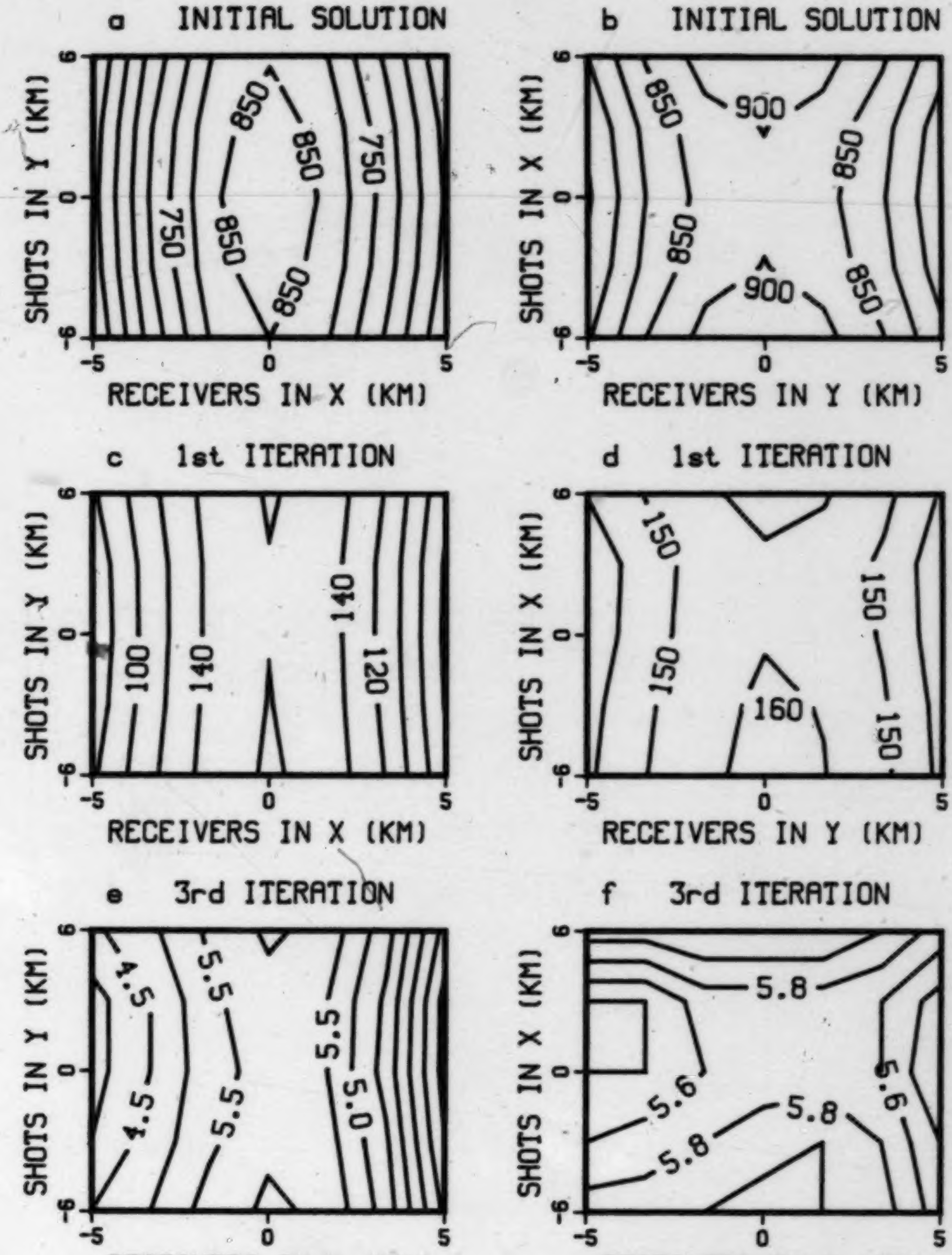

Figure 5.4 (a) to (f). Residual times between the computed and known model at each iteration step. Times are in milliseconds.

approximately the same for fifth iteration. Figure 5.5, a to f displays the decrease in residual times between the computed and the known model for the first three iterations. The residual times decrease rapidly even in the case of the addition of random noise. The resulting model (Figure 5.6), with the addition of 20 msec noise to the observations, converges closely to the known model (Figure 5.2). In general, the performance of this damped least-squares inversion is stable and reliable in producing a robust estimate of the model in the case of data with and without noise.

5.3 Application to Vancouver Island reflection data

The tomographic method is now applied to the travel-time data from one of a set of four Vibroseis [1] lines obtained in 1984 on Vancouver Island as a part of PROJECT LITHOPROBE. PROJECT LITHOPROBE is a Canadian collaborative geoscientific project involving a coordinated program of geophysical, geological and geochemical techniques to obtain the three-dimensional properties of the lithosphere. The seismic instrumentation consisted of a 120 channel DFS-5 digital recording system employing four synchronized vibrator sources along a geophone layout with a 90 m group spacing. The selected vibroseis sections used in this study were along a very crooked road. Figures 5.7 is an expanded map showing the shot and receiver locations. Although it is

---

[1] Registered trademark of Continental Oil Company.

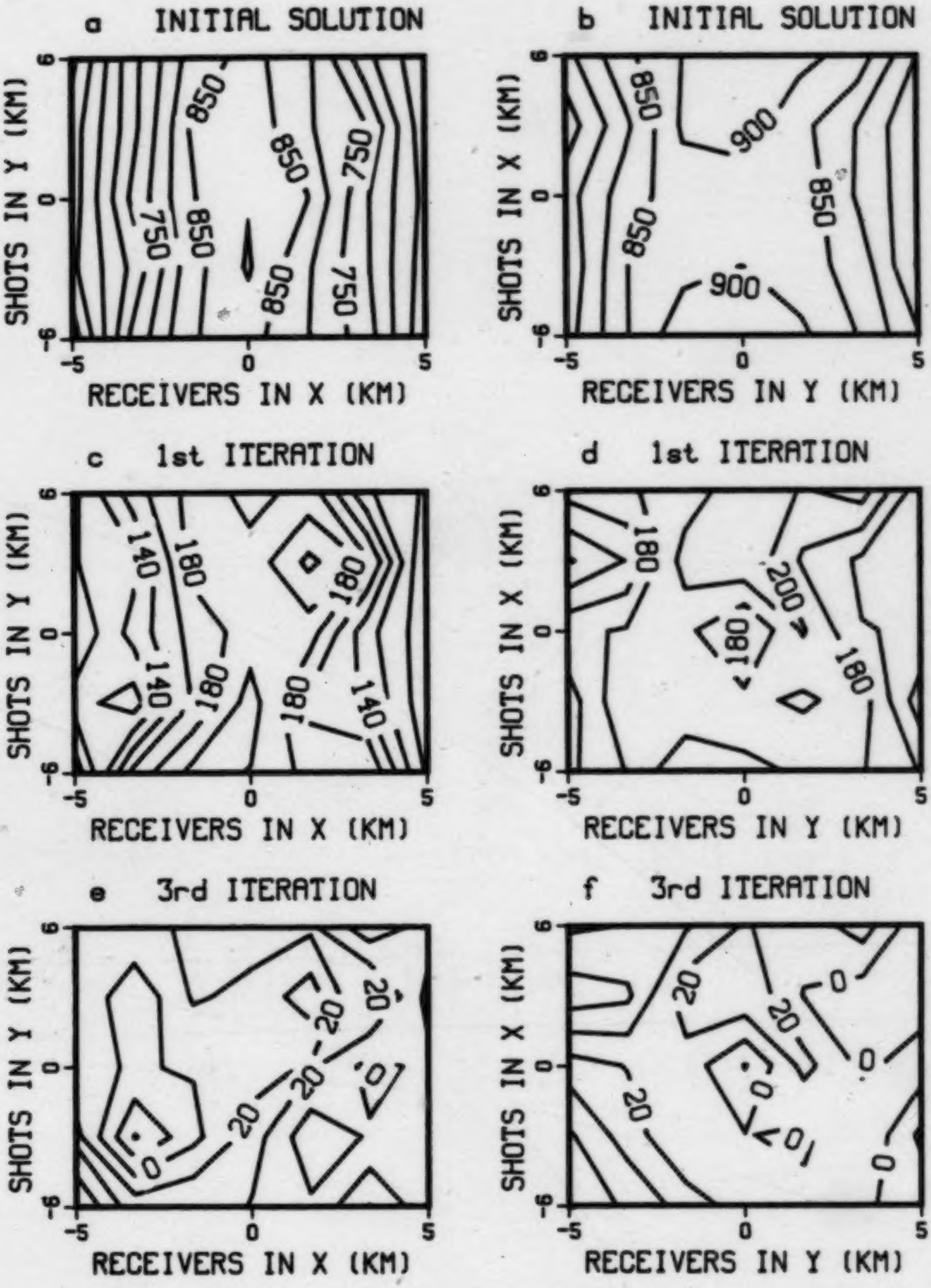

Figure 5.5 (a) to (f). Residual times between the computed and known model at each iteration step, with the introduction of random noise into the theoretical travel times. The standard deviation of the noise is 20 msec. Times are in milliseconds.

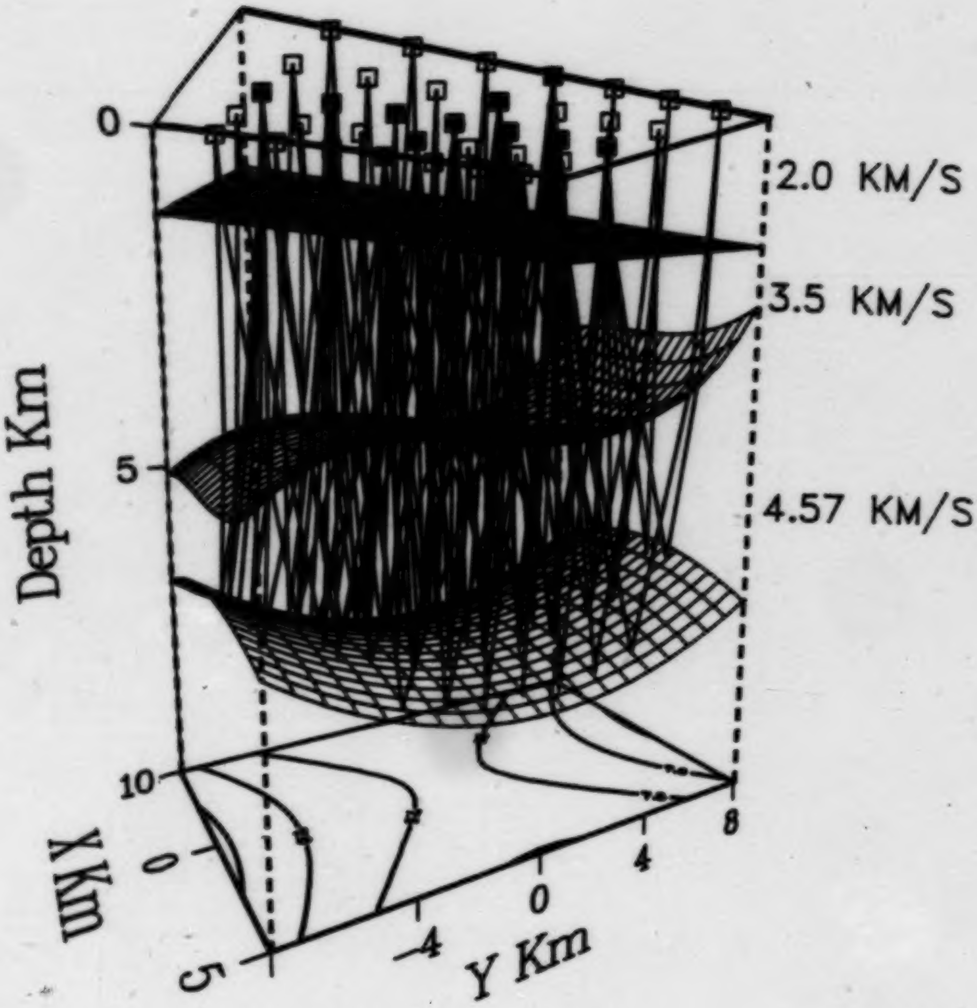

Figure 5.6 Three-dimensional plot of ray paths and the model obtained from the inversion procedure with the random noise added to the observations.

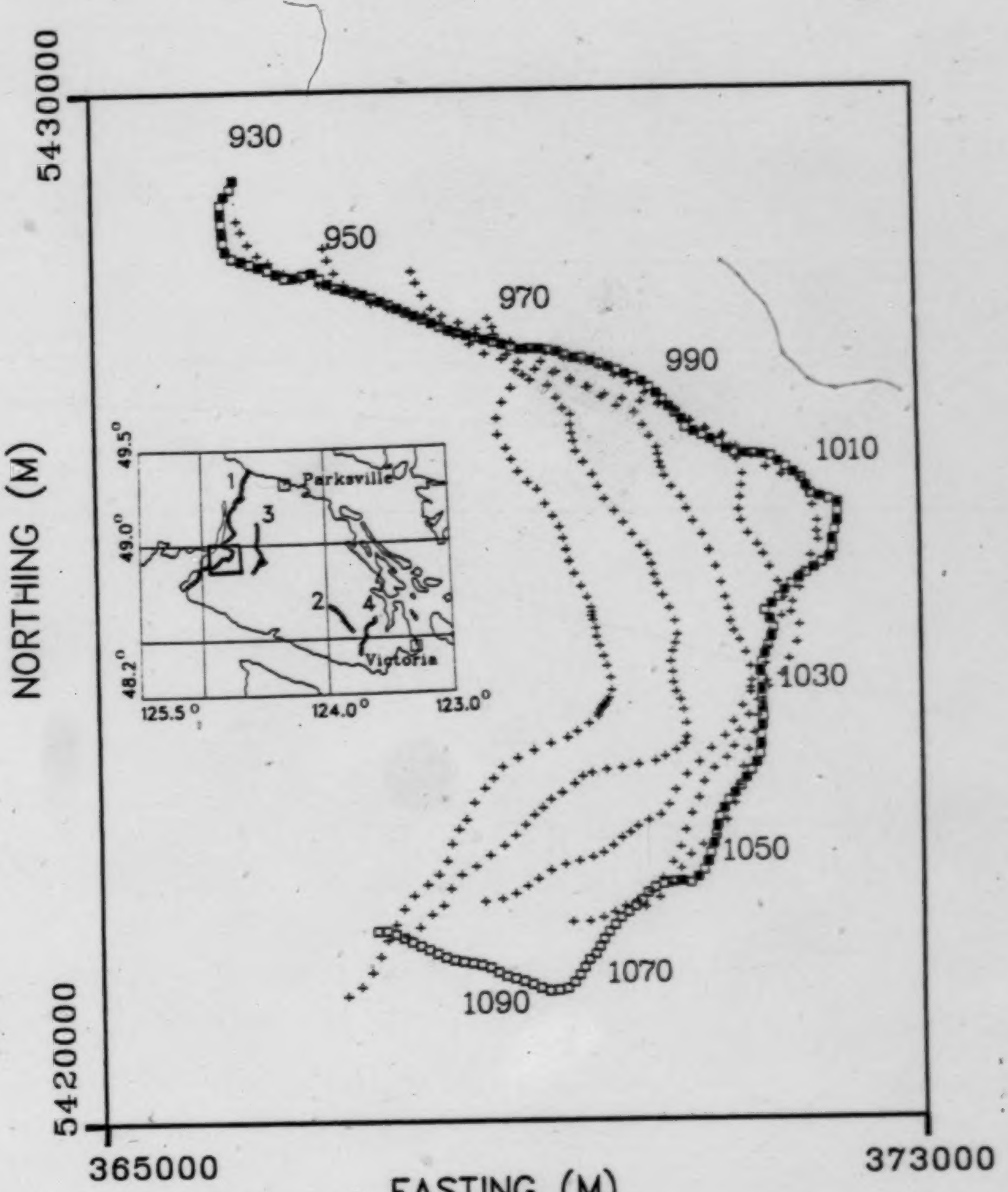
5430000
5420000
NORTHING (M)
365000
373000
EASTING (M)
930
950
970
990
1010
1030
1050
1070
1090
49.5°
49.0°
48.2°
125.5°
124.0°
123.0°
Parksville
Victoria
1
2
3
4

Figure 5.7 The expanded map of southern Vancouver Island shows the shot and receiver locations used in this study. Solid squares are sources; squares are receivers; crosses indicate an approximate surface projection of sub-surface reflecting points.

a two-dimensional reflection survey, it is possible to obtain a three-dimensional structure, because the sources and receivers are on a crooked line. The reflection mid-points, indicated by +'s in Figure 5.7 cover a three-dimensional subsurface.

Figures 5.8 and 5.9 show two selected records of the excellent original field data. There are two prominent bands of reflectors located approximately at 5 and 8 seconds. These two major reflectors are quite uniform and consistent throughout all the sections. The first reflector, (C), around 5 seconds has been called decollement zone. It has been interpreted as a detached plate of oceanic crust that was emplaced in the Miocene, about 18 m.y. ago. The second reflector, (E), is the top of the underthrusting oceanic crust which is currently subducting under the west coast (Yorath et al., 1985). Both records clearly indicate that the subduction zone dips towards the northeast of the reflection profile. Figure 5.10 displays the frequency-domain migrated section in this region. Both the decollement and the subduction zones indicate dipping to the northeast of the reflection profile.

The analyses of first-break arrivals and previous seismic refraction studies (McMechan and Spence, 1983, Spence, 1984, and others) indicate that the sedimentary layer in this region is nearly horizontal and its velocity and thickness are 6 km/s and 1.5 km respectively. Therefore, the sedimentary layer is assumed to be horizontal, and its

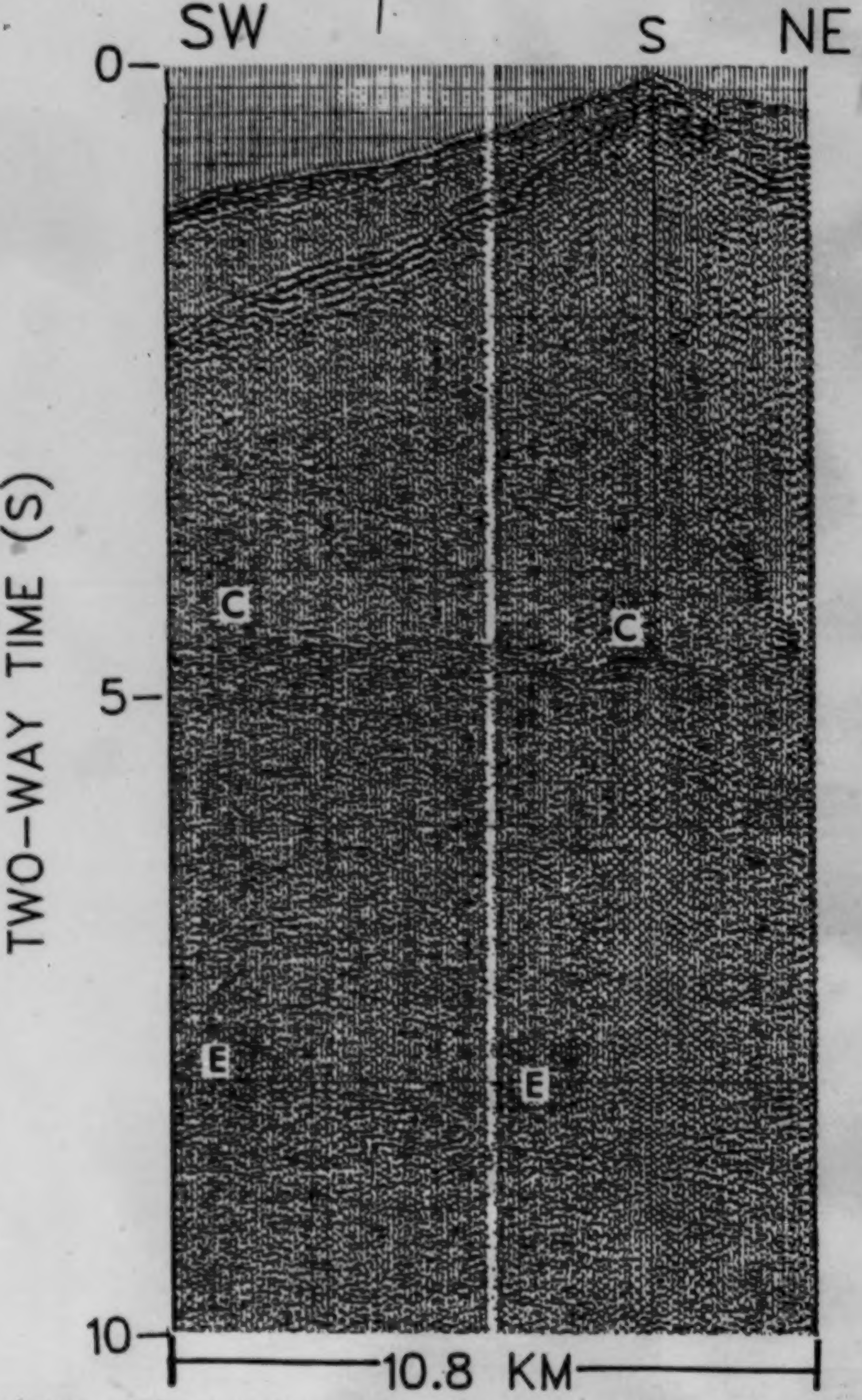

Figure 5.8 Example of a selected record. Ground length is approximately 10.8 km. Reflecting horizons C and E were used in this study.

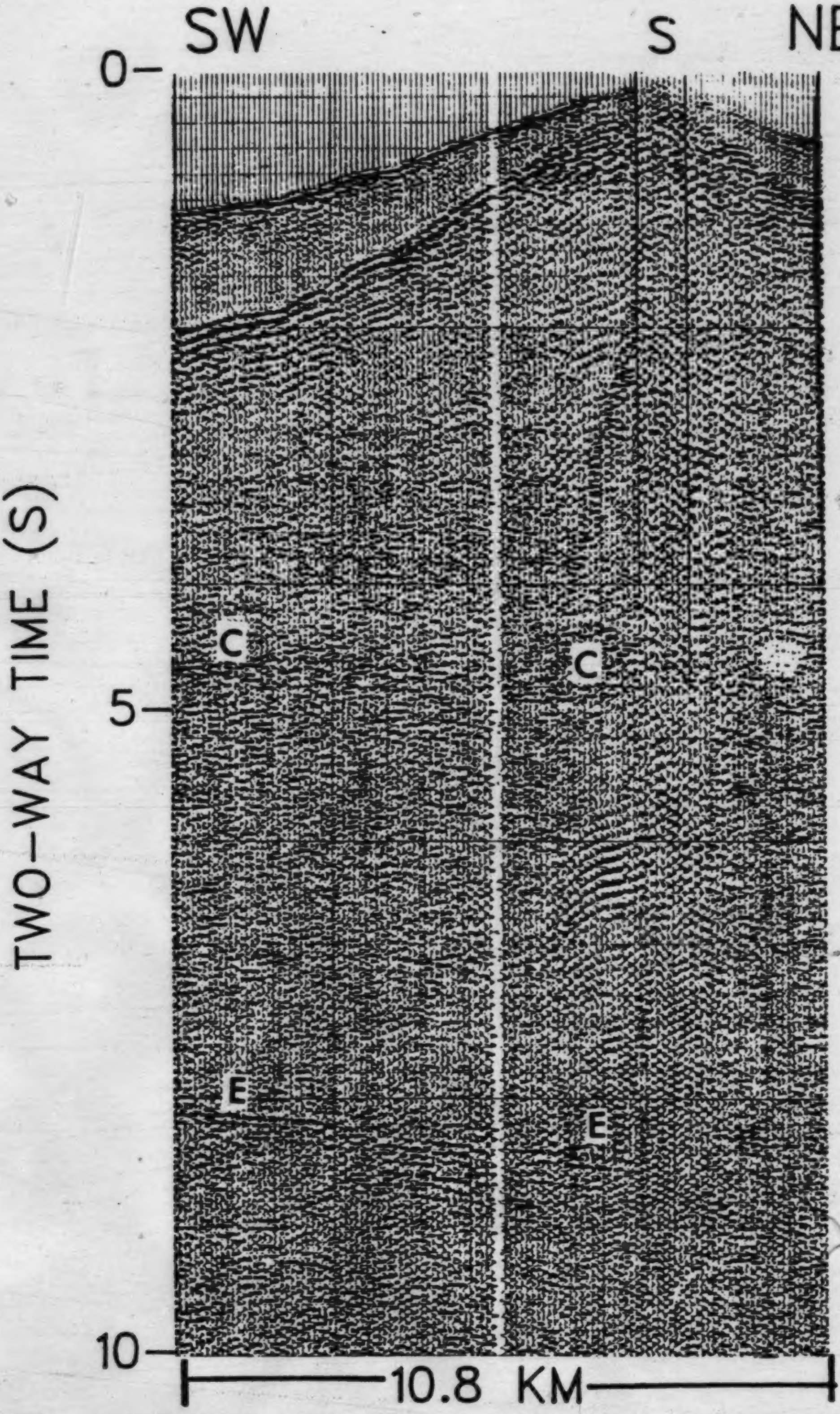

Figure 5.9 Another example of a selected record. Ground length is approximately 10.8 km. Reflecting horizons C and E were used in this study.

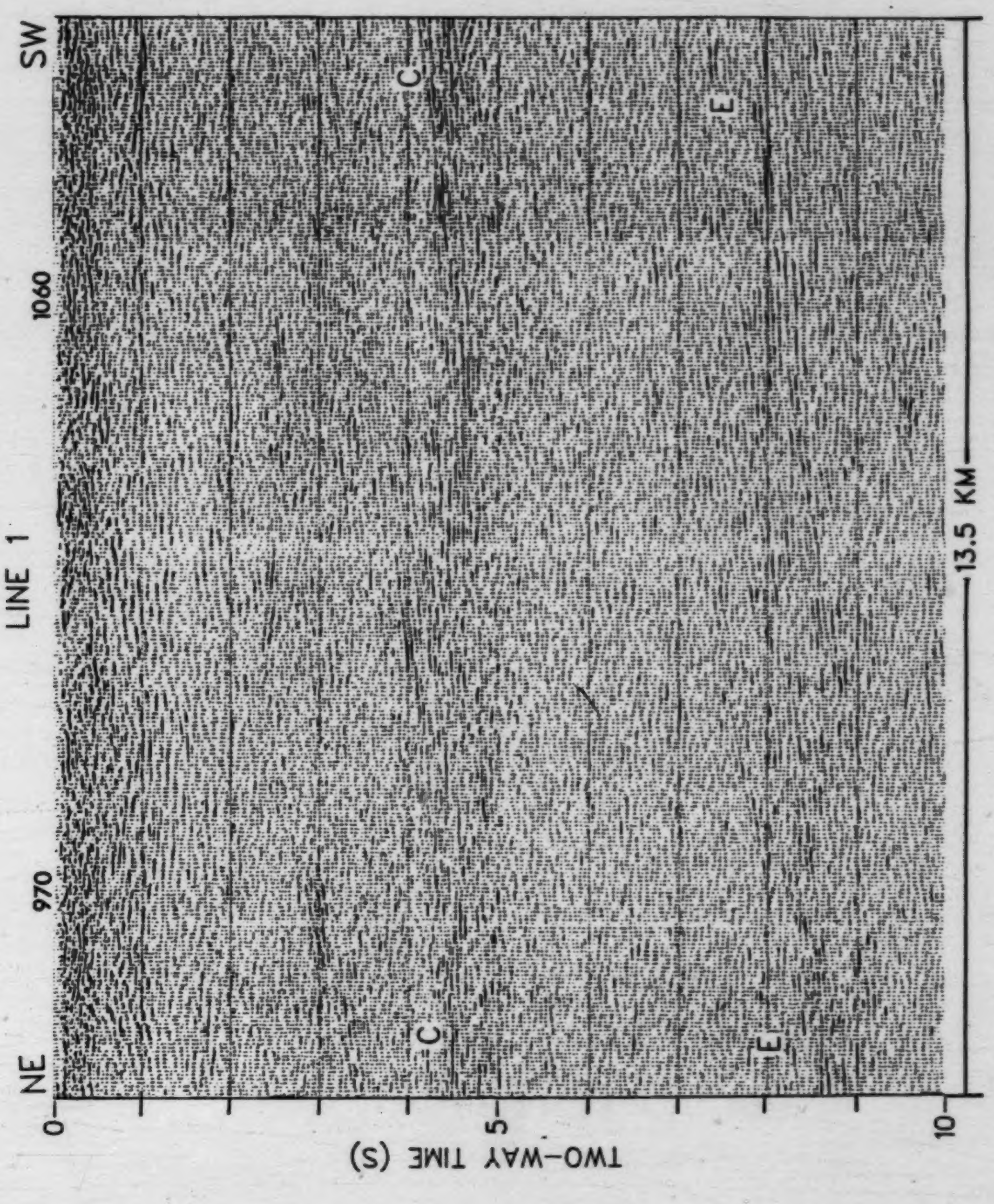

Figure 5.10 The corresponding frequency-domain migrated section in this region. C is the decollement zone and E, the subduction zone.

parameters remain constant in solving for lower layers.

The objective is to determine the interval velocity as well as the structure of both the decollement zone and subduction zone by inverting the travel-time data. Travel times were picked for both reflectors from original recordings. The accuracy of picking the arrivals is about 10 msec. To invert the second reflector, we first assumed the initial model to be a cubic polynomial surface. However, we found that several eigenvalues were zero during the inversion process. Since we used a small set of data, we expected that the observations might not be adequate to determine the model parameters of a cubic polynomial surface. By eliminating all zero eigenvalues, we found that a plane interface was adequate to model this small set of data. During the inversion process the eigenvalue corresponding to the velocity parameter was quite small, therefore, two approaches were used to determine the model parameters of the plane layer: (1) excluding the velocity parameter in the inversion procedure, (2) including velocity parameter in the inversion procedure. Both approaches yielded very similar results. I will display only the result from the second approach, and also I show an example later how the damping factor affected the resolution matrix in these two cases. Figure 5.11 shows the structure of the decollement zone obtained from the damped least-squares inversion. In four iterations the standard error is 14 msec and this accuracy is excellent in crustal seismology. The

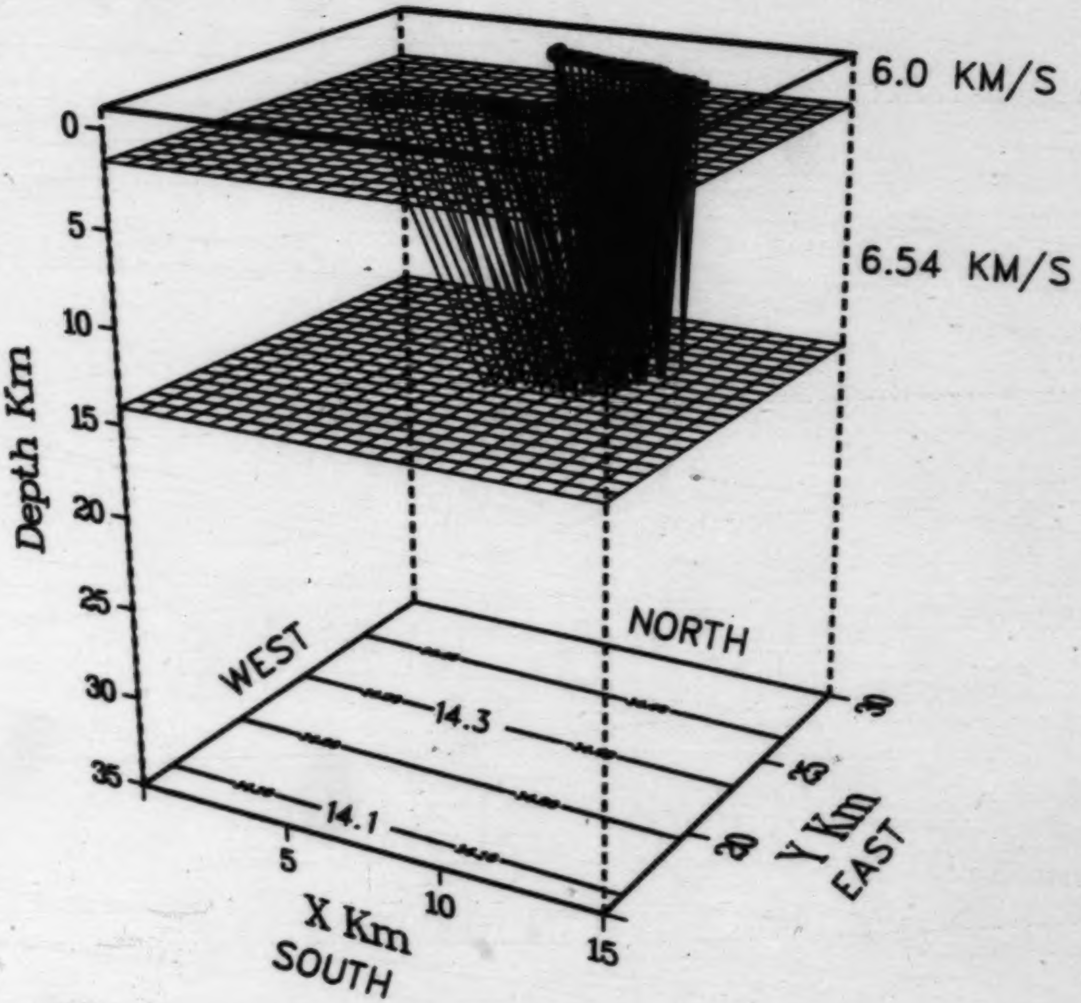
6.0 KM/S
6.54 KM/S
0
5
10
15
20
25
30
35
Depth Km
WEST
NORTH
14.3
14.1
5
10
15
X Km
SOUTH
30
25
20
Y Km
EAST

Figure 5.11 The structure of the decollement zone obtained from the inversion procedure.

decollement zone dips approximately 1.6° to the northeast, with a minimum depth of about 14 km.

The inversion of the subduction zone is achieved by freezing the model paramters of the first two layers. As before, a plane interface is adequate to fit the observations and also the eigenvalue corresponding to the velocity parameter is small. Figure 5.12 displays the structure of the subduction zone obtained from the inversion procedure. In five iterations the standard error is 24 msec and this accuracy is acceptable because of the difficulty and uncertainty in picking the travel times. The subduction zone dips approximately 8.4° to the northeast and has a minimum depth of about 25 km.

The reliability of the damped least-squares solution can be measured by its resolution and covariance matrices. The diagonal elements of the resolution matrix are a useful measure of resolution. As before, if the diagonal elements of the resolution matrix are unity, all model parameters are uniquely determined. Otherwise, the estimates of the model parameters are expressed as a weighted average of the true values. Figures 5.13a and 5.13b are the resolution matrices for the subduction zone in two cases: (1) excluding the velocity parameter in the inversion procedure, and (2) including the velocity parameter. The peaks represent the magnitude of the diagonal elements. If the velocity parameter is not included in the inversion procedure, the fluctuation of the solution due to the small eigenvalue is

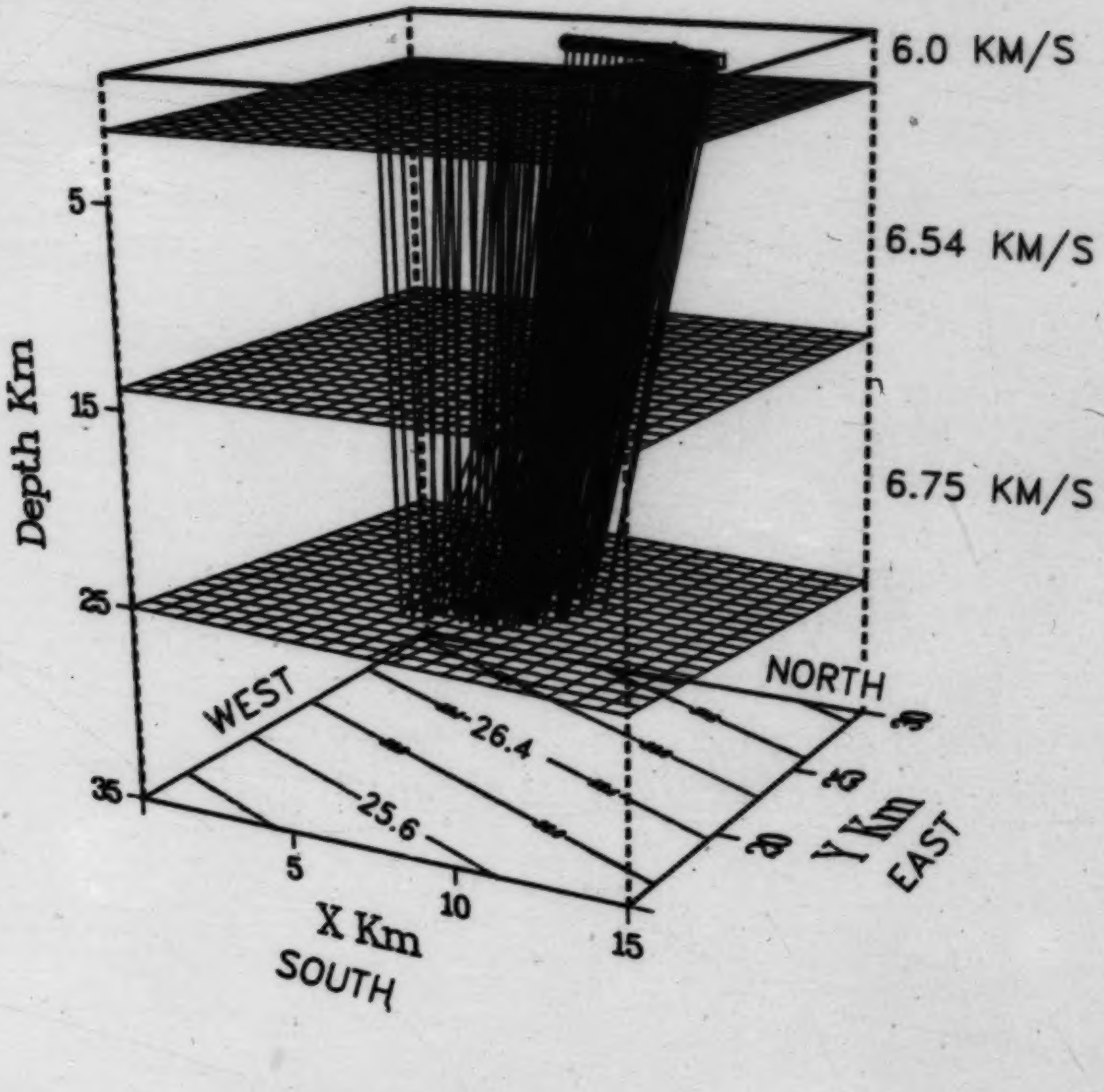
6.0 KM/S
6.54 KM/S
6.75 KM/S
Depth Km
5
15
25
35
WEST
NORTH
26.4
25.6
5
10
15
X Km
SOUTH
20
25
30
Y Km
EAST

Figure 5.12 The structure of the subduction zone obtained from the inversion procedure.

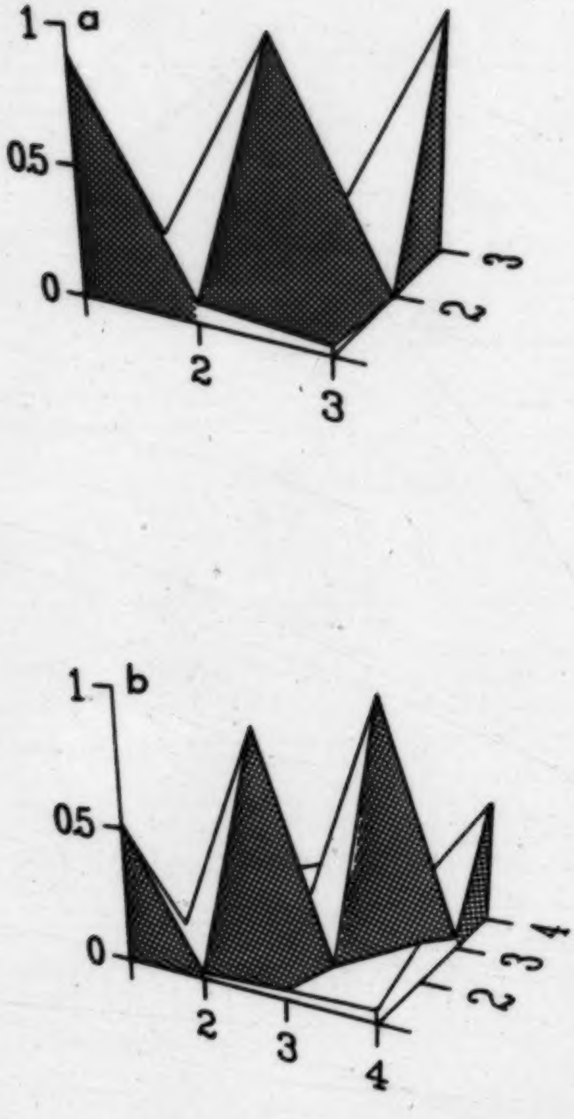

Figure 5.13 The resolution matrices for the subduction zone. The order of model parameters from 1 to 4 is d, b, a, and V. (a) velocity parameter is not included; (b) velocity parameter is included.

eliminated. Therefore, all the parameters of the plane should be well determined. This reflects in the resolution matrix, for the magnitude of the diagonal elements for the resolution matrix are fairly close to 1 (Figure 5.13a). However, the model parameters are not uniquely determined for the addition of the velocity parameter in the inversion process. The estimates of the resolution for the parameters a and b are 0.84 and 0.93 respectively, but the estimates for the parameters d and V have the values 0.52 and 0.48 respectively (Figure 5.13b). This implies that their estimates are a weighted average of the true solution and also the parameters d and V are correlated to each other. The corresponding covariance matrices in these two cases are shown in Figures 5.14a and 5.14b. The magnitude of the diagonal elements for the covariance matrices are relatively small, we concluded that the computed model was fairly reliable.

Seismic data are often displayed in a form such that the reflection "events" appear to be directly below the receiver stations as if the elastic waves have travelled vertically down and back to the surface. This will represent the true subsurface position only if the reflecting zones are horizontal. Where there is dip the true reflecting postion may be found by "migrating" the dipping segments to such a position that the ray paths are normal to the reflecting surface. The change in reflection time between adjacent traces (apparent dip) can be used to determine the

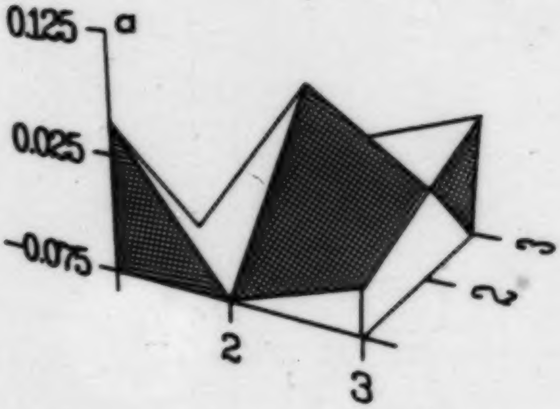

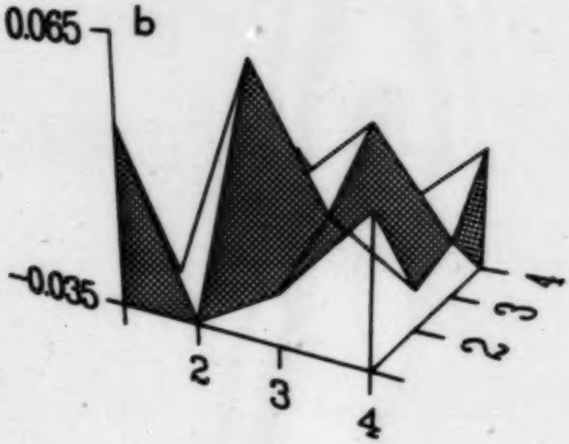

Figure 5.14 The covariance matrices for the subducted plate. The order of model parameters from 1 to 4 is d, b, a, and V. (a) velocity parameter is not included; (b) velocity parameter is included.

actual position along the profile of the reflecting surface. The true reflecting points are displaced both laterally and vertically from their recorded positions. Transformation of apparent reflecting positions to true positions is referred as migration. Because of the crooked lines, each source-receiver pair had to be considered individually in the migration process. An algorithm that had as its input the northing, easting of each source and receiver, the travel time and the stepout time(i.e. the first derivative with respect to horizontal distance) was written.

Structural maps of both the decollement and subduction zones are generated by simple ray migration. The dipping segments of reflection 'events' are migrated back to a position that the ray paths are normal to the reflecting surface. The migrated positions of depths are displayed on Figure 5.15 and 5.16. The structural maps of the top of the decollement and subduction zones (Figures 5.15 and 5.16) may be more complicated because of the existence of faults. In general, both horizons dip to the northeast. The contours of both structural maps are generated by linear extrapolation among the depths obtained by the simple migration of four reflection profiles. Because of the sparse data in this region, the maps only indicate the approximate structure of both zones. To confirm the usefulness of the inversion procedure, we found that the computed model obtained from the inversion procedure was consistent with the interpretation from the structural maps.

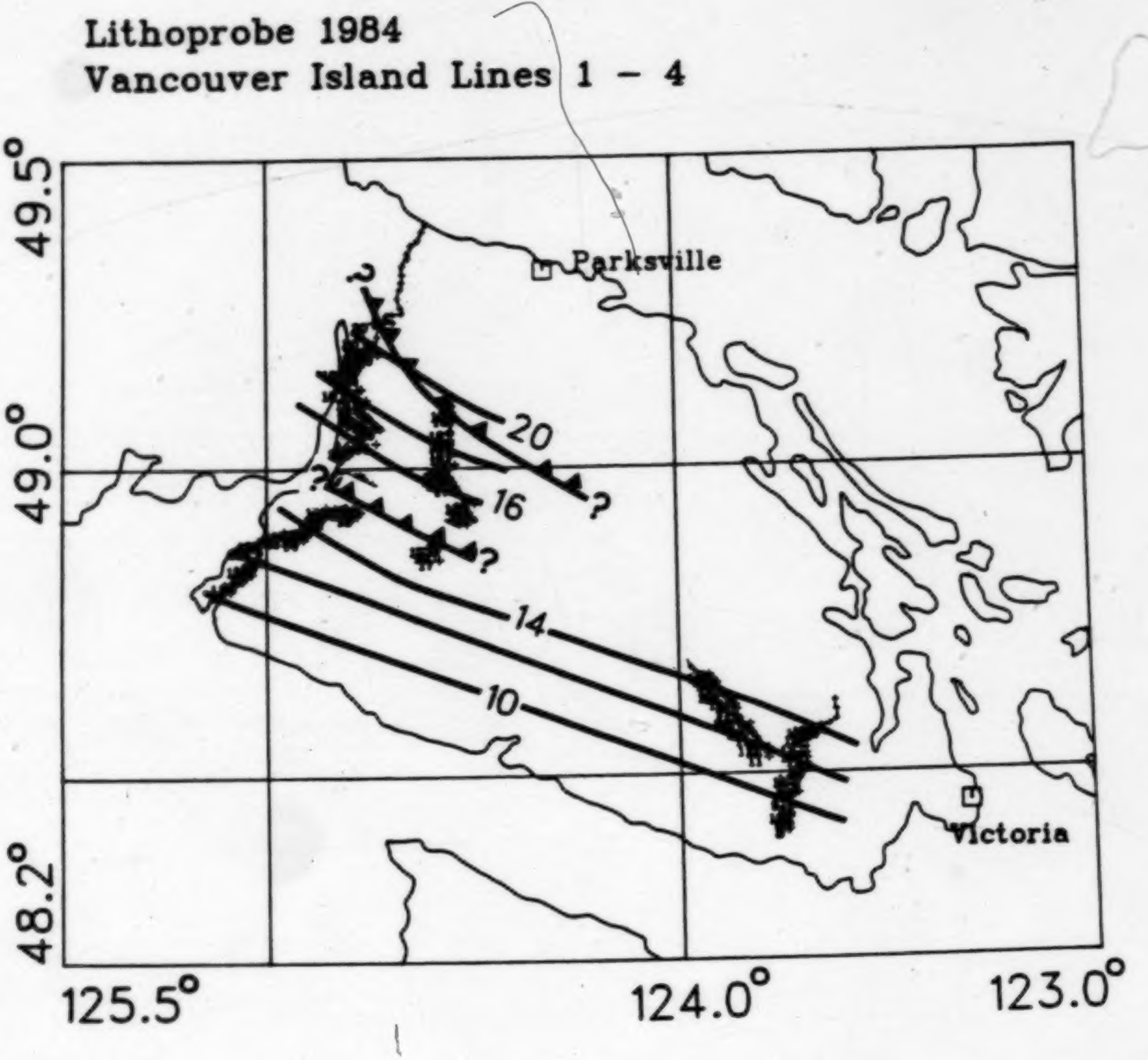
Lithoprobe 1984
Vancouver Island Lines 1 - 4
Parksville
Victoria
20
16
14
10
?
49.5°
49.0°
48.2°
125.5°
124.0°
123.0°

Figure 5.15 Structural map of the decollement zone obtained by simple migration.

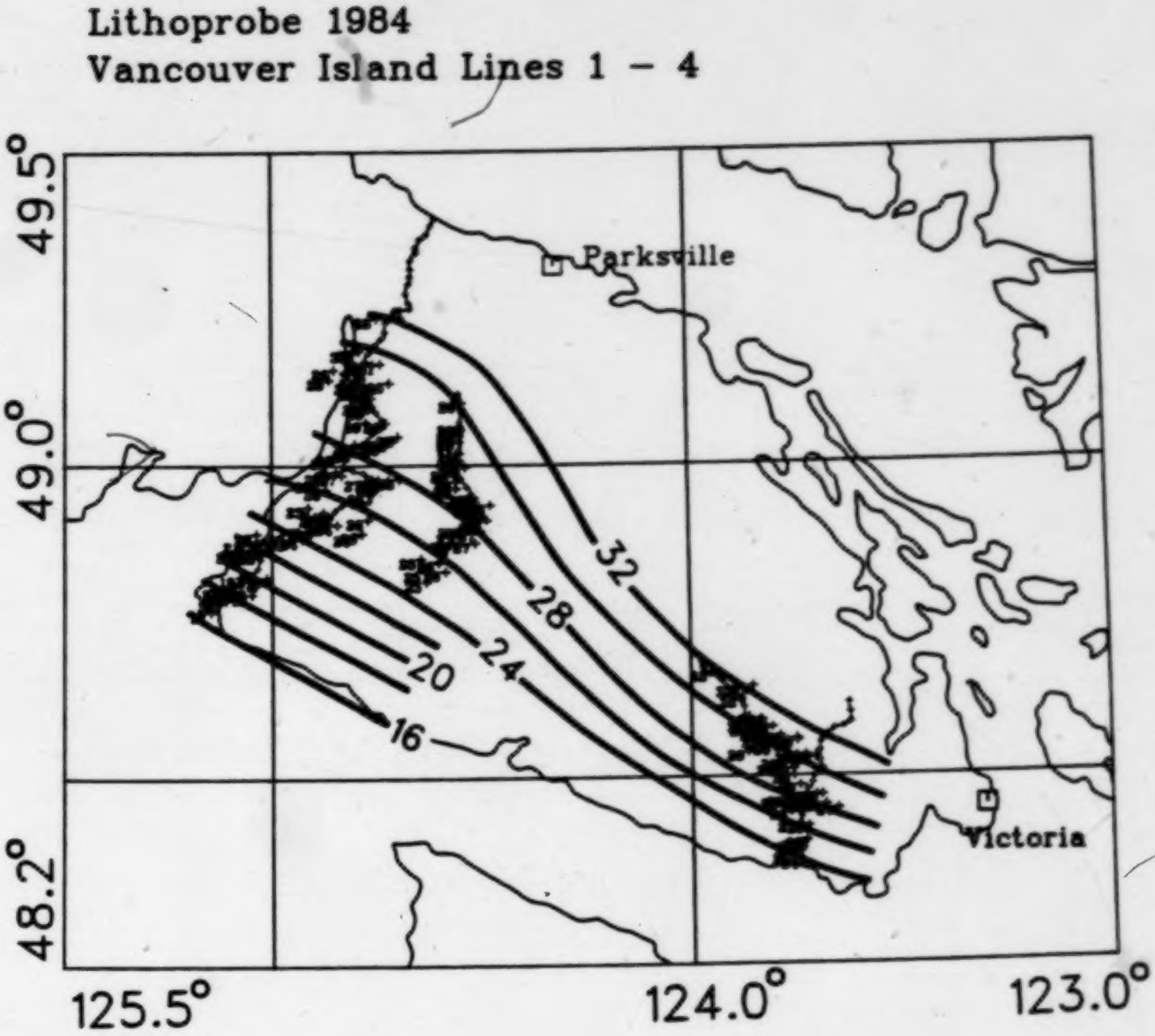
Lithoprobe 1984
Vancouver Island Lines 1 - 4
49.5°
49.0°
48.2°
125.5°
124.0°
123.0°
Parksville
Victoria
32
28
24
20
16

Figure 5.16 Structural map of the subduction zone obtained by simple migration.

5.4 Conclusion

The three-dimensional ray-tracing algorithm has been shown to be fast, accurate, and efficient in tracing seismic rays from sources to receivers through a number of polynomial surfaces. The seismic tomographic technique has demonstrated in both synthetic data, with or without noise, and with real field observations, to produce a stable and plausible model within a few iterations. Furthermore, this technique is particularly useful for imaging the three-dimensional subsurface when the seismic lines are constrainted to paths along crooked mountain roads.

The quality of the Vancouver Island reflection record sections is much better than those obtained in deeper crustal studies anywhere in the world. This has allowed us to image clearly the modern underthrusting oceanic plate and an older slab making up the crust of Vancouver Island. The process of crustal thickening by overthrusting and underthrusting is demonstrated clearly in Figure 5.10. A schematic diagram of the underthrusting slab is also shown in Figure 5.17.

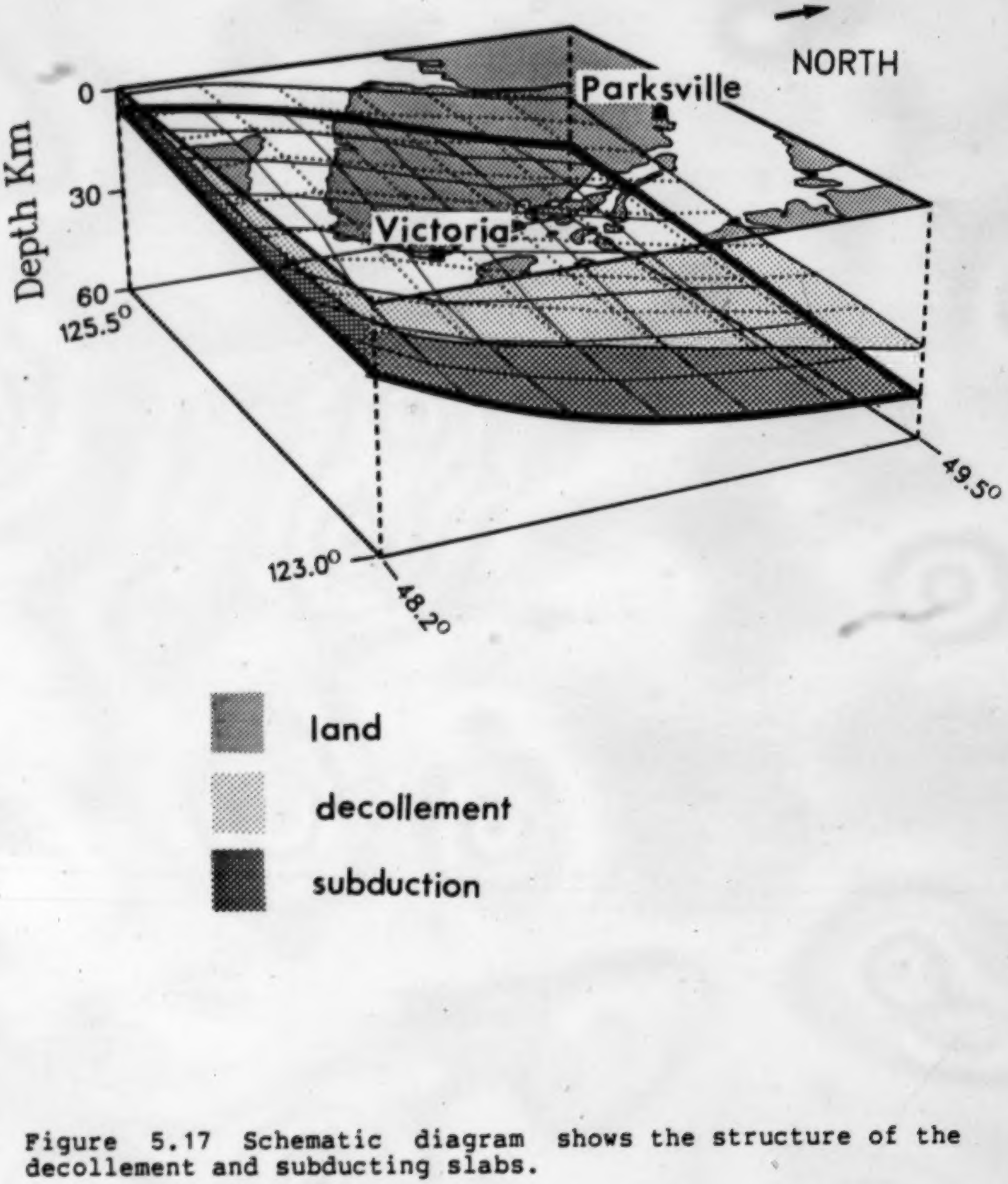
NORTH
Parksville
Victoria
Depth Km
0
30
60
125.5°
123.0°
48.2°
49.5°
land
decollement
subduction

Figure 5.17 Schematic diagram shows the structure of the decollement and subducting slabs.

6. CONCLUSIONS

The major accomplishments and conclusions of this thesis are summarized here.

1. A new three-dimensional ray tracing algorithm has been developed for use in seismic tomography where the interface can be modelled by discontinuous, or faulted, plane surfaces described by a polynomial of any degree. The method is fast, accurate and efficient in tracing seismic rays from sources to receivers through a number of polynomial surfaces, including intersecting surfaces of plane interfaces.
2. The inversion scheme demonstrates the viability of constructing the three-dimensional structure and velocity from seismic refraction and/or reflection data.
3. The new spatial refraction recording developed by E. R. Kanasewich proves to be very promising in locating possible faults and delineating the three-dimensional structure of the crust.
4. The large separation between recording sites (about 6.5 km) for the Saskatchewan data and the use of only a small portion of Vancouver Island data limit us to assuming a plane-layered model in both cases.
5. The crustal structure beneath southern Saskatchewan shows the existence of a low velocity zone and significant crustal faults, defining a series of north-south trending blocks. This anomaly correlates well with the gravity and aeromagnetic anomalies. The

faults on the Moho are clearly defined by the seismic data and have vertical displacement of up to 5 km in a crustal section nearly 50 km thick.

6. The tomographic technique has been used effectively to obtain three-dimensional structure and velocity from seismic reflection data obtained during PROJECT LITHOPROBE Phase 1, on Vancouver Island. Imaging by the seismic tomographic technique has demonstrated that the subducting plate under Vancouver Island dips at 8° to 10° under the North American continent and shows some significant curvature that needs to be studied in greater detail.
7. The magnitude of the singular values indicate how well the model parameters are determined. The eigenvalues corresponding to the velocity parameters in both the Saskatchewan and Vancouver Island data were an order of magnitude smaller than the parameters of the planes. Thus the parameters of the planes are relatively well-determined compared to the velocity parameters. Furthermore, the velocity parameters correlate with the depths of the planes. The resulting models were weighted averages of the true structures of the earth.

BIBLIOGRAPHY

Aki, K., and Lee, W. H., 1976, Determination of three-dimensional velocity anomalies under a seismic array using first P arrival times from local earthquakes: J. Geophys. Res., 81, 4381-4399.

Aki, K. and Richards, P., 1980, Quantitative Seismology theory and methods: vol.2. Freeman Publ. Co., San Francisco, California, 675-709.

Backus, G. E. and Gilbert, J. F., 1970, Uniqueness in the inversion of inaccurate gross earth data: Phil. Trans. Roy. Soc. Lond.: 266, 123-192.

Backus, G. E. and Gilbert, J. F., 1968, The resolving power of gross earth data: Geophys. J. 16, 169-205.

Bailes, A. H. and McRitchie, W. D., 1978, The transition from low to high grade metamorphism in the Kisseynew sedimentary gneiss belt, Manitoba: Geological Survey of Canada, paper 78-10, 155-178.

Bell, C. K., 1971, History of the Superior- Churchill boundary in Manitoba: Geological Survey of Canada, special paper 9, 5-10.

Berry, M. J. and Forsyth, D. A., 1975, Structure of Canadian Cordillera from seismic refraction and other data: Can. J. Earth Sci., 182-208.

Bube, K. P., and Resnick, J. R., 1984, Well-determined and poorly determined features in seismic tomography: 54th Annual SEG Meeting.

Burwash, R. A., and Culbert, R. R., 1976, Multivariate geochemical and mineral patterns in the Precambrain basement of Western Canada: Can. J. Earth Sci., 13, 1-18.

Burwash, R. A., Krupicka, J., and Culbert, R. R., 1973, Cratonic reactivation in the Precambrian basement of Western Canada III, Crustal evolution: Can. J. Earth Sci., 10, 283-291.

Camfield, P. A. and Gough, D. I., 1977, A possible plate boundary in North America: Can. J. Earth Sci., 14, 1229-1238.

Cerveny, V. and Ravindra, R., 1971, Theory of seismic head waves: University of Toronto press.

Cerveny, V., 1966, On dynamic properties of reflected and head waves in the n-layered Earth's crust: Geophys. J. R. Astro. Soc., 11, 139-147.

Chander, R., 1977, On tracing seismic rays with specfied end points in layers of constant velocity and plane interfaces: Geophys. Prosp., 25, 120-124.

Chandra, N. N. and Cumming, C. L., 1972, Seismic refraction studies in western Canada: Can. J. Earth Sci., 9, 1099-1109.

Condie, K. C., 1976, The Wyoming Archean province in the Western United States. In B. F. Windley (editor), The early history of the earth: J. Wiley and Sons, New York, N.Y., 499-510.

Cutler, R. T., Bishop, T. N., Wyld, H. W., Shuey, R. T., Kroeger, R. A., Jones, R. C., and Rathbun, M. L., 1984, Seismic tomography formulation and methodology: 54th Annual SEG Meeting.

Delandro, W., and Moon, W., 1982, Seismic structure of Superior-Churchill Precambrian boundary zone: J. Geophys. Res., 87, 6884-6888.

Devaney, A. J., 1984, Geophysical diffraction tomography: IEEE Trans. Geosci. and Remote Sens., GE-22, 3-13.

Ermanovics, I. F. and Froese, E., 1978, Metamorphism of the Superior Province in Manitoba: Geological Survey of Canada, paper 78-10, 17-24.

Ermanovics, I. F. and Wanless, R. K., 1983, Isotopic age studies and tectonic interpretation of Superior province in Manitoba: Geological Survey of Canada, paper 82-12, 22.

Forsythe, G. E. Malcolm, M., and Moler, C., 1977, Computer methods for mathematical computations: prentice Hall, Englewood Cliffs, N. J.

Forsythe, G. E. and Moler, C., 1967, Computer solution of linear algebraic system: prentice Hall, Englewood Cliffs, N. J.

Gerhard, L., Anderson, S., Lefever, J. and Carlson, C., 1982, Geological development, origin, and energy mineral resources of Williston Basin, North Dakota: Bull. Seism. Soc. Am., 66, 989-1020.

Gjoystdal, H., and Ursin, B., 1981, Inversion of reflection times in three-dimensions: Geophysics, 86, 972-983.

Golub, G. H. and Kahan, W., 1965, Calculating the singular values and pseudoinverse of a matrix: Siam J. Numer. Anal., 2, 205-224.

Golub, G. H., and Reinsch C., 1970, Singular value decomposition and least-squares solution, *in* Wilkson, J., and Reinsch, C., Eds., Handbook for automatic computation, II, linear algebra: Springer-Verlag.

Green, A., Berry, M., Spencer, C., Kanasewich, E., Chiu, S., Clowes, R., Yorath, C., Stewart, D., Unger, J and Poole, W., 1984, Recent seismic reflection studies in Canada. (Manuscript submitted for publication)

Green, A. G., Cumming, G, L., and Cedarwell, D., 1979, Extension of the Superior- Churchill boundary zone into southern Canada: Can. J. Earth Sci., 16, 1691-1701.

Green, A. G., Hajnal, Z., and Weber, W., 1985, An evolutionary model of the western Churchill province and western margin of the Superior province in Canada and the north-central United States: Tectonophysics (in press).

Green, A. G., Stephenson, O. G., Mann, G. D., Kanasewich, E. R., Cumming, C. L., Hajnal, Z., Mair, J. A., West, G. F., 1980, Cooperative seismic surveys across the Superior-Churchill boundary zone in southern Canada:

Can. J. Earth Sci., 17, 617-637.

Green, A. G., 1981, Results of a seismic reflection survey across the fault zone between the Thompson nickel belt and the Churchill tectonic province, northern Manitoba: Can. J. Earth Sci., 18, 13-25.

Hajnal, Z., Fowler, M. R., Mereu, R. F., Kanasewich, E. R., Cumming, G. L., Green, A. G., and Mair, A., 1984, An initial analysis of the Earth's crust under the Williston Basin: 1979 COCRUST experiment: J. Geophys. Res., 10, 9381-9400.

Hawley, B. W., Zandt, G., and Smith, R. B., 1981, Simultaneous inversion for hypocenters and lateral velocity variations: J. Geophys. Res., 86, 7073-7086.

Hoerl, A. E., and Kennard, R. W., 1970, Ridge regression: biased estimation for nonorthogonal problem: Technometrices, 12, 55-67.

Hoerl, A. E., Kennard, R. W., and Baldwin, K. F., 1975, Ridge regression: Some simulation: Communications in Statistics, 4, 105-123.

Jackson, D. D., 1972, Interpretation of inaccurate, insufficient data: Geophys. J. R. Astro. Soc., 28, 97-109.

Jackson, D. D., 1979, The use of a priori data to resolve non-uniqueness in linear inversion: Geophys. J. R. Astro. Soc., 57, 137-157.

Kak, A. C., 1979, Computerized tomography with X-ray emission and ultrasound sources: Proc IEEE, 67,, 1245-1272.

Kanasewich, E. R., 1981, Time sequence analysis in geophysics: Third edition, University of Alberta press, Edmonton, Alberta.

Kanasewich, E. R., and Chiu, S. K., 1985, Least-squares inversion of spatial seismic refraction data: Bull. Seism. Soc. Am., in press.

Kanasewich, E. R., Clowes, R. M. and McClougham, C. H., 1969, A buried Precambrian rift in Western Canada: Tectophysics, 8, 513-527.

Kazmierczak, Z., 1980, Seismic crustal studies in Saskatchewan: M. Sc., thesis, University of Alberta.

Lawless, J. F., and Wang, P., 1976, A simulation of ridge and other regression estimators: Communications in

Statistics, A5, 307-323.

Lawson, C. L. and Hanson, R. J., 1974, Solving least-squares problems: prentice Hall, Englewood Cliffs, N. J.

Levenberg, K., 1944, A method for the solution of certain nonlinear problems in least squares: Q. Appl. Math., 2, 164-168.

Lewry, J. F. and Sibbald, T. I., 1977, Variation in lithology and tectonometamorphic relationships in the Precambrain basement of northern Saskatchewan: Can. J. Earth Sci., 14, 1452-1467.

Lewry, J. F., Sibbald, T. I., and Rees, C. J. 1978, Metamorphic patterns and their relation to tectonism and plutonism in the Churchill province in northern Saskatchewan: Geological Survey of Canada, paper 78-10, 139-154.

Lewry, J. F., Stauffer, M. R. and Fumertan S., 1981, A Cordilleran type batholithic belt in the Churchill province in northern Saskatchewan: Precambrain Research, 14, 277-313.

Lewry, J. F., Sibbald, T. I. and Schledewitz, D. C., 1983, Variation in character of Archean basement in the western Churchill province and its significance: Geologic Association of Canada, paper in press.

Lines, L. R., and Trietel, S., 1984, A reveiw of least-squares inversion and its applications to geophysical problem: Geophys. Prosp., 32, 159-186.

Macrides, C., 1983, Interpretation of seismic refraction profiles in southern Saskatchewan: M. Sc., thesis, University of Alberta.

Marquart, D. W., 1963, An algorithm for least-squares estimation of nonlinear parameters: J. Soc. Indust. Appl. Math., 11, 55-67.

Maureau, G. T., 1964, Crustal structure in western Canada: M. Sc., thesis, University of Alberta.

McCamy, K. and Meyer, R. P., 1964, A correlation method of apparent velocity measurement: J. Geophys. Res., 69, 691-699.

McMechan, G. A. and Spence, G. D., 1983, P-wave velocity structure of the Earth's crust beneath Vancouver Island: Can. J. Earth Sci., 20, 742-752.

Miller, W. and Wrathall, C., 1980, Software for roundoff analysis of matrix algorithms: Academic press, N. Y.

Norton, S. J. and Linzer, M., 1979, Ultrasonic reflectivity tomography: reconstruction with circular transducer arrays: Ultra. Imaging, 1, 154-184.

Porter, J. W., Price, R. A. and McCrossan R. G., 1982, The western Canada sedimentary basin, Phil. trans. Roy. Soc. Lond A 305, 169-192.

Powell, M. J., A hybrid method for nonlinear equations, *In* Rabinowitz, P., Ed., Numerical methods for nonlinear alegraic equations, Gordon and Breach Inc.

Price, R. A. and Douglas, R. J., 1972, Variations in tectonic styles in Canada: Geological Association of Canada, special paper 11, 381-623.

Sereda, I. T., 1978, A crustal reflection spread study in southeast Saskatchewan and southeast Manitoba: M. Sc., thesis, University of Saskatchewan.

Shahriar, M., 1982, Refraction data from southern Saskatchewan: A detailed interpretation of the 1979 east-west CO-CRUST profile: M. Sc., thesis, University of Alberta.

Spence G. D., 1984, Seismic structure across the active subduction zone of western Canada: Unpublished PhD thesis, University of British Columbia.

Stark, H. and Paul, I., 1981, An investigation of computerized tomography by direct fourier inversion and optimum interpolation: IEEE, Trans. Biomed. Eng., BME-28, 496-505.

Stark, P. A., 1970, Introduction to Numerical methods: MacMillan Publ. Co., London, 87-114.

Stewart, G. W., 1973, Introduction to matrix computation: Academic press, N. Y.

Theobald, C. M., 1974, Generalizations of mean square error applied to ridge regression: J. of the Roy. Stat. Soc., Ser. B, 36, 103-106.

Yorath, C. J., Clowes, R., Sutherland Brown, A., Brandon, M., Massey, N., Green, A., Spencer, C., Kanasewich, E., and Hyndman, R., 1985, LITHOPROBE- PHASE 1: Southern Vancouver Island: Preliminary analysis of reflection seismic profiles and surface geological studies. (submitted to publication)

APPENDIX ---COMPUTER PROGRAMS

```
C
C     THIS PROGRAM DESIGNED TO DETERMINE THE CRUSTAL
C     STRUCTURE OF SASKATCHEWAN SPATIAL REFRACTION DATA.
C
C    IT COMPUTES SEISMIC RAY TRACING WITH SPECIFIED
C    END POINTS IN LAYERS OF CONSTANT VELOCITY AND PLANE
C    INTERFACES.
C
C    IMPROVEMENT OF MODEL BY DAMPED LEAST-SQUARES ITERATIONS
C
C
      DIMENSION X1(40), A(20), B(20), C(20), D(20)
      DIMENSION X(40),Z(20),V(20),VT(20),F(50),FCN(20)
      DIMENSION XRCR(100),YRCR(100),ZRCR(100), AZM(100)
      DIMENSION DIST(100), RMATR(300,20),W(20)
      DIMENSION TOBS(140),T(140),TERR(300),TNPT(20)
      DIMENSION WK(3000), PAR(20), AJINV(50,50), COEFF(20)
      REAL AMATRX(300,20), U(300,20), V1(300,20)
      REAL FLOC1(4), FLOC2(4), SCALE(20)
      INTEGER IFACE(20),IFAULT(10),INDEX(10),IDER(20)
      INTEGER IVDER(20), ICHAR(70), ID(140)
      COMMON/ABCD/ NP, A, B, C, D, IFACE
      COMMON X
      COMMON/XYZ/ X0, Y0, Z0, XN1, YN1, ZN1
      COMMON/FCEPT/X1CEPT,Y1CEPT,X2CEPT,Y2CEPT,XF2LCN
      COMMON/VV/IDIM,NV,V,IFLAG,IREFR,NORFL,NUFAUL,NUPLAY
      EXTERNAL CALFUN
      DATA INDEX/10*0/
C
C     UNIT 1 -- OUTPUT FOR JACOBIAN MATRIX
C     UNIT 2 -- OUTPUT FOR RESOLUTION MATRIX
C               AND COVARIANCE MATRIX
C     UNIT 3 -- OUTPUT FOR PLOTTING TRAVEL TIME CURVES
C     UNIT 4 -- *SINK*
C     UNIT 5 -- INPUT DATA
C     UNIT 6 -- OUTPUT DATA
C     UNIT 7 -- INPUT DATA FOR ITERATION IF IREAD=99
C     UNIT 8 -- TEMPORARY STORE FILE FOR UNIT 7
C
C
   10 FORMAT(10I6)
   11 FORMAT(10I6)
   12 FORMAT(I5, F14.6, 10E16.6 )
   14 FORMAT(12F12.6)
   15 FORMAT(2I6, 6E16.6)
   16 FORMAT('0      NS01A ROUTINE IS USED')
   17 FORMAT('0      NLSYST ROUTINE IS USED')
   20 FORMAT(10I6)
   24 FORMAT(A4)
   30 FORMAT( 10F14.6)
   31 FORMAT(10F14.4)
   32 FORMAT(12F9.4)
```

```
 33  FORMAT(I6,2X,12F9.4)
 40  FORMAT( I6, 5F12.4)
 45  FORMAT( I7, 10F12.4)
 50  FORMAT(I6, 10F12.4)
 55  FORMAT('0  INPUT OF X, Y, V, ',I7, 4F10.4)
 54  FORMAT ('  THE INDEX OF I  FROM NLSYST =', I3)
 67  FORMAT('0  TIME FROM MODEL ', 10F10.4)
 68  FORMAT('0  TIME RESIDUALS ', 10F10.4)
 69  FORMAT('STANDARD ERROR ESTIMATE= ',F10.5,
    &  'ERROR MEAN=',  F10.5)
 70  FORMAT(' DAMPING FACTOR =', F10.5)
 71  FORMAT(' ERROR  -- NPTS .LE. NC' )
 72  FORMAT(' ERROR RETURN FROM SVD ROUTINE', I6)
 73  FORMAT(' ERROR ESTIMATE FROM SVD', F12.5)
 74  FORMAT(' OLD COEFF OF MODELS ', 10F9.4 )
 76  FORMAT('INPUT IRC: (I6)'/,
    + ' INPUT NPARS(I6) ')
 77  FORMAT(10I6)
 79  FORMAT(2E12.6)
 80  FORMAT(' NEW COEFF OF MODELS ', 10F9.4 )
C
C   WK -- WORK VECTOR LENGTH
C   MODIT -- NUMBER OF ITERATIONS FOR THE MODEL
C   MAXIT -- MAX NUMBER OF ITERATIONS TO SOLVE THE NONLINEAR
C            SYSTEMS.
C
C    DELT = THE STEP SIZE FOR THE PARTIAL DERIVATIVE
C    XTOL = THE TOLERANCE OF X
C    FTOL = THE TOLERANCE OF FUNCTION CALFUN
C    MAXFUN = MAX NUMBER TO CALL FUNCTION CALFUN
C    DMAX = GENERAL ESTIMATE OF DISTANCE FROM SOLUTION
C    ACC = ACCURACY
C    IDIM = DIMENSION OF THE PROBLEM
C    KLAYER = THE K-LAYER(PLANE) TO START WITH
C    NP = MAX NUMBER OF PLANE IN THE MODEL
C    INDEXF = NUMBER FOR THE FAULT PLANE
C    IFAULT = CONTAIN THE INDEX OF FAULT PLANE
C    ISCASE -- SPECIAL CASE IF ISCASE .GT. 0
C    RELERR USED FOR GENERALIZED INVERSE TO DELETE
C       SMALL EIGENVALUES.
C    IF (ISCASE.EQ.1) THE 1ST PLANE NOT USE IN THE SOLUTION
C    OF THE ITERATION IN THE MODEL CONTAINING 2 FAULTS.
C    IF (ISCASE.EQ.2) THE 2ST PLANE NOT USE IN THE SOLUTION
C    OF THE ITERATION IN THE MODEL CONTAINING 2 FAULTS.
C    VR -- THE REDUCTION VELOCITY
C   IF (JVR.GT.0) TOBS = TOBS + DIST/VR
C   IF NORFL.GT.0  DON'T COMPUTE DERIVATIVE OF VELOCITY
C   NUFAUL -- THE FAULT INFO. FOR CRUSTAL LAYERS
C
      VR = 8.0
C
      MDIM = 300
      NDIM = 50
      RAD = 3.14159/180.0
      IUNIT = 7
C
C    READ IN PARAMETERS FOR THE NONLINEAR EQNS
C
      DO 19 I=1,40
      X(I) = 0.0
      F(I) = 0.0
   19 CONTINUE
C
      READ(5,11) IFLAG,ISUB,IPRINT,JACOB,NSHOT,NUPLAY,
     &   IHOERL, ISCASE
      READ(5,15) MODIT, MAXIT, DELTA, XTOL, FTOL, TTOL
      WRITE(6,15) MODIT, MAXIT, DELTA, XTOL, FTOL, TTOL
      READ(5,12) MAXFUN, DMAX, ACC,RELERR,CONST,DFACTR
      WRITE(6,12) MAXFUN, DMAX, ACC,RELERR,CONST,DFACTR
      READ(5,10) IDIM, KLAYER, NP, INDEXF, NORFL
      WRITE(6,10) IDIM, KLAYER, NP, INDEXF, NORFL
C
C    READ THE PLANE COEFFS
C    MAKE SURE ALL THE COEFFS OF C(I) = 1.0
C
      IF ( ISUB .EQ. 1) WRITE(6,16)
      IF ( ISUB .EQ. 2) WRITE(6,17)
C
C    READ IN INTERFACE INFORMATION
C
      DO 300 I= 1, NP
      READ(5,14) A(I), B(I), C(I), D(I), VT(I)
      WRITE(6,14) A(I), B(I), C(I), D(I), VT(I)
  300 CONTINUE
C
C    READ IN LOCATIONS OF THE FAULTS
C
      READ(5,14) (FLOC1(I), I=1,4)
      READ(5,14) (FLOC2(I), I=1,4)
C
C    READ IN THE FAULT INFORMATION
C
      IF(INDEXF) 21, 21, 22
   21 IFAULT(1) = 0
      GO TO 23
   22 READ(5,20) (IFAULT(I), I= 1, INDEXF)
      WRITE(6,20) (IFAULT(I), I= 1, INDEXF)
C
   23 CONTINUE
C
      L1 = 1
C
      DO 400 L= KLAYER, NP
      IF( L .EQ. IFAULT(L1) ) GO TO 390
C
         DO 395 J=1,20
         DO 395 I=1,MDIM
         AMATRX(I,J)=0.0
```

```
 395     CONTINUE
C
C    NEQ = POINTS OF VERTICES IN THE PLANE
C    NPTS = NUMBER OF RECIEVERS
C    NFPTS = NUMBER OF FAULT POINTS TO BE DELETED
C
      NC = 4
        NCMAX = 4
        ERSAV = -999
        ITER = -1
 499    ITER = ITER+1
        TMEAN = 0.0
        ERROR = 0.0
        ICNT =0
        ICT = 0
        NPDMAX = 0
C
        IF (ITER) 406,406,403
 403    NUM = 6+NP+INDEXF
        REWIND 5
C
        DO 404 JJ1 = 1,NUM
        READ(5,24) DUM
 404    CONTINUE
C
C   READ IN UPDATED INPUT IF ITER>0
C
        REWIND 7
        REWIND 8
 406    CONTINUE
C
       DO 460 JJ=1,NSHOT
C
C  NPDER -- NUMBER OF PARTIAL DERIVATIVE
C  ISORIG -- = 0 IF SHOT IS AT L.H.S OF THE ORIGIN
C             = 1 IF SHOT IS AT R.H.S OF THE ORIGIN
C  ISRCR -- INTERCHANGE THE SHOT WITH THE RECIEVER
C  IREAD =99  READ IN INPUT FROM FILE 7
C  IF IFSHIF.LE.0 THE LOCATION OF FAULTS NOT CHANGED
C  IF IFSHIF.GT.0  FAULT 2 IS SHIFTED TO FAULT 1
C  IF IREFR .GT. 0 -- REFRACTION DATA
C  IF IREFR .LE. 0 -- REFLECTION DATA
C  IF NORFL .GT.0 INVERT REFLECTION DATA ONLY
C  IF NORFL .LE.0 INVERT BOTH REFRACTION AND REFLECTION
C
       JVR = 0
C
       READ(5,10)NEQ,NPTS,NFPTS,NPDER,ISORIG,ISRCR,
      &  IREAD, IFSHIF
       READ(5,10) IREFR, JVR, NUFAUL
       IF (NPDER .GT. NPDMAX) NPDMAX=NPDER
C
C
C    (X0,Y0,Z0) -- SOURCE  (XN1, YN1, ZN1) -- DETECTOR
```

```
C
      READ(5,30) X0, Y0, Z0, VN1
C
      XSAVE = X0
      YSAVE = Y0
      ZSAVE = Z0
C
C
      DO 401 K = 1, NPTS
      READ(5,40)ID(K),XRCR(K),YRCR(K),AZM(K),DIST(K),TOBS(K)
      IF ( JVR.GT.0) TOBS(K) = TOBS(K) + DIST(K)/VR
      ZRCR(K) = 0.0
 401  CONTINUE
C
      NV = NEQ+1
      V(NV) = VN1
      IF ( IREFR.LE.0 .AND. NPDER.EQ.2)
     +  CALL LINE(X0,Y0,XRCR(1),YRCR(1),FLOC2,X2CEPT,Y2CEPT)
C
C   INDEX(1) INDICATES THE NUMBER OF POINTS TO INSERT
C   OR DELETE TO A VECTOR. E.G. INDEX(1)=1 , THE
C   X VECTOR IS ADDED OR DELETED AT X(I), AND X(NEQ+I)
C   BY PAR(1) AND PAR(INDEX(1)+1)
C
      DO 402 I=1,10
 402  INDEX(1) = 0
C
      IF (NFPTS )  35, 35, 36
  36  READ(5,20) (INDEX(I), I=1,NFPTS)
      NPAR = 2*INDEX(1)
  35  CONTINUE
C
        IF (NPDER) 38,38,37
  37    READ(5,20) (IDER(I),I=1,NPDER)
  38    CONTINUE
C
C    INPUT HERE HAS TO INCLUDE ALL LOCATIONS OF THE FAULTS.
C    THOSE FAULT LOCATION (X VECTOR) WIL BE DELETED BEFORE
C    CALLING ROUTINE NS01A.
C    IFACE AND V VECTORS STILL CONTAIN THE INFORMATION OF
C    THE FAULT AND WILL NOT BE DELETED.
C
      INDX = 0
      IF (IREFR.LE.0 .AND. NPDER.EQ.2) INDX=IDER(2)-1
      DO 410 I = 1,NEQ
      READ(5,50) IFACE(I), XX, YY, V(I)
      X(I) = XX
      X(NEQ+I) = YY
      IF (I.EQ.INDX) X(I)=X2CEPT
      IF(I.EQ.INDX) X(NEQ+I) = Y2CEPT
C     WRITE(6,55) IFACE(I), XX, YY, V(I)
 410  CONTINUE
C
      IF (IREAD.EQ.99) GO TO 415
```

```
C
      IF (INDEX(1)) 412, 412, 413
 413  CALL DELETE( X, NEQ, PAR, INDEX)
C
      LX = 2*NEQ
C
 412  CONTINUE
C
C  IN 3-D NEED TO SOLVE NEQ*2 LINEAR EQUATIONS
C
      NEQ1 = NEQ
      IF (IDIM .EQ. 3) NEQ1= NEQ*2
C
 415  CONTINUE
C
      DO 430 J= 1, NPTS
      XN1 = XRCR(J)
      YN1 = YRCR(J)
      ZN1 = ZRCR(J)
      IDUM = 0
C
      IF (ISRCR) 306,306,305
C
C   INTERCHANGE THE  BETWEEN SHOT AND RECIEVERS
C
 305  X0 = XN1
      Y0 = YN1
      Z0 = ZN1
      XN1 = XSAVE
      YN1 = YSAVE
      ZN1 = ZSAVE
 306  CONTINUE
C
        IF (IREAD.EQ.99) CALL READF(IUNIT,NEQ,IFACE,X,VN1,
     + NFPTS,PAR, INDEX, NPDER, IDER)
        NEQ1 = NEQ
        IF (IDIM.EQ.3) NEQ1 = NEQ*2
        II = 10
C       WRITE(6,32) (V(I),I=1,NV)
C
C
        IF (ITER) 58,58,56
 56      DO 57 I=1,NPDER
         IVPT = IDER(I)
         IF ( I.EQ.1 .AND. IREFR.GT.0) IVPT=IVPT+1
         J1 = IFACE(IDER(I))
         IDF = J1
         IF (I.EQ.2 .AND. NPDER.EQ.3) J1 = J1 -1
         IF (IREFR.GT.0) V(IVPT) = VT(J1)
C
C  THE CASE OF FAULT IN CRUSTAL LAYERS FOR REFLECTION DATA
C
       IF (IDF-IABS(NUFAUL)) 52, 53,52
   53  IDIFF = ISIGN(1,NUFAUL)
```

```
      IDF = IDF + IDIFF
      IF ( IREFR.LE.0 .AND. NORFL.GT.0) V(IVPT) = VT(IDF)
      GO TO 908
 52   CONTINUE
C
C   ADD THESE 2 STATEMENTS FOR REFLCETION
C
        IF ( IREFR.LE.0 .AND. NORFL.GT.0) V(IVPT) = VT(J1)
        IF ( IREFR.LE.0 .AND. NORFL.GT.0) V(IVPT+1) = VT(J1)
C
 908  CONTINUE
C
C       WRITE(6,910) IVPT, J1, V(IVPT), VT(J1)
C 910   FORMAT(' VTEST ', 2I5, 2F10.4)
 57     CONTINUE
 58   CONTINUE
C
C     WRITE(6,32) (V(I), I=1,NV)
C
      IF (INDEX(1).LE.0) GO TO 435
C
C   COMPUTE THE LOCATION OF THE FAULT
C
      IF (IFSHIF) 310,310,315
 310  XF2LCN = FLOC2(1)
      CALL LINE(X0,Y0,XN1,YN1,FLOC1,X1CEPT,Y1CEPT)
      CALL LINE(X0,Y0,XN1,YN1,FLOC2,X2CEPT,Y2CEPT)
C
      GO TO 320
C
 315  XF2LCN = FLOC1(1)
      CALL LINE(X0,Y0,XN1,YN1,FLOC2,X1CEPT,Y1CEPT)
      CALL LINE(X0,Y0,XN1,YN1,FLOC1,X2CEPT,Y2CEPT)
 320  CONTINUE
C
      IF (INDEX(1).EQ.0) GO TO 325
      II = INDEX(1)
      GO TO (321, 324), II
 321  IK = INDEX(2)
      I2 = IFACE( IK)
      ITEST = IABS( I2 - IFACE(IK-1))
      IF ( ITEST.EQ.2) GO TO 323
      PAR(1) = X1CEPT
      PAR(2) = Y1CEPT
      GO TO 325
C
 323  PAR(1) = X2CEPT
      PAR(2) = Y2CEPT
      GO TO 325
C
 324  PAR(1) = X1CEPT
      PAR(2) = X2CEPT
      PAR(3) = Y1CEPT
      PAR(4) = Y2CEPT
 325  CONTINUE
C
C
C    SOLVE THE SYSTEM OF NON-LINEAR EQUATION
C
C    ROUTINE NS01A CAN BE FOUND IN THE FOLLOWING
C    REFERENCE:
C  POWELL, M. J., A HYBRID METHOD FOR NONLINEAR EQUATIONS,
C  IN RABINOWITZ, P., ED., NUMERICAL METHODS FOR
C  NONLINEAR ALEGRAIC EQUATIONS, GORDON AND BREACH INC.
C
  435 IF (ISUB .EQ. 1)
     + CALL NS01A(NEQ1,X,F,AJINV,NDIM,DELTA,DMAX,ACC,
     + MAXFUN, IPRINT, WK, PAR, INDEX)
C
C       IF ( ISUB .EQ. 2)
C      + CALL NLSYST(CALFUN,NEQ1,MAXIT,PAR,INDEX,X,F,DELTA,
C      +  XTOL, FTOL, II)
C
C    CHECK FOR THE DIFFERENT CONFIGURATIONS OF THE
C    FAULT MODELS
C
C       IF (ITER.GE.0)
C     + CALL RAYM(NEQ,X,IFACE,D,V,VT,NFPTS,INDEX,PAR,NPDER,
C     + IDER,ISRCR,ISORIG,NUPLAY, IALTR)
C
C       IDUM= IDUM+1
C       IF (IALTR.EQ.1 .AND. IDUM.LT.2) GO TO 435
C
C
      IF (INDEX(1) .GT. 0) CALL INSERT(X, NEQ, PAR, INDEX)
      LX = 2*NEQ
C      WRITE(6,32) (X(I), I=1,LX)
C
      DO 440 I=1,NEQ
 440  Z(I) = ZF(I)
      WRITE(6,33) ID(J), ( Z(I), I=1,NEQ)
C
      CALL TIME(X, Z, V, NEQ, TSUM, TNPT)
      T(J) = TSUM
C
C    SET UP THE JACOBIAN MATRIX
C    IDF -- THE ID NUMBER OF THE INTERFACE
C
      IF ( JACOB-99) 449,445,449
 445  IF( NPDER.LE.0) GO TO 449
      ICNT= ICNT+1
        DO 446 IK = 1,NPDER
        K1 = IDER(IK)
        IDF = IFACE(K1)
        IVPT = K1
        IF ( IK.EQ.1 .AND. IREFR.GT.0) IVPT=IVPT+1
C    LAST USE FOR THE LAST SEGMENT IN MODEL OF 2-FAULTS
        LAST = NPDER-IK
        IF (NPDER.EQ.1) LAST = 99
C
C   PDERR -- ROUTINE TO COMPUTE PARTIAL DER. OF 2-FAULTS OF
C            REFRACTION DATA
C   PDERL -- ROUTINE TO COMPUTE PARTIAL DER. OF REFLECTION
C            DATA. NO FAULT IS CONSIDERED.
C
        IF(IREFR.GT.0) CALL PDERR(X,Z,NEQ,K1,IVPT,FCN,
    &   LAST,NPDER)
        IF(IREFR.LE.0) CALL PDERL(X,Z,NEQ,K1,IVPT,FCN,IDF)
C
C   THE CASE OF FAULT IN CRUSTAL LAYERS FOR REFLECTION DATA
C
      IF (IDF-IABS(NUFAUL)) 443,442,443
 442  IDIFF = ISIGN(1, NUFAUL)
      IDF = IDF + IDIFF
 443  CONTINUE
C
C
C    THIS IS SPECIAL CASE OF MIDDLE LAYER OF THE HORST
C
        IF (LAST.EQ.1 .AND. NPDER.EQ.3) IDF=IDF-1
        IF ( IDF.EQ.ICASE) GO TO 446
C
        NCOEF = 4
        NCOEF1 = 3
C
C  IF  NOPERV = 0 -- NOT INCLUDE VELOCITY AS A PARAMETER
C
        NOPERV = 1
        IF (NOPERV.EQ.0) NCOEF = 3
        IF (NOPERV.EQ.0) NCOEF1 = 2
C
        K2 = ( IDF-(NUPLAY+1) )*NCOEF + 1
        NCC = K2 + NCOEF1
        I1 = 0
C
        IF ( NCC .GT. NCMAX) NCMAX=NCC
           DO 444 I=K2, NCC
           I1 = I1+1
 444       AMATRX(ICNT,I) = FCN(I1)
 446     CONTINUE
C
      WRITE(1,32) (AMATRX(ICNT,I),I=1,NCMAX)
 449  CONTINUE
C
      WRITE(8,20) NEQ, NFPTS, NPDER
      IF (NFPTS) 335,335,330
 330  NPAR = 2*INDEX(1)
      WRITE(8,20) (INDEX(I), I=1,NFPTS)
 335  CONTINUE
C
      IF (NPDER) 338,338,337
 337  WRITE(8,20) (IDER(I),I=1,NPDER)
 338  CONTINUE
C
      ITEST = NEQ-NUPLAY
      INDEX(NFPTS+1) = 0
      JD = 2
C
       DO 345 I = 1, NEQ
       IDUM = INDEX(JD)
       WRITE(8,50) IFACE(I),X(I),X(NEQ+I),V(I),Z(I)
C
C      IF ( I.GT.NUPLAY .AND. I.LE.ITEST .AND. I.NE.IDUM)
C     +  WRITE(2,50) IFACE(I),X(I),X(NEQ+I),V(I),Z(I)
C      IF ( I.EQ.INDEX(JD)) JD=JD+1
C
  345  CONTINUE
C
      IF (NFPTS .GT. 0) CALL DELETE(X, NEQ, PAR, INDEX)
C
 430  CONTINUE
C
      WRITE(6,54) II
C
       WRITE(6,67) (T(I), I=1,NPTS)
C    COMPUTE ERROR ESTIMATE
C
      DO 450 I = 1, NPTS
      ICT = ICT+1
      TERR(ICT) = TOBS(I)- T(I)
      TMEAN = TMEAN + TERR(ICT)
      ERROR = ERROR + TERR(ICT)**2
C
C    USE FOR PLOTTING 3-D TRAVEL TIME CURVES
C
      IDD = ID(I)
      IF (IREFR.LE.0 .AND. IDD.GT.0) IDD = ID(I)*(-1)
      WRITE(3,45) IDD,XRCR(I),YRCR(I),AZM(I),DIST(I),T(I),
     &  TOBS(I),TERR(ICT)
C
 450  CONTINUE
C
 460  CONTINUE
      TAVE = TMEAN/ICT
C
       WRITE(6,68) (TERR(I), I=1,ICT)
       WRITE(4,68) (TERR(I), I=1,ICT)
      ERROR = (ERROR/ICT)**0.5
      WRITE(6,69) ERROR,TAVE
      WRITE(4,69) ERROR,TAVE
      IF (ERROR .LE. TTOL) GO TO 400
C
      CONST = CONST*DFACTR
C     IF (ERROR .GE. ERSAV ) CONST = CONST/DFACTR
      WRITE (6,70) CONST
      WRITE (4,70) CONST
      ERSAV = ERROR
 465  CONTINUE
C
C
C
      IF (ITER .GE. MODIT) GO TO 710
C
      IF (JACOB-99) 469,466,469
 466  IF( ICNT .GE. NCMAX) GO TO 467
      WRITE(6,71) ICNT, NCMAX
      STOP
C
 467  CONTINUE
C
      IF ( IHOERL .LE. 0) GO TO 473
C
      CALL SCALM(AMATRX,ICNT,NCMAX,MDIM,SCALE)
      DO 461 I=1,ICNT
C     WRITE(1,32) (AMATRX(I,LK), LK=1,NCMAX)
 461  CONTINUE
      CALL DAMPR(AMATRX,ICNT,NCMAX,MDIM,TERR,SCALE,COEFF,
     &  DAMPF, ITER)
C
      IF ( IHOERL .GT.0 ) GO TO 472
C
C   COMPUTE THE EIGENVALUES AND EIGENVECTORS
C   THE ROUTINE SVD CAN BE FOUND AT THE FOLLOWING
C   REFERENCE:
C  FORSYTHE, G. E. MALCOLM, M., AND MOLER, C., 1977,
C  COMPUTER METHODS FOR  MATHEMATICAL COMPUTATIONS:
C  PRENTICE HALL, ENGLEWOODCLIFFS, N. J.
C
 473  CALL SVD(MDIM,ICNT,NCMAX,AMATRX,W,.TRUE.,U,.TRUE.,
     &  V1, IERR, WK)
C
C         DO 1000 I=1,ICNT
C         WRITE(1) (AMATRX(I,I1), I1=1,NCMAX)
C 1000    CONTINUE
C
C         WRITE(1) (TERR(I),I=1,ICNT)
C
      IF (IERR .EQ. 0) GO TO 468
      WRITE(6,72) IERR
      STOP
C
 468  CONTINUE
C
C   SOLVE FOR LEAST SQUARE SOLUTION
C
      CALL SOLSVD(MDIM,ICNT,NCMAX,W,U,V1,COEFF,TERR,RELERR,
     & CONST, RMATR)
C
C   COMPUTE THE STANDARD ESTIMATE FROM SVD
C
```

```
      CALL SDERR(MDIM,ICNT,NCMAX,AMATRX,COEFF,TERR,RERR)
      WRITE(4,73) RERR
      WRITE(6,73) RERR
C
C   UPDATE THE CHANGE OF THE PARAMETERS
C
C
 472    CONTINUE
C
        IK = NUPLAY+1
        NMODEL = NCMAX/NCOEF + IK - 1
        DO 471 K1 =IK,NMODEL
        K2 = (K1-(NUPLAY+1) )* NCOEF + 1
        WRITE(4,74) A(K1), B(K1), D(K1), VT(K1)
        WRITE(6,74) A(K1), B(K1), D(K1), VT(K1)
C
C    THIS IS A SPECIAL CASE NOT TO CHANGE THE COEFFS
C    OF THE THIS LAYER
C
        IF (K1.EQ.ISCASE) GO TO 480
C
        A(K1) = A(K1)+COEFF(K2)
        B(K1) = B(K1)+COEFF(K2+1)
        D(K1) = D(K1)+COEFF(K2+2)
        IF(NOPERV.NE.0) VT(K1) = VT(K1)+COEFF(K2+3)
 480    CONTINUE
C
C
        WRITE(4,80) A(K1), B(K1), D(K1), VT(K1)
        WRITE(6,80) A(K1), B(K1), D(K1), VT(K1)
 471    CONTINUE
C
 469  CONTINUE
C
C
      WRITE(4,76)
      READ(4,77) IRC, NPARS
      IF (NPARS .GT. 0) READ(4,79) ACC
      IF ( IRC .LE. 0) GO TO 800
C
        REWIND 7
        REWIND 8
C
C   UPDATE THE INPUT INFORMATION FOR RAY-TRACING
C
        DO 494 I=1,999
        READ(8,496,END=495) ICHAR
        WRITE(7,496) ICHAR
 496    FORMAT(100A4)
 494     CONTINUE
 495     CONTINUE
C
C
       GO TO 499
```

```
C
 390  L1 = L1+1
      IF (L1 .GT. INDEXF) IFAULT(L1) =0
C
 400  CONTINUE
C
      GO TO 800
 700  WRITE(6, 705) L, ITER
 705  FORMAT('PREVIOUS ERROR ','LAYER =',I3,4X,'ITER= ',I3)
      GO TO 800
 710  WRITE(6, 715) L
 715  FORMAT('MODEL ITERATIONS    ','LAYER = ',I3,4X)
 800  CONTINUE
C
      WRITE(6,808) ITER
 808  FORMAT(' THE NUMBER OF ITERATIONS =', I3)
      WRITE (6, 810)
 810  FORMAT('0  FINAL MODEL OF PLANE COEFFS' )
      WRITE(6,820)
 820  FORMAT(10X,'A',3X, 10X,'B',3X, 10X,'C',3X, 10X,'D',
     & 10X, 'VELOCITY')
      DO 830 I =1, NP
 830   WRITE(6,14) A(I), B(I), C(I), D(I), VT(I)
      STOP
      END
C
      REAL FUNCTION ZF(I)
      DIMENSION X(40), A(20), B(20), C(20), D(20), V(20)
      INTEGER IFACE(20)
      COMMON/ABCD/ NP, A, B, C, D, IFACE
      COMMON/VV/IDIM,NV,V,IFLAG,IREFR,NORFL,NUFAUL,NUPLAY
      COMMON X
      NEQ = NV-1
      J = NEQ+I
      K = IFACE(I)
      ZF = -( A(K)*X(I)+B(K)*X(J)+D(K) )
C      IF (IFLAG .EQ.1 ) WRITE(6,10) J, K, ZK
C  10  FORMAT('0  FROM ROUTINE ZF(I)', 2I8, F12.5)
      RETURN
      END
C
      SUBROUTINE CALFUN( X, F, N, PAR, INDEX)
      DIMENSION X(1), F(1), A(20), B(20), C(20), D(20), V(20)
      DIMENSION PAR(1)
      INTEGER IFACE(20), INDEX(1)
C
      COMMON/ABCD/ NP, A, B, C, D, IFACE
      COMMON/XYZ/ X0, Y0, Z0, XN1, YN1, ZN1
      COMMON/VV/IDIM,NV,V,IFLAG,IREFR,NORFL,NUFAUL,NUPLAY
C
C   CALCULATE THE JACOBIAN MATRIX FOR X(I) AND Y(I)
C   F(1 TO NEQ ) STORE THE PARTIAL DERIVATIVES
C       OF X(I)
C   F( NEQ+1 TO 2*NEQ ) STORE THE PARTIAL DERIVATIVES
```

```
C        OF Y(I)
C
      NEQ = N
      IF (IDIM .EQ. 3) NEQ=N/2
C
      IF ( IREFR.LE.0 .AND. NEQ.EQ.1) GO TO 310
C
      IF (INDEX(1) .GT. 0) CALL INSERT(X, NEQ, PAR, INDEX)
C
      DO 225 K=1,NEQ
C
      I = K
      J = NEQ+I
      II = IFACE(I)
      IF ( I .EQ. 1) GO TO 20
      IF ( I .EQ. NEQ) GO TO 25
C
      F(K)=( X(I)-X(I-1) -A(II) *( ZF(I)-ZF(I-1))) /
     & (( X(I)-X(I-1))
     & **2 +(X(J)-X(J-1))**2+(ZF(I)-ZF(I-1))**2)**0.5/V(I)
     &  +( X(I)-X(I+1) -A(II) *( ZF(I)-ZF(I+1)))/
     & (( X(I)-X(I+1))**2
     & +(X(J)-X(J+1))**2+(ZF(I)-ZF(I+1))**2)**0.5/V(I+1)
C
       GO TO 220
  20  F(K)=(X(I)-X0-A(II)*(ZF(I)-Z0))/(( X(I)-X0 )**2
     &  +(X(J)-Y0)**2 + (ZF(I)-Z0)**2  )**0.5 / V(I)
     &  +( X(I)-X(I+1) -A(II) *( ZF(I)-ZF(I+1)))/
     &    (( X(I)-X(I+1))**2
     &  +(X(J)-X(J+1))**2+(ZF(I)-ZF(I+1))**2)**0.5/V(I+1)
       GO TO 220
C
  25  F(K)=( X(I)-X(I-1) -A(II) *( ZF(I)-ZF(I-1)))/
     & (( X(I)-X(I-1))
     & **2+(X(J)-X(J-1))**2+(ZF(I)-ZF(I-1))**2)**0.5/V(I)
     & +(X(I)-XN1-A(II)*(ZF(I)-ZN1) ) /( (X(I)-XN1)**2
     &  +(X(J)-YN1)**2 + (ZF(I)-ZN1)**2 )**0.5 / V(I+1)
C
 220   IF(IFLAG.EQ.1) WRITE(6,30) NEQ,I,J,K,II,A(II),F(K)
       IF (IFLAG.EQ.1)  WRITE(6,35) (X(LL), LL = 1,N)
 225   CONTINUE
C
       IF (IDIM .EQ. 2) GO TO 300
       IF (IDIM-3) 300, 230, 300
C
 230   N2 = NEQ*2
       NEQ1 = NEQ+1
       DO 245 K = NEQ1, N2
       I = K-NEQ
       J = NEQ+I
       II = IFACE(I)
       IF ( I .EQ. 1) GO TO 40
       IF ( I .EQ. NEQ) GO TO 50
C
```

```
       F(K)=( X(J)-X(J-1) -B(II) *( ZF(I)-ZF(I-1)))
     & /(( X(I)-X(I-1))
     & **2+(X(J)-X(J-1))**2+(ZF(I)-ZF(I-1))**2)**0.5/V(I)
     &  +( X(J)-X(J+1) -B(II) *( ZF(I)-ZF(I+1)))
     & /(( X(I)-X(I+1))**2
     & +(X(J)-X(J+1))**2+(ZF(I)-ZF(I+1))**2)**0.5/V(I+1)
        GO TO 240
C
  40   F(K)=( X(J)-Y0 -B(II)*(ZF(I)-Z0))/( (X(I)-X0)**2
     &  +(X(J)-Y0)**2 + (ZF(I)-Z0)**2 )**0.5 / V(I)
     &  +( X(J)-X(J+1) -B(II) *( ZF(I)-ZF(I+1)))
     &  /(( X(I)-X(I+1))**2
     & +(X(J)-X(J+1))**2+(ZF(I)-ZF(I+1))**2)**0.5/V(I+1)
        GO TO 240
C
  50   F(K)=( X(J)-X(J-1) -B(II) *( ZF(I)-ZF(I-1)))
     & /(( X(I)-X(I-1))
     & **2+(X(J)-X(J-1))**2+(ZF(I)-ZF(I-1))**2)**0.5/V(I)
     &  +( X(J)-YN1-B(II)*(ZF(I)-ZN1))/((X(I)-XN1)**2
     &  +(X(J)-YN1)**2 + (ZF(I)-ZN1)**2 )**0.5 / V(I+1)
C
 240    IF(IFLAG.EQ.1) WRITE(6,30) NEQ,I,J,K,II,A(II),F(K)
        IF (IFLAG.EQ.1)  WRITE(6,35) (X(LL), LL = 1,N)
 245   CONTINUE
C
 300   CONTINUE
C
   30   FORMAT('PARS -- CALFUN', 5I6,2F8.2, F14.6)
   35   FORMAT('X VALUES- CALFUN', 6F12.6)
C
C
       N1 = NEQ
       IF (INDEX(1) .GT. 0) CALL DELETE(X, NEQ, PAR, INDEX)
       IF (INDEX(1) .GT. 0) CALL DELETE(F, N1, PAR, INDEX)
       RETURN
C
C   THIS IS A SPECIAL CASE FOR REFLECTION
C   IN ONLY ONE LAYER
C    F(1) -- PARTIAL DERIVATIVE FOR X(I)
C    F(2) -- PARTIAL DERIVATIVE FOR Y(I)
C
 310   I = NEQ
       J = NEQ+I
       II = IFACE(I)
        F(1)=( X(I)-X0 -A(II) * (ZF(I)-Z0) ) /(( X(I)-X0 )**2
     &  +(X(J)-Y0)**2 + (ZF(I)-Z0)**2  )**0.5 / V(I)
     &  +( X(I)-XN1 -A(II) *(ZF(I)-ZN1) ) /( (X(I)-XN1)**2
     &  +(X(J)-YN1)**2 + (ZF(I)-ZN1)**2 )**0.5 / V(I+1)
C
C
        F(2)=( X(J)-Y0 -B(II) *(ZF(I)-Z0) ) /( (X(I)-X0)**2
     &  +(X(J)-Y0)**2 + (ZF(I)-Z0)**2 )**0.5 / V(I)
     &  +( X(J)-YN1 - B(II) *(ZF(I)-ZN1) )/ ( (X(I)-XN1)**2
     &  +(X(J)-YN1)**2 + (ZF(I)-ZN1)**2 )**0.5 / V(I+1)
```

```
      RETURN
      END
C
      SUBROUTINE READF(IUNIT,NNEQ,IFACE, X,VN1,NFPTS,PAR,
     +  INDEX,NPDER, IDER)
C
C    ROUTINE TO READ THE DATA FROM FILE 7
C
      DIMENSION X(1), PAR(1), V(20)
      INTEGER INDEX(1), IDER(1), IFACE(1)
      COMMON/VV/IDIM,NV,V,IFLAG,IREFR,NORFL,NUFAUL,NUPLAY
C
      READ(IUNIT,100) NNEQ, NFPTS, NPDER
      IF (NFPTS) 20,20,10
   10 READ(IUNIT,100)  (INDEX(I),I=1,NFPTS)
   20 CONTINUE
C
      IF (NPDER) 40,40,30
   30 READ(IUNIT,100)   (IDER(I), I=1,NPDER)
   40 CONTINUE
C
  100 FORMAT(10I6)
C
      DO 50 I=1,NNEQ
      READ(IUNIT,110) IFACE(I), X(I), X(NNEQ+I), V(I)
  110 FORMAT(I6, 10F12.4)
   50 CONTINUE
C
      NV = NNEQ+1
      V(NV) = VN1
C
      IF ( NFPTS .GT. 0) CALL DELETE(X,NNEQ,PAR,INDEX)
      RETURN
      END
      SUBROUTINE TIME(X, Z, V, NEQ, SUM, TNPT)
C
C    FUNCTION TO COMPUTE THE TRAVEL TIME
C
      REAL X(40), Z(20), V(20), TNPT(20)
      COMMON/XYZ/ X0, Y0, Z0, XN1, YN1, ZN1
C
      NEQ1 = NEQ+1
      SUM = 0.0
      DO 100 I=1,NEQ1
      J = NEQ + I
      IF ( I .EQ. 1) GO TO 10
      IF ( I .EQ. NEQ1) GO TO 20
      SUM = SUM+( (X(I)-X(I-1))**2 +(X(J)-X(J-1))**2
     & +(Z(I)-Z(I-1))**2 ) **0.5/V(I)
      TNPT(I) = SUM
      GO TO 100
   10 SUM = SUM+( (X(I)-X0)**2 +(X(J)-Y0)**2
     & +(Z(I)-Z0)**2 )**0.5/ V(I)
      TNPT(I) = SUM
      GO TO 100
 20   SUM = SUM+( (XN1-X(I-1))**2 +(YN1-X(J-1))**2
     & +(ZN1-Z(I-1))**2 ) **0.5/ V(I)

       TNPT(I) = SUM
100   CONTINUE
C
      RETURN
      END
      SUBROUTINE INVERS(NDIM, N, B)
C
C     THIS SUBROUTINE COMPUTES THE INVERSE OF MATRIX B
C     THE OUTPUT OF INVERSE MATRIX IS A
C
C NDIM--THE DIMENSION OF B AS DEFINED IN THE MAIN PROGRAM
C N--THE ORDER OF MATRIX B (I.E. THE NUMBER OF COLUMNS)
C B--INPUT MATRIX TO BE INVERTED
C A-- OUTPUT INVERTED MATRIX
C     RE-ASSIGN A INTO B MATRIX AS OUTPUT
C
      DIMENSION  B(NDIM,N), A(40,40), R(100), C(100)
C
      DO 10 I=1,N
      DO 10 J=1,N
 10   A(I,J) = 0.
C
      DO 40 L=1,N
      DEL = B(L,L)
         DO 30 I=1,L
         C(I)=0.
         R(I)=0.
              DO 20 J=1,L
              C(I)=DBLE(C(I))+DBLE(A(I,J))*DBLE(B(J,L))
 20           R(I)=DBLE(R(I))+DBLE(B(L,J))*DBLE(A(J,I))
 30      DEL = DBLE(DEL) -DBLE(B(L,I))*DBLE(C(I))
C
      C(L)=-1.
      R(L)=-1.
C
      DO 40 I=1,L
      C(I)=C(I)/DEL
      DO 40 J=1,L
      A(I,J)=DBLE(A(I,J))+DBLE(C(I))*DBLE(R(J))
 40   B(I,J) = A(I,J)
C
      RETURN
      END
C
      SUBROUTINE SOLSVD(MDIM,M, N, W,U,V,X,B,RELERR,
     &  CONST, RMATR)
C
C   THIS ROUTINE SOLVES FOR X(N) SUCH THAT
C   ||B-AX|| = MININMUM
C
```

```
      REAL U(MDIM,N),V(MDIM,N),RMATR(MDIM,N),W(N),X(N),B(M)
C
C
C      DO 32 I=1,N
C  32  WRITE(6,322) (V(I,J), J=1,N)
C 322  FORMAT(' MATRIX V ', 6F12.6)
      WRITE(6,323) (W(I), I=1,N)
 323  FORMAT(' VECTOR W ', 6F10.4)
C
C
C   COMPUTE THE ABSOLUTE TOLERANCE, RELERR IS THE RELATIVE
C   ERROR IN THE DATA
C
      TAU = RELERR*W(1)
C
C   COMPUTE THE RANK OF A
C
      IF (W(1) .GE. TAU) GO TO 50
      WRITE(6,340) W(1), TAU
 340  FORMAT(' THE MAX SING. ', F10.6,' LT TAU ', F10.6)
      STOP
  50  CONTINUE
      DO 60 I =2,N
      IF ( W(I) .GE. TAU) GO TO 60
      NRANK = I-1
      COND = W(1)/W(NRANK)
      GO TO 70
  60  CONTINUE
C
      NRANK = N
      COND = W(1)/W(N)
  70  CONTINUE
C
      WRITE(6,345) W(1), TAU
 345  FORMAT('THE MAX SING.= ',F10.6,5X,' TAU= ', F10.6)
      WRITE (6,350) NRANK, COND
 350  FORMAT('PSEDUO RANK= ',I4,5X,'COND. NUMBER= ',E14.6)
C
C     COMPUTE THE SOLUTION
C
      CALL ZERO(X,N)
      DO 110 J=1,NRANK
      S = 0.
         DO 90 I = 1,M
         S = S + DBLE(U(I,J))*DBLE(B(I))
  90     CONTINUE
C
C   APPLY MARQUART DAMPING FACTOR
C
         IF (CONST.LE.0.0) S = S/W(J)
         IF(CONST.GT.0.0)  S=S*W(J)/ (W(J)**2 + CONST)
         DO 100 I = 1,N
            X(I) = DBLE(X(I))+S*V(I,J)
 100     CONTINUE
 110  CONTINUE
      WRITE(6,360)
 360  FORMAT(' THE SOLUTION ARE ')
      WRITE(6,370) (X(I), I=1,N)
 370  FORMAT(4(F10.4,2X))
C
C      CALL VVT( V, MDIM, N, NRANK, W, RMATR, 0)
C
C      WRITE(6,380)
C 380  FORMAT( '  THE RESOLUTION MATRIX ARE')
C      DO 120 I= 1,N
C      WRITE(6,365) (RMATR(I,J), J=1,N)
C 365  FORMAT(12F8.4)
C 120  CONTINUE
C
      RETURN
      END
C
      SUBROUTINE ZERO(X,N)
      DIMENSION X(N)
      DO 10 I = 1,N
      X(I) = 0.
  10  CONTINUE
      RETURN
      END
      SUBROUTINE INSERT(X, NEQ, PAR, INDEX)
C
C    INSERT THE ELEMENTS FORM VECTOR PAR INTO X VECTOR
C
      REAL X(40), PAR(20), XSAVE(40)
      INTEGER INDEX(10)
C
      IF (INDEX(1).EQ.0) RETURN
C
      LXY = 2*NEQ
      DO 100 I=1,LXY
      XSAVE(I) = X(I)
 100  CONTINUE
C
      NPAR = INDEX(1)
      LX = NEQ+ NPAR
      L = 1
      LL = 1
C
      NUM = INDEX(1)+2
      DO 105 I = NUM, 10
 105  INDEX(I) = 0
C
      DO 110 I=1,LX
      IF ( INDEX(L+1) -I) 10, 20, 10
  10  X(I) = XSAVE(LL)
      X(I+LX) = XSAVE(LL+NEQ)
      LL = LL+1
      GO TO 110
```

```
C
  20  X(I) = PAR(L)
      X(I+LX) = PAR(L+NPAR)
      L = L+1
 110  CONTINUE
C
      NEQ = NEQ + NPAR
      RETURN
      END
C
      SUBROUTINE DELETE(X, NEQ, PAR, INDEX)
      REAL X(40), PAR(20), XSAVE(40)
      INTEGER INDEX(10)
C
      IF (INDEX(1).EQ.0) RETURN
C
      LXY = 2*NEQ
      DO 100 I=1,LXY
      XSAVE(I) = X(I)
 100  CONTINUE
C
      L = 1
      LL = 1
      LX = NEQ-INDEX(1)
C
      NUM = INDEX(1)+2
      DO 105 I = NUM, 10
 105  INDEX(I) = 0
C
      DO 110 I=1,NEQ
      IF ( INDEX(L+1) .EQ. I) GO TO 10
      X(LL) = XSAVE(I)
      X(LL+LX) = XSAVE(I+NEQ)
      LL = LL+1
      GO TO 40
C
  10  L = L+1
  40  CONTINUE
C
 110  CONTINUE
      NEQ = NEQ - INDEX(1)
      RETURN
      END
C
C
      SUBROUTINE LINE(X1,Y1,XN1,YN1,FLOC,XCEPT,YCEPT)
      REAL FLOC(1)
C
C   THE PROGRAM FIRST FINDS THE EQUATION OF 2 LINES
C   Y = AX + B, THEN SOLVE THE INTERSECTION POINT
C   BETWEEN THESE TWO LINES
C
      X2 = FLOC(1)
      Y2 = FLOC(2)
      XN2 = FLOC(3)
      YN2 = FLOC(4)
C
      IERR = 3
      IF (ABS(XN1-X1).LE. .1E-5 .AND. ABS(XN2-X2).LE. .1E-5)
     +  IERR = 1
      IF (ABS(YN1-Y1).LE. .1E-5 .AND. ABS(YN2-Y2).LE. .1E-5)
     +  IERR = 2
      GO TO (1,2,3), IERR
    1 WRITE(6,100)
  100 FORMAT(' ERROR RETURN, BOTH LINES // TO Y AXIS ')
      RETURN
    2 WRITE(6,110)
  110 FORMAT(' ERROR RETURN, BOTH LINES // TO X AXIS ')
      RETURN
    3 CONTINUE
C
      IF (ABS(XN1-X1).LE. .1E-5 .OR. ABS(XN2-X2).LE. .1E-5)
     +  GO TO 10
      IF (ABS(YN1-Y1).LE. .1E-5 .OR. ABS(YN2-Y2).LE. .1E-5)
     +  GO TO 20
C
      A1 = (YN1-Y1)/( DBLE(XN1)-DBLE(X1))
      A2 = (YN2-Y2)/( DBLE(XN2)-DBLE(X2))
      B1 = Y1- A1*X1
      B2 = Y2- A2*X2
      XCEPT = (B2-B1)/(A1-A2)
      YCEPT = (A2*B1-A1*B2)/(DBLE(A2)-DBLE(A1))
      GO TO 30
C
   10 IF (ABS(XN1-X1) - .1E-5 ) 11, 11, 12
   11 A1 = 999.
      B1 = X1
      A2 = (YN2-Y2)/( DBLE(XN2)-DBLE(X2))
      B2 = Y2- A2*X2
      XCEPT = X1
      YCEPT = A2*X1 + B2
      GO TO 30
C
   12 A2 = 999.
      B2 = X2
      A1 = (YN1-Y1)/( DBLE(XN1)-DBLE(X1))
      B1 = Y1- A1*X1
      XCEPT = X2
      YCEPT = A1*X2 + B1
      GO TO 30
C
   20 IF (ABS(YN1-Y1) -.1E-5 ) 21, 21, 23
   21 A1 = 0.0
      B1 = Y1
      A2 = (YN2-Y2)/( DBLE(XN2)-DBLE(X2))
      B2 = Y2- A2*X2
      YCEPT = Y1
      XCEPT = (YCEPT-B2)/A2
      GO TO 30
C
  23  CONTINUE
      A2 = 0.0
      B2 = Y2
      A1 = (YN1-Y1)/( DBLE(XN1)-DBLE(X1))
      B1 = Y1- A1*X1
      YCEPT = Y2
      XCEPT = (YCEPT-B1)/A1
  30  CONTINUE
C
      RETURN
      END
      SUBROUTINE VVVT(V, MDIM, M, N, W, DAMP, SIGMA2)
C
C    COMPUTE THE PRODUCT OF TWO MATRIX
C    C = V * V(TRANSPOSE)
C    RW -- EIGENVALUE OF THE RESOLUTION MATRIX
C    CW -- EIGENVALUE OF THE COVARIANCE MATRIX
C
      DIMENSION V(30,30), RMATR(30,30), CMATR(30,30), W(N)
      REAL SUM
C
C
      DO 50 I =1,M
      DO 40 J= 1,M
      SUM = 0.0
      SUM1 = 0.0
C
         DO 30 K = 1,N
         RW = W(K)/ (W(K)+DAMP)
         CW = W(K)/ (W(K)+DAMP)**2
         SUM = SUM + V(I,K)*V(J,K) *RW
         SUM1 = SUM1 + V(I,K)*V(J,K) *CW
  30     CONTINUE
      RMATR(I,J) = SUM
      CMATR(I,J) = SUM1 * SIGMA2
  40  CONTINUE
  50  CONTINUE
C
C  WRITE OUT THE COVARIANCE AND RESOLUTION MATRIX
C
      WRITE(2,500) M, N
      DO 100 I=1,M
      WRITE(2,510) (RMATR(I,J), J=1,N)
 100  CONTINUE
C
      WRITE(2,520)
 520  FORMAT(///, 'COVARIANCE MATRIX')
C
      DO 110 I=1,M
      WRITE(2,510) (CMATR(I,J), J=1,N)
 110  CONTINUE
C
```

```
 500  FORMAT(2I5)
 510  FORMAT(12F9.3)
      RETURN
      END
      SUBROUTINE PDERR(X,Z,NEQ,ILAYER,IVPT,FCN,LAST,NPDER)
C
C   ILAYER --LAYER TO COMPUTE THE IMPROVEMENT OF SOLUTION
C   FCN -- STORE THE PARTIAL DERIVATIVE
C   THIS ROUTINE IS DESIGNED FOR THE LAYER WHICH HAS
C   TWO FAULTS.
C
C    IF LAST = 99 -- HEAD WAVE PROPAGATE ONE PLANE LAYER
C        WITHOUT ANY STRUCTURE
C    IF LAST = 1 -- COMPUTE THE PARTIAL DERIVATIVE OF THE
C       MIDDLE LAYER FOR THE HORST STRUCTURE
C
      DIMENSION X(1), Z(1), FCN(1), V(20)
      COMMON/XYZ/ X0, Y0, Z0, XN1, YN1, ZN1
      COMMON/VV/IDIM,NV,V,IFLAG,IREFR,NORFL,NUFAUL,NUPLAY
C
      T3 = 0.0
C
      DO 5 K =1,4
      FCN(K) = 0.0
  5   CONTINUE
C
C   MAKE SURE THE P.DERATIVE TAKEN AT THE RIGHT POINT
C  DESIGN FOR 2D FAULT HAVING 3 DERIVATIVES.
      IMID = -99
      IF ( NPDER.EQ.3) IMID = 1
C
      I = ILAYER
      J = NEQ+I
C
C   LAST = IMID -- ONLY THE DERIVATIVE OF THE VELOCITY
C   OF THE MIDDLE LAYER OF THE HORST STRUCTURE
C
      IF ( LAST.EQ.IMID) GO TO 50
      IF ( I.EQ.1) GO TO 20
      IF ( I.EQ.NEQ) GO TO 30
C
       T1=-(Z(I)-Z(I-1))/((X(I)-X(I-1))**2+(X(J)-X(J-1))**2
     &  +(Z(I)-Z(I-1))**2)**0.5/V(I)
C
        T2=(Z(I+1)-Z(I))/((X(I+1)-X(I))**2+(X(J+1)-X(J))**2
     &     +(Z(I+1)-Z(I))**2) **0.5/V(I+1)
C
C   T3 IS USED FOR PLANE LAYER
C
      I = I+2
      J = J+2
       IF ( LAST.EQ.99)
     & T3=(Z(I)-Z(I-1))/((X(I)-X(I-1))**2+(X(J)-X(J-1))**2
     &  +(Z(I)-Z(I-1))**2)**0.5/V(I)
```

```
C
      GO TO 40
  20  T1=-(Z(I)-Z0)/((X(I)-X0)**2+(X(J)-Y0)**2+(Z(I)-Z0)**2)
     &  **0.5/V(I)
      T2=(Z(I+1)-Z(I))/((X(I+1)-X(I))**2+(X(J+1)-X(J))**2
     &   +(Z(I+1)-Z(I))**2) **0.5/V(I+1)
C
      I = I+1
      J = J+1
      IF ( LAST.EQ.99)
     & T3=(ZN1-Z(I))/((XN1-X(I))**2+(YN1-X(J))**2
     & +(ZN1-Z(I))**2 )  **0.5/V(I+1)
C
      GO TO 40
C
  30  T1=-(Z(I)-Z(I-1))/((X(I)-X(I-1))**2+(X(J)-X(J-1))
     & **2+(Z(I)-Z(I-1))**2) **0.5/V(I)
      T2=(ZN1-Z(I))/((XN1-X(I))**2+(YN1-X(J))**2+(ZN1-Z(I))
     &  **2)**0.5/V(I+1)
  40  CONTINUE
C
C     IF LAST=99 MEANS ONLY THE HEAD WAVE PROPAGATE THRU
C     A PLANE
C
      I = ILAYER
      J = NEQ+I
      T1 = T1+T2
      FCN(1) = X(I)*T1 + X(I+1) * T3
      FCN(2) = X(J)*T1 + X(J+1) * T3
      FCN(3) = T1 + T3
C
C   COMPUTE THE DERIVATIVE OF THE VELOCITY
C
  50  CONTINUE
C
      I = IVPT
      J = NEQ+I
C
      T4=-((X(I)-X(I-1))**2+(X(J)-X(J-1))**2
     &  +(Z(I)-Z(I-1))**2)**0.5/ V(I)**2

C
C 50   T3=-((X(I)-X0)**2+(X(J)-Y0)**2+(Z(I)-Z0)**2)
C      &  **0.5/ V(I)**2
C       GO TO 70
C
C  60  T3=-((X(I)-X(I-1))**2+(X(J)-X(J-1))**2
C      & +(Z(I)-Z(I-1))**2) **0.5/V(I)**2
C  70  CONTINUE
C
      FCN(4) = T4
C
      RETURN
      END
      SUBROUTINE PDERL(X, Z, NEQ, ILAYER, IVPT, FCN, IDF)
C
C
C    ILAYER --LAYER TO COMPUTE THE IMPROVEMENT OF SOLUTION
C    FCN -- STORE THE PARTIAL DERIVATIVE
C    THIS ROUTINE IS DESIGNED FOR THE REFLECTED DATA
C
      DIMENSION X(1), Z(1), FCN(1), V(20)
      COMMON/XYZ/ X0, Y0, Z0, XN1, YN1, ZN1
      COMMON/VV/IDIM,NV,V,IFLAG,IREFR,NORFL,NUFAUL,NUPLAY
C
C    MAKE SURE THE P.DERATIVE TAKEN AT THE RIGHT POINT
C
      I = ILAYER
      J = NEQ+I
C
      IF ( I.EQ.1) GO TO 20
      IF ( I.EQ.NEQ) GO TO 30
C
      T1=-(Z(I)-Z(I-1))/((X(I)-X(I-1))**2+(X(J)-X(J-1))**2
     &    +(Z(I)-Z(I-1))**2)**0.5/V(I)
      T2= (Z(I+1)-Z(I))/((X(I+1)-X(I))**2+(X(J+1)-X(J))**2
     &    +(Z(I+1)-Z(I))**2) **0.5/V(I+1)
      T3= -((X(I)-X(I-1))**2+(X(J)-X(J-1))**2
     &    +(Z(I)-Z(I-1))**2)**0.5/ V(I)**2
      T4= -( (X(I+1)-X(I))**2+(X(J+1)-X(J))**2
     &    +(Z(I+1)-Z(I))**2) **0.5/V(I+1)**2
C
      GO TO 40
   20 T1= -(Z(I)-Z0)/((X(I)-X0)**2+(X(J)-Y0)**2+(Z(I)-Z0)
     & **2) **0.5/V(I)
      T2= (Z(I+1)-Z(I))/((X(I+1)-X(I))**2+(X(J+1)-X(J))**2
     &  +(Z(I+1)-Z(I))**2) **0.5/V(I+1)
      T3= -((X(I)-X0)**2+(X(J)-Y0)**2+(Z(I)-Z0)**2)
     &  **0.5/ (V(I)**2)
      T4= -((X(I+1)-X(I))**2+(X(J+1)-X(J))**2
     &   +(Z(I+1)-Z(I))**2) **0.5/ (V(I+1)**2)
C
      GO TO 40
C
   30 T1= -(Z(I)-Z(I-1))/((X(I)-X(I-1))**2+(X(J)-X(J-1))**2
     &    +(Z(I)-Z(I-1))**2) **0.5/V(I)
      T2= (ZN1-Z(I))/((XN1-X(I))**2+(YN1-X(J))**2+(ZN1-Z(I))
     &    **2)**0.5/V(I+1)
      T3= -((X(I)-X(I-1))**2+(X(J)-X(J-1))**2
     &    +(Z(I)-Z(I-1))**2) **0.5/ (V(I)**2)
      T4= -((XN1-X(I))**2+(YN1-X(J))**2+(ZN1-Z(I))**2)
     &  **0.5/ (V(I+1)**2)
   40 CONTINUE
C
C    IF NUPLAY.EQ.0 -- SPECIAL CASE : NO UPPER LAYER
C
```

```
      IF(NUPLAY.NE.0) T1=T1+T2
      IF(NUPLAY.EQ.0) T1=T1*2
      FCN(1) = X(I)*T1
      FCN(2) = X(J)*T1
      FCN(3) = T1
C
      FCN(4) = T4 + T3
      IF (NORFL.LE.0) FCN(4) = 0.
C
C    THE CASE OF CRUSTAL FAULT FOR REFLECTION DATA
C
      IF ( IABS(NUFAUL)-IDF) 43,42,43
   42 FCN(1) = 0.0
      FCN(2) = 0.0
      FCN(3) = 0.0
      FCN(4) = T3
   43 CONTINUE
C
C
      IDUM =1
      IF (IDUM.EQ.1) GO TO 80
      I = IVPT - 1
      J = NEQ+I
      IF ( I.EQ.1) GO TO 50
      IF ( I.EQ.NEQ) GO TO 60
C
      T3=-((X(I)-X(I-1))**2+(X(J)-X(J-1))**2
     &  +(Z(I)-Z(I-1))**2)**0.5/ V(I+1)**2
C     I= I+1
C     T4=-((X(I)-X(I-1))**2+(X(J)-X(J-1))**2
C    &  +(Z(I)-Z(I-1))**2)**0.5/ V(I)**2
      GO TO 70
C
 50   T3=-((X(I)-X0)**2+(X(J)-Y0)**2+(Z(I)-Z0)**2)
     &  **0.5/ V(I)**2
      T4 = -(( XN1-X(I))**2+(YN1-X(J))**2+(ZN1-Z(I))**2)
     &  **0.5/ V(I+1)**2
C
  60  CONTINUE
      GO TO 70
C
C
C 60  T3=-((X(I)-X(I-1))**2+(X(J)-X(J-1))**2
C   & +(Z(I)-Z(I-1))**2) **0.5/V(I)**2
  70  CONTINUE
C
      FCN(4) = T3 + T4
C
  80  CONTINUE
      RETURN
      END
      SUBROUTINE SDERR(MDIM, M, N, A, X, B, RERR)
      DIMENSION A(MDIM,N), X(M), B(M)
C
```

```
      RSQ = 0.
      DO 20 I=1,M
         RI = 0.
           DO 10 J=1,N
              RI = RI+X(J)*A(I,J)
  10       CONTINUE
      RSQ = RSQ + (RI-B(I))**2
  20  CONTINUE
C
      RERR = SQRT(RSQ/FLOAT(M))
      RETURN
      END
C
      SUBROUTINE SCALM(X, NROW, NCOL, IX, D)
C
C   IX -- ROW DIMENSION OF X IN THE CALLING PROGRAM
C   D -- SCALING FACTORS OF IN EACH COL. OF X MATRIX
C
      REAL X(IX,NCOL), D(NCOL)
C
      DO 50 J =1,NCOL
        SUM = 0.0
C
        DO 40 I=1, NROW
          SUM = SUM+X(I,J)**2
  40    CONTINUE
        D(J)= SQRT(SUM)
C
        DO 30 I=1,NROW
          X(I,J) =X(I,J)/D(J)
  30    CONTINUE
C
  50  CONTINUE
      RETURN
      END
C
C
C   SUBROUTINE DAMPR -- COMPUTE THE DAMPING FACTOR OF THE
C   RIDGE ESTIMATOR FROM HOERL & KENNARD METHOD(1975)
C
      SUBROUTINE DAMPR(X,NROW,NCOL,IX,Y,D,B,DAMP,ITER)
C
C   SOLVE FOR LEAST SQUARE SOLUTION OF    Y= XB
C   Y -- NUMBER OF OBSERVATION = NROW
C   X -- JOCABIAN MATRIX (IN THIS CASE)
C   B -- THE SOLUTION OF THE LEAST SQUARE MATRIX(OUTPUT)
C   D -- THE COLUMN SCALE FACTOR (INPUT)
C   K -- DAMPING RIDGE FACTOR
      REAL X(IX,NCOL), B(NCOL), Y(NROW), D(NCOL)
      REAL XTX(30,30), XSTAR(300,300), WORK(300)
      REAL V(30,30), VT(30,30), C(30), W(30), ALPHA(30)
      REAL ALPSQ(30)
      REAL VK(30)
C
```

```
      IXX = 300
      IC = 30
      IVV = 30
C
C   COMPUTE X(TRANPOSE)*X  VMULFM -- FROM IMSL LIBRARY
C
      CALL VMULFM(X,X,NROW,NCOL,NCOL,IX,IX,XTX,IC,IERR)
C
C   COMPUTE SINGULAR VALUE DECOMPOSITION
C
      CALL SVD(IC,NCOL,NCOL,XTX,W,.TRUE.,V,.TRUE.,VT,
     &  IERR,WORK)
      IF ( IERR.EQ.0) GO TO 10
      WRITE (6,100) IERR
  100 FORMAT( ' ERROR FROM SVD  IERR=', I4)
      RETURN
C
C
   10 CALL VMULFF(X,V,NROW,NCOL,NCOL,IX,IC,XSTAR,IXX,IERR)
C
C       DO 101 I=1,NROW
C       WRITE(6,102) (XSTAR(I,J), J=1,NCOL)
C 102   FORMAT(' XSTAR=', 12F9.5)
C 101   CONTINUE
C
C
      L = NCOL
      M = NROW
C
C   COMPUTE XSTAR*Y
C
      CALL VMULFM(XSTAR,Y,NROW,NCOL, 1,IXX,NROW,C,IC,IERR)
C
      ALPSUM = 0.0
      DO 20 I=1,L
      ALPHA(I) =  C(I)/W(I)
      ALPSQ(I) = ALPHA(I)**2
      ALPSUM = ALPSUM+ALPSQ(I)
      WRITE(6,160) ALPHA(I), C(I), W(I)
   20 CONTINUE
C
C     CALL VABMXF(ALPSQ, L, 1, JV, VMAX)
C
      YSUM = 0.0
      DO 30 I=1,NROW
      YSUM=YSUM+ Y(I)*Y(I)
   30 CONTINUE
C
      TSUM = 0.0
      DO 40 I=1,NCOL
      TSUM=TSUM + C(I)* ALPHA(I)
   40 CONTINUE
C
      RSQ = YSUM-TSUM
      SIGMA2 = (YSUM-TSUM)/(NROW-NCOL)
C
C    THE DAMPING FACTOR
C
      RKSUM = 0.0
C
      DO 45 J=1,NCOL
      VK(J) = SIGMA2/ALPSQ(J)
   45 CONTINUE
C
      WRITE(6,106) (VK(J), J=1,NCOL)
  106 FORMAT(' K VALUES= ', 5F15.5)
C
C  TEST WHETHER TO USE DAMPING FACTOR OR LS
C
      ERROR = 0.05
      TEST1 =  (ERROR **2) *NROW
      DAMP = NCOL*SIGMA2/ALPSUM
      WRITE(6,110) DAMP, SIGMA2, RSQ
      WRITE(4,110) DAMP, SIGMA2, RSQ
C
      IF (RSQ.LT. TEST1) DAMP = 0.0
      WRITE(6,110) DAMP, SIGMA2, RSQ
      WRITE(4,110) DAMP, SIGMA2, RSQ
  110 FORMAT(' DAMPING FACTOR =', F9.6,'  SIGMA2= ', E11.4,
     &  '   RESIDUAL SUM= ', E11.4)
C
      CALL VVVT(V, IXX, NCOL, NCOL, W, DAMP, SIGMA2)
C
C
C    COMPUTE THE SOLUTION OF B
C
      DO 50 J=1,NCOL
      ALPHA(J) = W(J)/ ( W(J)+DAMP) * ALPHA(J)
   50 CONTINUE
C
      WRITE(1,160) (ALPHA(J), J=1,NCOL)
  160 FORMAT(' ALPHA=', 4F12.5)
C
      DO 170 I = 1, NCOL
      WRITE(1,180) (V(I,J), J=1,NCOL)
  180 FORMAT( 'V', 12F10.5)
  170 CONTINUE
C
      WRITE(6,120) (W(J), J=1,NCOL)
  120 FORMAT( ' EIGENVALUES=', 4F12.5)
      CALL VMULFF(V,ALPHA,L,L, 1,IC,IC,B,L,IERR)
C
C   TRANSFOR THE SOLUTION FROM STANDARDIZATION TO
C   THE ORIGINAL MODEL
C
      DO 60 J = 1,L
      B(J) = B(J)/D(J)
   60 CONTINUE
```

```
C
      WRITE(6,130) ( B(J), J=1,L)
  130 FORMAT(' SOLUTION=', 4F12.5)
C
      RETURN
      END
```

```
C
C   THIS PROGRAM COMPUTES SEISMIC RAY TRACING WITH SPECIFIED
C   END POINTS OF CONSTANT VELOCITY AND POLYNOMIAL
C   SURFACES.
C
C    IMPROVEMENT OF MODEL BY DAMPED LEAST-SQUARES ITERATIONS
C
C
      DIMENSION X1(40), A(10,10)
      DIMENSION X(40),Z(20),V(20),VT(20),F(40),FCN(20)
      DIMENSION XRCR(100),YRCR(100),ZRCR(100), AZM(100)
      DIMENSION DIST(100),RMATR(300,20),W(20)
      DIMENSION TOBS(100),T(100),TERR(300),TNPT(20)
      DIMENSION WK(3000),PAR(20),AJINV(40,40),COEFF(20)
      REAL AMATRX(300,20), U(300,20), V1(300,20)
      REAL SCALE(20), RANDM(100)
      INTEGER IFACE(20),IDER(20)
      INTEGER IVDER(20), ICHAR(70), ID(140)
      COMMON/ABCD/ A, NSURF, IFACE
      COMMON X
      COMMON/XYZ/ X0, Y0, Z0, XN1, YN1, ZN1
      COMMON/VV/ V, NV, IFLAG
      EXTERNAL CALFUN
      DATA COEFF/20*0.0/
C
C     UNIT 2 -- OUTPUT FOR RESOLUTION MATRIX
C               AND COVARIANCE MATRIX
C     UNIT 3 -- OUTPUT FOR PLOTTING TRAVEL TIME CURVES
C     UNIT 4 -- *SINK*
C     UNIT 5 -- INPUT DATA
C     UNIT 6 -- OUTPUT DATA
C     UNIT 7 -- INPUT DATA FOR ITERATION IF IREAD=99
C     UNIT 8 -- TEMPORARY STORE FILE FOR UNIT 7
C
C
   10 FORMAT(10I6)
   12 FORMAT(I5, F14.6, 10E16.6 )
   14 FORMAT(12F10.5)
   13 FORMAT(10F10.5)
   15 FORMAT(2I6, 6E16.6)
   24 FORMAT(A4)
   30 FORMAT( 12F10.4)
   31 FORMAT(10F14.4)
   32 FORMAT(11F11.3)
   33 FORMAT(I6,2X,12F9.4)
   37 FORMAT(I6,12F9.3/12F9.3)
   40 FORMAT( I6, 10F12.4)
   55 FORMAT('0  INPUT OF X, Y, V, ',I7, 4F10.4)
   54 FORMAT ('  THE INDEX OF I  FROM NLSYST =', I3)
   67 FORMAT('0  TIME FROM MODEL ', 10F10.4)
   68 FORMAT('0  TIME RESIDUALS ', 10F10.4)
   69 FORMAT('STANDARD ERROR= ',F10.5,'  ERROR MEAN=',
     &   F10.5)
   70 FORMAT(' DAMPING FACTOR =', F10.5)
   71 FORMAT(' ERROR  -- NPTS LE. NC' )
   72 FORMAT(' ERROR RETURN FROM SVD ROUTINE', I6)
   73 FORMAT(' ERROR ESTIMATE FROM SVD', F12.5)
   74 FORMAT(' OLD COEFF OF MODELS ', 5F10.5 )
   76 FORMAT('INPUT IF IRC'/,
     + ' INPUT NPARS(I6) ')
   77 FORMAT(10I6)
   79 FORMAT(2E12.6)
   80 FORMAT(' NEW COEFF OF MODELS ', 5F10.5 )
C
C   WK -- WORK VECTOR LENGTH
C   MODIT -- NUMBER OF ITERATIONS FOR THE MODEL
C   MAXIT -- MAX NUMBER OF ITERATIONS FOR THE NONLINEAR
C            SYSTEMS.
C
C     DELT = THE STEP SIZE FOR THE PARTIAL DERIVATIVE
C     XTOL = THE TOLERANCE OF X
C     FTOL = THE TOLERANCE OF FUNCTION CALFUN
C     MAXFUN = MAX NUMBER TO CALL FUNCTION CALFUN
C     DMAX = GENERAL ESTIMATE OF DISTANCE FROM SOLUTION
C     ACC = ACCURACY
C     KLAYER = THE K-LAYER(PLANE) TO START WITH
C     NSURF = MAX NUMBER OF PLANE IN THE MODEL
C     IF (NRANDOM .LE.0) NO RANDOM NOISE APPLIED TO DATA
C     RDELT -- STANDARD DEVIATION OF RANDOM NOISE
C     IORDER -- ORDER OF THE POLYNOMIAL
C
      IA = 10
      NCMAX = 11
      MDIM = 300
      NDIM = 40
      RAD = 3.14159/180.0
      IUNIT = 7
C
C     READ IN PARAMETERS FOR THE NONLINEAR EQNS
C
      DO 19 I=1,40
      X(I) = 0.0
      F(I) = 0.0
   19 CONTINUE
C
      READ(5,10) IFLAG,IPRINT,JACOB,NSHOT,NUPLAY,IHOERL
      READ(5,15) MODIT,MAXIT,DELTA,XTOL,FTOL,TTOL,RDELT
      WRITE(6,15) MODIT,MAXIT,DELTA,XTOL,FTOL,TTOL,RDELT
      READ(5,12) MAXFUN, DMAX, ACC, RELERR,CONST,DFACTR
      WRITE(6,12) MAXFUN, DMAX, ACC, RELERR,CONST,DFACTR
      READ(5,10) KLAYER, NSURF, NRANDM, IORDER
      WRITE(6,10)  KLAYER, NSURF, NRANDM, IORDER
C
C   GENERATE RANDOM NOISE
C
      IF(NRANDM.GT.0) CALL RANDOM( NRANDM, RDELT, RANDM)
C
```

```
C    READ THE SURFACE COEFFS
C
C    READ IN INTERFACE INFORMATION
C
      NCMAX1 = NCMAX -1
      DO 105 I= 1, NSURF
        DO 100 J=1,IA
 100   A(I,J) = 0.0
C
      READ(5,14) (A(I,J), J=1,IA), VT(I)
      WRITE(6,14) (A(I,J), J=1,IA), VT(I)
 105  CONTINUE
C
      DO 400 L= KLAYER, NSURF
C
         DO 110 J=1,20
         DO 110 I=1,MDIM
         AMATRX(I,J)=0.0
 110     CONTINUE
C
C    NEQ = POINTS OF VERTICES IN THE PLANE
C    NPTS = NUMBER OF RECIEVERS
C
        ERSAV = -999
        ITER = -1
 499    ITER = ITER+1
        TMEAN = 0.0
        ERROR = 0.0
        ICNT =0
        ICT = 0
        NPDMAX = 0
        KR = 0
C
        IF (ITER) 406,406,403
 403    NUM = 4+NSURF
        REWIND 5
C
        DO 404 JJ1 = 1,NUM
        READ(5,24) DUM
 404    CONTINUE
C
C   READ IN UPDATED INPUT IF ITER>0
C
        REWIND 7
        REWIND 8
 406    CONTINUE
C
      DO 410 JJ=1,NSHOT
C
C  NPDER -- NUMBER OF PARTIAL DERIVATIVE
C  ISRCR -- INTERCHANGE THE SHOT WITH THE RECIEVER
C  IREAD =99  READ IN INPUT FROM FILE 7
C  IOFSET = 0, USED IN ROUTINE CHGMOD AS ZERO OFFSET
C  IOFSHT = 0, MAKE SHOT AND RCR THE SAME LOCATION
```

```
C
      READ(5,10)NEQ,NPTS,NPDER,ISRCR,IREAD,INDEX,IOFSET,
     &  IOFSHT
      IF (NPDER .GT. NPDMAX) NPDMAX=NPDER
C
C     IF (IREAD.EQ.99) GO TO 143
C
C
C
        IF (NPDER) 138,138,137
 137    READ(5,10) (IDER(I),I=1,NPDER)
 138    CONTINUE
C
C    (X0,Y0,Z0) -- SOURCE  (XN1, YN1, ZN1) -- DETECTOR
C
C   IF Z0 IS NEGATIVE -- Z0  IS ABOVE SEA LEVEL
C
      READ(5,40) ITEMP, X0, Y0, Z0, VN1
C
C
      XSAVE = X0
      YSAVE = Y0
      ZSAVE = Z0
C
C   IF ZRCR IS NEGATIVE -- ZRCR IS ABOVE SEA LEVEL
C
      DO 112 K = 1, NPTS
      READ(5,40) ID(K), XRCR(K),YRCR(K), ZRCR(K), TOBS(K)
C     ZRCR(K) = 0.0
C
 112  CONTINUE
C
C    READ IN INITIAL SOLUTION FOR THE RAY-TRACING
C
      DO 140 I = 1,NEQ
      READ(5,40) IFACE(I), X(I),X(NEQ+I), V(I)
      WRITE(6,55) IFACE(I), X(I),X(NEQ+I), V(I)
 140  CONTINUE
 143  CONTINUE
C
C
      IF(NRANDM.LE.0) GO TO 119
C
      DO 118 K=1,NPTS
        KR = KR+1
        TOBS(K) = TOBS(K) +RANDM(KR)
 118  CONTINUE
 119  CONTINUE
C
C
      NV = NEQ+1
      V(NV) = VN1
C
C
      DO 430 J= 1, NPTS
      XN1 = XRCR(J)
      YN1 = YRCR(J)
      ZN1 = ZRCR(J)
      IDUM = 0
C
      IF (ISRCR) 306,306,305
C
C   INTERCHANGE BETWEEN SHOT AND RECIEVER LOCATION
C
 305  X0 = XN1
      Y0 = YN1
      Z0 = ZN1
      XN1 = XSAVE
      YN1 = YSAVE
      ZN1 = ZSAVE
 306  CONTINUE
C
C
      IF (IOFSHT) 423,422,423
 422  X0 = XN1
      Y0 = YN1
 423  CONTINUE
C
       IF (IREAD.EQ.99 )
     + CALL READF(IUNIT,NEQ,IFACE,X,VN1,INDEX,NPDER,IDER)
C
C  IN 3-D NEED TO SOLVE NEQ*2 LINEAR EQUATIONS
C
      NEQ1 = NEQ
      IF (INDEX .EQ. 3) NEQ1= NEQ*2
       WRITE(6,32) (V(I),I=1,NV)
C
C
       IF (ITER) 158,158,156
 156    DO 157 I=1,NPDER
        IVPT = IDER(I)
        J1 = IFACE(IDER(I))
C
C   ASSIGN VELOCITY FOR REFLCETION
C
          V(IVPT) = VT(J1)
          V(IVPT+1) = VT(J1)
C
C
C        WRITE(6,90) IVPT, J1, V(IVPT), VT(J1)
C 90    FORMAT(' VTEST ', 2I5, 2F10.4)
 157    CONTINUE
 158   CONTINUE
C
C   SOLVE THE SYSTEM OF NON-LINEAR EQUATION
C
C   ROUTINE NS01A CAN BE FOUND IN THE FOLLOWING
C   REFERENCE:
C  POWELL, M. J., A HYBRID METHOD FOR NONLINEAR EQUATIONS,
C  IN RABINOWITZ, P., ED., NUMERICAL METHODS FOR
C  NONLINEAR ALEGRAIC EQUATIONS, GORDON AND BREACH INC.
C
        CALL NS01A(NEQ1,X,F,AJINV,NDIM,DELTA,DMAX, ACC,
      + MAXFUN, IPRINT, WK, INDEX)
C
C
        LX = 2*NEQ
        WRITE(6,32) (X(I), I=1,LX)
C
       DO 440 I=1,NEQ
 440   Z(I) = ZF(I)
       WRITE(6,33) ID(J), ( Z(I), I=1,NEQ)
C
       WRITE(1,37)ID(J),X0,Y0,Z0,(X(I),X(I+NEQ),
      &  Z(I),I=1,NEQ),XN1,YN1, ZN1
C
       CALL TIME(X, Z, V, NEQ, TSUM, TNPT)
       T(J) = TSUM
C
C   SET UP THE JACOBIAN MATRIX
C   IDF -- THE ID NUMBER OF THE INTERFACE
C
       IF ( JACOB-99) 449,445,449
 445   IF( NPDER.LE.0) GO TO 449
       ICNT= ICNT+1
         DO 446 IK = 1,NPDER
         K1 = IDER(IK)
         IDF = IFACE(K1)
C
C   PDERL -- ROUTINE TO COMPUTE DERIVATIVES
C
         IF(IORDER.EQ.1)CALL PDER1(X,Z,NEQ,K1,FCN,INDEX,
      &  NCMAX,IOFSET)
         IF(IORDER.EQ.2)CALL PDER2(X,Z,NEQ,K1,FCN,INDEX,
      &  NCMAX,IOFSET)
         IF(IORDER.EQ.3)CALL PDER3(X,Z,NEQ,K1,FCN,INDEX,
      &  NCMAX,IOFSET)
C
            DO 444 I=1,NCMAX
 444        AMATRX(ICNT,I) = FCN(I)
 446      CONTINUE
C
C      WRITE(1,32) (AMATRX(ICNT,I),I=1,NCMAX)
 449   CONTINUE
C
       WRITE(8,10) NEQ, NPDER, INDEX, ID(J)
C
       IF (NPDER) 338,338,337
 337   WRITE(8,10) (IDER(I),I=1,NPDER)
 338   CONTINUE
C
C
        DO 345 I = 1, NEQ
       WRITE(8,40) IFACE(I),X(I),X(NEQ+I),V(I),Z(I)
  345  CONTINUE
C
 430  CONTINUE
C
       WRITE(6,67) (T(I), I=1,NPTS)
C    COMPUTE ERROR ESTIMATE
C
      DO 450 I = 1, NPTS
      ICT = ICT+1
      TERR(ICT) = TOBS(I)- T(I)
      TMEAN = TMEAN + TERR(ICT)
      ERROR = ERROR + TERR(ICT)**2
C
C    USE FOR PLOTTING 3-D TRAVEL TIME CURVES
C
      WRITE(3,40)ID(I),XRCR(I),YRCR(I),ZRCR(I),T(I),TOBS(I),
     &  TERR(ICT)
C
 450  CONTINUE
C
 410  CONTINUE
      TAVE = TMEAN/ICT
C
       WRITE(6,68) (TERR(I), I=1,ICT)
       WRITE(4,68) (TERR(I), I=1,ICT)
      ERROR = (ERROR/ICT)**0.5
      WRITE(6,69) ERROR,TAVE
      WRITE(4,69) ERROR,TAVE
      IF (ERROR .LE. TTOL) GO TO 400
C
      CONST = CONST*DFACTR
C     IF (ERROR .GE. ERSAV ) CONST = CONST/DFACTR
      WRITE (6,70) CONST
      WRITE (4,70) CONST
      ERSAV = ERROR
 465  CONTINUE
C
C
C
      IF (ITER .GE. MODIT) GO TO 710
C
      IF (JACOB-99) 469,466,469
 466  IF( ICNT .GE. NCMAX) GO TO 467
      WRITE(6,71) ICNT, NCMAX
      STOP
C
 467  CONTINUE
C
      IF ( IHOERL .LE. 0) GO TO 473
C
      CALL SCALM(AMATRX,ICNT,NCMAX,MDIM,SCALE)
      DO 461 I=1,ICNT
C     WRITE(1,32) (AMATRX(I,LK), LK=1,NCMAX)
```

```
 461  CONTINUE
      CALL DAMPR(AMATRX,ICNT,NCMAX,MDIM,TERR,SCALE,COEFF,
     &  DAMPF,ITER)
C
      IF ( IHOERL .GT.0 ) GO TO 472
C
C   COMPUTE THE EIGENVALUES AND EIGENVECTORS
C
C   COMPUTE THE EIGENVALUES AND EIGENVECTORS
C   THE ROUTINE SVD CAN BE FOUND AT THE FOLLOWING
C   REFERENCE:
C  FORSYTHE, G. E. MALCOLM, M., AND MOLER, C., 1977,
C  COMPUTER METHODS FOR  MATHEMATICAL COMPUTATIONS:
C  PRENTICE HALL, ENGLEWOODCLIFFS, N. J.
C
C
 473  CALL SVD(MDIM,ICNT,NCMAX,AMATRX,W,.TRUE.,U,.TRUE.,
     &  V1, IERR, WK)
C
C         DO 190 I=1,ICNT
C         WRITE(1) (AMATRX(I,I1), I1=1,NCMAX)
C 190     CONTINUE
C
C         WRITE(1) (TERR(I),I=1,ICNT)
C
       IF (IERR .EQ. 0) GO TO 468
       WRITE(6,72) IERR
       STOP
C
 468   CONTINUE
C
C    SOLVE FOR LEAST SQUARE SOLUTION
C
       CALL SOLSVD(MDIM,ICNT,NCMAX,W,U,V1,COEFF,TERR,
      & RELERR, CONST, RMATR)
C
C    COMPUTE THE STANDARD ESTIMATE FROM SVD
C
       CALL SDERR(MDIM,ICNT,NCMAX,AMATRX,COEFF,TERR,RERR)
       WRITE(4,73) RERR
       WRITE(6,73) RERR
C
C    UPDATE THE CHANGE OF THE PARAMETERS
C
C
 472     CONTINUE
C
         IK = NUPLAY+1
C        NMODEL = NCMAX/NCMAX + IK - 1
C
        IF(IORDER.EQ.1)CALL CHGM1(IK,A,IA,NCMAX,VT,COEFF,
       & INDEX,IOFSET)
        IF(IORDER.EQ.2)CALL CHGM2(IK,A,IA,NCMAX,VT,COEFF,
       & INDEX,IOFSET)
      IF(IORDER.EQ.3)CALL CHGM3(IK,A,IA,NCMAX,VT,COEFF,
     & INDEX,IOFSET)
C
 469  CONTINUE
C
C
      WRITE(4,76)
      READ(4,77) IRC, NPARS
      IF (NPARS .GT. 0) READ(4,79) ACC
      IF ( IRC .LE. 0) GO TO 800
C
        REWIND 7
        REWIND 8
C
C   UPDATE THE INPUT INFORMATION
C
        DO 494 I=1,999
        READ(8,496,END=495) ICHAR
        WRITE(7,496) ICHAR
 496    FORMAT(100A4)
 494     CONTINUE
 495     CONTINUE
C
C
      GO TO 499
C
C
 400  CONTINUE
C
      GO TO 800
 700  WRITE(6, 705) L, ITER
 705  FORMAT(' ERROR',' LAYER = ',I3,4X,'ITER= ',I3)
      GO TO 800
 710  WRITE(6, 715) L
 715  FORMAT('MODEL ITERATIONS  ','LAYER = ', I3, 4X)
 800  CONTINUE
C
      WRITE(6,808) ITER
 808  FORMAT(' THE NUMBER OF ITERATIONS =', I3)
      WRITE (6, 810)
 810  FORMAT('0  FINAL MODEL OF PLANE COEFFS' )
      WRITE(6,820)
 820  FORMAT(10X,'A',3X, 10X,'B',3X, 10X,'C',3X, 10X,'D',
     & 10X, 'VELOCITY')
      DO 830 I =1, NSURF
 830   WRITE(6,14) (A(I,J), J=1,IA), VT(I)
      STOP
      END
C
      REAL FUNCTION ZF(I)
      DIMENSION X(40), A(10,10), V(20)
      INTEGER IFACE(20)
      COMMON/ABCD/ A,NSURF,IFACE
      COMMON/VV/ V,NV,IFLAG
      COMMON X
      NEQ = NV-1
      J = NEQ+I
      K = IFACE(I)
C
      ZF = -(A(K,2)*X(J)**3+A(K,3)*X(J)**2+A(K,4)*X(J)
     &       +A(K,5)*X(I)*X(J)**2+A(K,6)*X(J)*X(I)**2
     &       +A(K,7)*X(I)*X(J) + A(K,8)*X(I)**3
     &       +A(K,9)*X(I)**2 + A(K,10)*X(I) ) - A(K,1)
C
C       IF (IFLAG .EQ.1 ) WRITE(6,10) J, K, ZF
   10 FORMAT('0  FROM ROUTINE ZF(I)', 2I8, F12.5)
      RETURN
      END
C
      REAL FUNCTION DZX(I)
      DIMENSION X(40), A(10,10), V(20)
      INTEGER IFACE(20)
      COMMON/ABCD/ A,NSURF,IFACE
      COMMON/VV/ V,NV,IFLAG
      COMMON X
      NEQ = NV-1
      J = NEQ+I
      K = IFACE(I)
      DZX =A(K,5)*X(J)**2+2*A(K,6)*X(I)*X(J)+A(K,7)*X(J)
     &      +3*A(K,8)*X(I)**2 + 2*A(K,9)*X(I) + A(K,10)
       DZX = (-1)*DZX
C
      RETURN
      END
C
      REAL FUNCTION DZY(I)
      DIMENSION X(40), A(10,10), V(20)
      INTEGER IFACE(20)
      COMMON/ABCD/ A,NSURF,IFACE
      COMMON/VV/ V,NV,IFLAG
      COMMON X
      NEQ = NV-1
      J = NEQ+I
      K = IFACE(I)
      DZY = 3*A(K,2)*X(J)**2 + 2*A(K,3)*X(J) + A(K,4)
     & +2*A(K,5)*X(I)*X(J)+A(K,6)*X(I)**2+A(K,7)*X(I)
       DZY = (-1)*DZY
C
      RETURN
      END
      SUBROUTINE CALFUN( X, F, N, INDEX)
      DIMENSION X(1), F(1), A(10,10), V(20)
      INTEGER IFACE(20)
C
      COMMON/ABCD/ A,NSURF,IFACE
      COMMON/XYZ/ X0, Y0, Z0, XN1, YN1, ZN1
      COMMON/VV/ V,NV,IFLAG
C
```

```
C   CALCULATE THE JACOBIAN MATRIX
C
C     IF INDEX = 1 -- X DIMENSION ONLY
C     IF INDEX = 2 -- Y DIMENSION ONLY
C     IF INDEX = 3 -- BOTH X AND Y DIMENSIONS
C
      NEQ = N
      IF (INDEX .EQ. 3) NEQ=N/2
C
      IF ( NEQ.EQ.1) GO TO 310
C
      DO 100 K=1,NEQ
C
      I = K
      J = NEQ+I
      II = IFACE(I)
      IF ( I .EQ. 1) GO TO 20
      IF ( I .EQ. NEQ) GO TO 25
C
      F(K)=( X(I)-X(I-1)+ DZX(I)*( ZF(I)-ZF(I-1)))
     & /(( X(I)-X(I-1))
     & **2+(X(J)-X(J-1))**2+(ZF(I)-ZF(I-1))**2)**0.5/V(I)
     & +( X(I)-X(I+1)+ DZX(I)*( ZF(I)-ZF(I+1)))
     & /(( X(I)-X(I+1))**2
     &+(X(J)-X(J+1))**2+(ZF(I)-ZF(I+1))**2)**0.5/V(I+1)
C
       GO TO 120
  20  F(K)=( X(I)-X0+DZX(I)*(ZF(I)-Z0))/((X(I)-X0)**2
     &  +(X(J)-Y0)**2 + (ZF(I)-Z0)**2  )**0.5 / V(I)
     &  +(X(I)-X(I+1)+ DZX(I)*(ZF(I)-ZF(I+1)))
     &  /(( X(I)-X(I+1))**2
     &+(X(J)-X(J+1))**2+(ZF(I)-ZF(I+1))**2)**0.5/V(I+1)
       GO TO 120
C
  25  F(K)=(X(I)-X(I-1)+ DZX(I)*(ZF(I)-ZF(I-1)))
     & /(( X(I)-X(I-1))
     & **2+(X(J)-X(J-1))**2+(ZF(I)-ZF(I-1))**2 )**0.5/V(I)
     &  +( X(I)-XN1 + DZX(I)*(ZF(I)-ZN1))/( (X(I)-XN1)**2
     &  +(X(J)-YN1)**2 + (ZF(I)-ZN1)**2 )**0.5 / V(I+1)
C
 120   XTEMP =  DZX(I)
       IF(IFLAG.EQ.1) WRITE(6,30) NEQ,I,J,K,XTEMP,F(K)
       IF (IFLAG.EQ.1)  WRITE(6,35) (X(LL), LL = 1,N)
 100   CONTINUE
C
C
       IF (INDEX-3) 300, 230, 300
C
 230   N2 = NEQ*2
       NEQ1 = NEQ+1
       DO 245 K = NEQ1, N2
       I = K-NEQ
       J = NEQ+I
       II = IFACE(I)
      IF ( I .EQ. 1) GO TO 60
      IF ( I .EQ. NEQ) GO TO 70
C
      F(K)=( X(J)-X(J-1)+ DZY(I)*(ZF(I)-ZF(I-1)))
     & /(( X(I)-X(I-1))
     & **2+(X(J)-X(J-1))**2+(ZF(I)-ZF(I-1))**2)**0.5/V(I)
     &  +( X(J)-X(J+1)+ DZY(I)*( ZF(I)-ZF(I+1)))
     & /(( X(I)-X(I+1))**2
     &+(X(J)-X(J+1))**2+(ZF(I)-ZF(I+1))**2)**0.5/V(I+1)
       GO TO 240
C
  60  F(K)=(X(J)-Y0+DZY(I)*(ZF(I)-Z0))/((X(I)-X0)**2
     &  +(X(J)-Y0)**2 + (ZF(I)-Z0)**2 )**0.5 / V(I)
     &  +(X(J)-X(J+1)+ DZY(I)*(ZF(I)-ZF(I+1)))
     & /(( X(I)-X(I+1))**2
     &+(X(J)-X(J+1))**2+(ZF(I)-ZF(I+1))**2)**0.5/V(I+1)
       GO TO 240
C
  70  F(K)=( X(J)-X(J-1)+ DZY(I)*(ZF(I)-ZF(I-1)))
     & /(( X(I)-X(I-1))
     & **2+(X(J)-X(J-1))**2+(ZF(I)-ZF(I-1))**2)**0.5/V(I)
     &  +( X(J)-YN1+ DZY(I)*(ZF(I)-ZN1) )/((X(I)-XN1)**2
     &  +(X(J)-YN1)**2 + (ZF(I)-ZN1)**2 )**0.5/V(I+1)
C
 240   YTEMP =  DZY(I)
       IF(IFLAG.EQ.1) WRITE(6,30) NEQ,I,J,K,YTEMP,F(K)
       IF (IFLAG.EQ.1)  WRITE(6,35) (X(LL), LL = 1,N)
 245  CONTINUE
C
 300  CONTINUE
C
   30  FORMAT('PARS -- CALFUN', 4I6,2E16.5, F14.6)
   35  FORMAT('X VALUES- CALFUN', 10F10.4)
C
       RETURN
C
C
C   THIS IS A SPECIAL CASE FOR REFLECTION
C   IN ONLY ONE LAYER
C
 310  I = NEQ
      J = NEQ+I
      II = IFACE(I)
       F(1)=( X(I)-X0+ DZX(I)*(ZF(I)-Z0)) /(( X(I)-X0 )**2
     &  +(X(J)-Y0)**2 + (ZF(I)-Z0)**2  )**0.5 / V(I)
     &  +( X(I)-XN1+ DZX(I)*(ZF(I)-ZN1))/( (X(I)-XN1)**2
     &  +(X(J)-YN1)**2 + (ZF(I)-ZN1)**2 )**0.5 / V(I+1)
C
C
       F(2)=( X(J)-Y0+ DZY(I)*(ZF(I)-Z0))/( (X(I)-X0)**2
     &  +(X(J)-Y0)**2 + (ZF(I)-Z0)**2 )**0.5 / V(I)
     &  +( X(J)-YN1+ DZY(I)*(ZF(I)-ZN1))/( (X(I)-XN1)**2
     &  +(X(J)-YN1)**2 + (ZF(I)-ZN1)**2 )**0.5 / V(I+1)
      RETURN
      END
C
      REAL FUNCTION DFX(I)
      DIMENSION X(40), A(10,10), V(20)
      INTEGER IFACE(20)
      COMMON/ABCD/ A,NSURF,IFACE
      COMMON/VV/ V,NV,IFLAG
      COMMON X
      NEQ = NV-1
      J = NEQ+I
      K = IFACE(I)
      DFX = A(K,5)*X(J)**2+2*A(K,6)*X(I)*X(J)+A(K,7)*X(J)
     &      +3*A(K,8)*X(I)**2 + 2*A(K,9)*X(I) + A(K,10)
C
      RETURN
      END
C
      REAL FUNCTION DFY(I)
      DIMENSION X(40), A(10,10), V(20)
      INTEGER IFACE(20)
      COMMON/ABCD/ A,NSURF,IFACE
      COMMON/VV/ V,NV,IFLAG
      COMMON X
      NEQ = NV-1
      J = NEQ+I
      K = IFACE(I)
      DFY = 3*A(K,2)*X(J)**2 + 2*A(K,3)*X(J) + A(K,4)
     & +2*A(K,5)*X(I)*X(J) +A(K,6)*X(I)**2 + A(K,7)*X(I)
C
      RETURN
      END
C
      SUBROUTINE XOFF(NEQ,X,XN1,YN1)
      DIMENSION X(1)
      DO 10 I=1,NEQ
      X(I) =XN1
      X(NEQ+I) = YN1
   10 CONTINUE
      RETURN
      END
C
      SUBROUTINE XYGRID(ID,X0,Y0,NGX,NGY,DX,DY,XRCR,
     & YRCR, DIST)
C
      DIMENSION XRCR(1), YRCR(1), DIST(1), ID(1)
      JJ = 0
C
      DO 20 I = 1, NGX
        DO 10 J=1,NGY
        JJ = JJ+1
        ID(JJ) = JJ
        XRCR(JJ) = X0+(I-1)*DX
        YRCR(JJ) = Y0+(J-1)*DY
        DIST(JJ)=SQRT((XRCR(JJ)-X0)**2+(YRCR(JJ)-Y0)**2)
   10    CONTINUE
   20  CONTINUE
       RETURN
       END
C
       SUBROUTINE CHGM3(IDFACE,A,IA,NCMAX,VT,COEFF,INDEX,
     & IOFSET)
C
C    FOR THIRD-ORDER SURFACE
C
       DIMENSION A(10,10),VT(1),COEFF(1)
C
 1000  FORMAT(' OLD COEFF OF MODELS ', 6F10.5 )
 1010  FORMAT(' NEW COEFF OF MODELS ', 6F10.5 )
C
       IK = IDFACE
C
       GO TO (10,20,30), INDEX
   10  WRITE(4,1000) (A(IK,K2), K2=1,IA), VT(IK)
       WRITE(6,1000) (A(IK,K2), K2=1,IA), VT(IK)
       A(IK,1) = A(IK,1)+COEFF(1)
       A(IK,8) = A(IK,8)+COEFF(2)
       A(IK,9) = A(IK,9)+COEFF(3)
       A(IK,10) = A(IK,10)+COEFF(4)
       IF (IOFSET.NE.0) VT(IK)= VT(IK)+COEFF(5)
       WRITE(4,1010) (A(IK,K2), K2=1,IA), VT(IK)
       WRITE(6,1010) (A(IK,K2), K2=1,IA), VT(IK)
       GO TO 50
C
  20   WRITE(4,1000) (A(IK,K2), K2=1,IA), VT(IK)
       WRITE(6,1000) (A(IK,K2), K2=1,IA), VT(IK)
       A(IK,1) = A(IK,1)+COEFF(1)
       A(IK,2) = A(IK,2)+COEFF(2)
       A(IK,3) = A(IK,3)+COEFF(3)
       A(IK,4) = A(IK,4)+COEFF(4)
       IF (IOFSET.NE.0) VT(IK)= VT(IK)+COEFF(5)
       WRITE(4,1010) (A(IK,K2), K2=1,IA), VT(IK)
       WRITE(6,1010) (A(IK,K2), K2=1,IA), VT(IK)
       GO TO 50
C
  30   WRITE(4,1000) (A(IK,K2), K2=1,IA), VT(IK)
       WRITE(6,1000) (A(IK,K2), K2=1,IA), VT(IK)
C
        DO 35 K2 = 1,IA
   35  A(IK,K2) = A(IK,K2)+COEFF(K2)
       IF (IOFSET.NE.0) VT(IK)= VT(IK)+COEFF(IA+1)
       WRITE(4,1010) (A(IK,K2), K2=1,IA), VT(IK)
       WRITE(6,1010) (A(IK,K2), K2=1,IA), VT(IK)
   50  CONTINUE
C
       RETURN
       END
       SUBROUTINE CHGM2(IDFACE,A,IA,NCMAX,VT,COEFF,INDEX,
     &  IOFSET)
```

```
C
C   FOR SECOND ORDER SURFACE
C
      DIMENSION A(10,10),VT(1),COEFF(1)
C
 1000 FORMAT(' OLD COEFF OF MODELS ', 6F10.5 )
 1010 FORMAT(' NEW COEFF OF MODELS ', 6F10.5 )
C
      IK = IDFACE
C
      GO TO (10,20,30), INDEX
  10  WRITE(4,1000) (A(IK,K2), K2=1,IA), VT(IK)
      WRITE(6,1000) (A(IK,K2), K2=1,IA), VT(IK)
      A(IK,1) = A(IK,1)+COEFF(1)
      A(IK,4) = A(IK,8)+ 0.0
      A(IK,5) = A(IK,9)+COEFF(2)
      A(IK,6) = A(IK,10)+COEFF(3)
      IF (IOFSET.NE.0) VT(IK)= VT(IK)+COEFF(5)
      WRITE(4,1010) (A(IK,K2), K2=1,IA), VT(IK)
      WRITE(6,1010) (A(IK,K2), K2=1,IA), VT(IK)
      GO TO 50
C
 20   WRITE(4,1000) (A(IK,K2), K2=1,IA), VT(IK)
      WRITE(6,1000) (A(IK,K2), K2=1,IA), VT(IK)
      A(IK,1) = A(IK,1)+COEFF(1)
      A(IK,2) = A(IK,2)+ 0.0
      A(IK,3) = A(IK,3)+COEFF(2)
      A(IK,4) = A(IK,4)+COEFF(3)
      IF (IOFSET.NE.0) VT(IK)= VT(IK)+COEFF(5)
      WRITE(4,1010) (A(IK,K2), K2=1,IA), VT(IK)
      WRITE(6,1010) (A(IK,K2), K2=1,IA), VT(IK)
      GO TO 50
C
 30   WRITE(4,1000) (A(IK,K2), K2=1,IA), VT(IK)
      WRITE(6,1000) (A(IK,K2), K2=1,IA), VT(IK)
C
      A(IK,1) = A(IK,1)+COEFF(1)
      A(IK,2) = A(IK,2)+ 0.0
      A(IK,3) = A(IK,3)+ COEFF(2)
      A(IK,4) = A(IK,4)+ COEFF(3)
      A(IK,5) = A(IK,5)+ 0.0
      A(IK,6) = A(IK,6)+ 0.0
      A(IK,7) = A(IK,7)+ COEFF(4)
      A(IK,8) = A(IK,8)+ 0.0
      A(IK,9) = A(IK,9)+COEFF(5)
      A(IK,10) = A(IK,10)+COEFF(6)
C
      IF (IOFSET.NE.0) VT(IK)= VT(IK)+COEFF(7)
      WRITE(4,1010) (A(IK,K2), K2=1,IA), VT(IK)
      WRITE(6,1010) (A(IK,K2), K2=1,IA), VT(IK)
  50  CONTINUE
C
      RETURN
      END
      SUBROUTINE CHGM1(IDFACE,A,IA,NCMAX,VT,COEFF,INDEX,
     &  IOFSET)
C
C   FOR FIRST ORDER SURFACE
C
      DIMENSION A(10,10),VT(1),COEFF(1)
C
 1000 FORMAT(' OLD COEFF OF MODELS ', 6F10.5 )
 1010 FORMAT(' NEW COEFF OF MODELS ', 6F10.5 )
C
      IK = IDFACE
C
      GO TO (10,20,30), INDEX
  10  WRITE(4,1000) (A(IK,K2), K2=1,IA), VT(IK)
      WRITE(6,1000) (A(IK,K2), K2=1,IA), VT(IK)
      A(IK,1) = A(IK,1)+COEFF(1)
      A(IK,4) = A(IK,8)+ 0.0
      A(IK,5) = A(IK,9)+ 0.0
      A(IK,6) = A(IK,10)+COEFF(2)
      IF (IOFSET.NE.0) VT(IK)= VT(IK)+COEFF(3)
      WRITE(4,1010) (A(IK,K2), K2=1,IA), VT(IK)
      WRITE(6,1010) (A(IK,K2), K2=1,IA), VT(IK)
      GO TO 50
C
 20   WRITE(4,1000) (A(IK,K2), K2=1,IA), VT(IK)
      WRITE(6,1000) (A(IK,K2), K2=1,IA), VT(IK)
      A(IK,1) = A(IK,1)+COEFF(1)
      A(IK,2) = A(IK,2)+ 0.0
      A(IK,3) = A(IK,3)+ 0.0
      A(IK,4) = A(IK,4)+COEFF(2)
      IF (IOFSET.NE.0) VT(IK)= VT(IK)+COEFF(3)
      WRITE(4,1010) (A(IK,K2), K2=1,IA), VT(IK)
      WRITE(6,1010) (A(IK,K2), K2=1,IA), VT(IK)
      GO TO 50
C
 30   WRITE(4,1000) (A(IK,K2), K2=1,IA), VT(IK)
      WRITE(6,1000) (A(IK,K2), K2=1,IA), VT(IK)
C
      A(IK,1) = A(IK,1)+COEFF(1)
      A(IK,2) = A(IK,2)+ 0.0
      A(IK,3) = A(IK,3)+ 0.0
      A(IK,4) = A(IK,4)+ COEFF(2)
      A(IK,5) = A(IK,5)+ 0.0
      A(IK,6) = A(IK,6)+ 0.0
      A(IK,7) = A(IK,7)+ 0.0
      A(IK,8) = A(IK,8)+ 0.0
      A(IK,9) = A(IK,9)+ 0.0
      A(IK,10) = A(IK,10)+COEFF(3)
C
      IF (IOFSET.NE.0) VT(IK)= VT(IK)+COEFF(4)
      WRITE(4,1010) (A(IK,K2), K2=1,IA), VT(IK)
      WRITE(6,1010) (A(IK,K2), K2=1,IA), VT(IK)
  50  CONTINUE
```

```
C
      RETURN
      END
C
      SUBROUTINE PDER3(X,Z,NEQ,ILAYER,FCN,INDEX,NCMAX,IOFSET)
C
C    FOR THE THIRD-ORDER SURFACE
C
C   THIS ROUTINE IS DESIGNED FOR THE REFLECTED DATA
C
      DIMENSION X(1), Z(1), FCN(1), V(20)
      COMMON/XYZ/ X0, Y0, Z0, XN1, YN1, ZN1
      COMMON/VV/ NV, V, IFLAG
C
C
      I = ILAYER
      J = NEQ+I
C
      IF ( I.EQ.1) GO TO 20
      IF ( I.EQ.NEQ) GO TO 30
C
      T1=-(Z(I)-Z(I-1))/((X(I)-X(I-1))**2+(X(J)-X(J-1))**2
     &    +(Z(I)-Z(I-1))**2)**0.5/V(I)
      T2= (Z(I+1)-Z(I))/((X(I+1)-X(I))**2+(X(J+1)-X(J))**2
     &    +(Z(I+1)-Z(I))**2) **0.5/V(I+1)
      T3= -((X(I)-X(I-1))**2+(X(J)-X(J-1))**2
     &    +(Z(I)-Z(I-1))**2)**0.5/ V(I)**2
      T4= -( (X(I+1)-X(I))**2+(X(J+1)-X(J))**2
     &    +(Z(I+1)-Z(I))**2) **0.5/V(I+1)**2
C
      GO TO 40
  20  T1= -(Z(I)-Z0)/((X(I)-X0)**2+(X(J)-Y0)**2+(Z(I)-Z0)
     & **2) **0.5/V(I)
      T2=(Z(I+1)-Z(I))/((X(I+1)-X(I))**2+(X(J+1)-X(J))**2
     &   +(Z(I+1)-Z(I))**2) **0.5/V(I+1)
      T3=-((X(I)-X0)**2+(X(J)-Y0)**2+(Z(I)-Z0)**2)
     &  **0.5/ (V(I)**2)
      T4= -( (X(I+1)-X(I))**2 +(X(J+1)-X(J))**2
     &   +(Z(I+1)-Z(I))**2) **0.5/ (V(I+1)**2)
C
      GO TO 40
C
  30  T1=-(Z(I)-Z(I-1))/((X(I)-X(I-1))**2+(X(J)-X(J-1))
     &     **2+(Z(I)-Z(I-1))**2) **0.5/V(I)
      T2= (ZN1-Z(I))/((XN1-X(I))**2+(YN1-X(J))**2
     & +(ZN1-Z(I))**2)**0.5/V(I+1)
      T3= -((X(I)-X(I-1))**2+(X(J)-X(J-1))**2
     &    +(Z(I)-Z(I-1))**2) **0.5/ (V(I)**2)
      T4= -((XN1-X(I))**2+(YN1-X(J))**2+(ZN1-Z(I))**2)
     &  **0.5/ (V(I+1)**2)
  40  CONTINUE
C
      T12 = T1+T2
      T34 = T3+T4
```

```
C
      GO TO (50,60,70), INDEX
  50  NCMAX = 5
      IF (IOFSET.EQ.0) NCMAX=NCMAX-1
      FCN(1) = T12
      FCN(2) = T12*X(I)**3
      FCN(3) = T12*X(I)**2
      FCN(4) = T12*X(I)
      FCN(5) = T34
      GO TO 90
C
  60  NCMAX = 5
      IF (IOFSET.EQ.0) NCMAX=NCMAX-1
      FCN(1) = T12
      FCN(2) = T12*X(J)**3
      FCN(3) = T12*X(J)**2
      FCN(4) = T12*X(J)
      FCN(5) = T34
      GO TO 90
C
  70  IF (IOFSET.EQ.0) NCMAX=NCMAX-1
      FCN(1) = T12
      FCN(2) = T12 * X(J)**3
      FCN(3) = T12 * X(J)**2
      FCN(4) = T12 * X(J)
      FCN(5) = T12 * X(I)* X(J)**2
      FCN(6) = T12 * X(J)* X(I)**2
      FCN(7) = T12 * X(I)* X(J)
      FCN(8) = T12 * X(I)**3
      FCN(9) = T12 * X(I)**2
      FCN(10) = T12 * X(I)
      FCN(11) = T34
C
  90  CONTINUE
C
      RETURN
      END
C
C
      SUBROUTINE PDER2(X,Z,NEQ,ILAYER,FCN,INDEX,NCMAX,
     &  IOFSET)
C
C    FOR SECOND ORDER SURFACE
C
C   THIS ROUTINE IS DESIGNED FOR THE REFLECTED DATA
C
      DIMENSION X(1), Z(1), FCN(1), V(20)
      COMMON/XYZ/ X0, Y0, Z0, XN1, YN1, ZN1
      COMMON/VV/ NV, V, IFLAG
C
C
      I = ILAYER
      J = NEQ+I
C
```

```
      IF ( I.EQ.1) GO TO 20
      IF ( I.EQ.NEQ) GO TO 30
C
      T1=-(Z(I)-Z(I-1))/((X(I)-X(I-1))**2+(X(J)-X(J-1))**2
     &    +(Z(I)-Z(I-1))**2)**0.5/V(I)
      T2= (Z(I+1)-Z(I))/((X(I+1)-X(I))**2+(X(J+1)-X(J))**2
     &    +(Z(I+1)-Z(I))**2) **0.5/V(I+1)
      T3= -((X(I)-X(I-1))**2+(X(J)-X(J-1))**2
     &    +(Z(I)-Z(I-1))**2)**0.5/ V(I)**2
      T4= -( (X(I+1)-X(I))**2+(X(J+1)-X(J))**2
     &    +(Z(I+1)-Z(I))**2) **0.5/V(I+1)**2
C
      GO TO 40
   20 T1=-(Z(I)-Z0)/((X(I)-X0)**2+(X(J)-Y0)**2+(Z(I)-Z0)
     & **2)**0.5/V(I)
      T2= (Z(I+1)-Z(I))/((X(I+1)-X(I))**2+(X(J+1)-X(J))**2
     &   +(Z(I+1)-Z(I))**2) **0.5/V(I+1)
      T3= -((X(I)-X0)**2+(X(J)-Y0)**2+(Z(I)-Z0)**2)
     & **0.5/ (V(I)**2)
      T4= -( (X(I+1)-X(I))**2 +(X(J+1)-X(J))**2
     &   +(Z(I+1)-Z(I))**2) **0.5/ (V(I+1)**2)
C
      GO TO 40
C
   30 T1=-(Z(I)-Z(I-1))/((X(I)-X(I-1))**2+(X(J)-X(J-1))**2
     &    +(Z(I)-Z(I-1))**2) **0.5/V(I)
      T2= (ZN1-Z(I))/((XN1-X(I))**2+(YN1-X(J))**2
     &   +(ZN1-Z(I))**2) **0.5/V(I+1)
      T3= -((X(I)-X(I-1))**2+(X(J)-X(J-1))**2
     &    +(Z(I)-Z(I-1))**2) **0.5/ (V(I)**2)
      T4= -((XN1-X(I))**2+(YN1-X(J))**2+(ZN1-Z(I))**2)
     & **0.5/ (V(I+1)**2)
   40 CONTINUE
C
      T12 = T1+T2
      T34 = T3+T4
C
      GO TO (50,60,70), INDEX
   50 NCMAX = 4
      IF (IOFSET.EQ.0) NCMAX=NCMAX-1
      FCN(1) = T12
      FCN(2) = T12*X(I)**2
      FCN(3) = T12*X(I)
      FCN(4) = T34
      GO TO 90
C
   60 NCMAX = 4
      IF (IOFSET.EQ.0) NCMAX=NCMAX-1
      FCN(1) = T12
      FCN(2) = T12*X(J)**2
      FCN(3) = T12*X(J)
      FCN(4) = T34
      GO TO 90
C
```

```
   70  NCMAX = 7
       IF (IOFSET.EQ.0) NCMAX=NCMAX-1
       FCN(1) = T12
       FCN(2) = T12 * X(J)**2
       FCN(3) = T12 * X(J)
       FCN(4) = T12 * X(I)* X(J)
       FCN(5) = T12 * X(I)**2
       FCN(6) = T12 * X(I)
       FCN(7) = T34
C
   90  CONTINUE
C
       RETURN
       END
       SUBROUTINE PDER1(X,Z,NEQ,ILAYER,FCN,INDEX,NCMAX,
     &  IOFSET)
C
C    FOR FIRST ORDER SURFACE
C
C   THIS ROUTINE IS DESIGNED FOR THE REFLECTED DATA
C
       DIMENSION X(1), Z(1), FCN(1), V(20)
       COMMON/XYZ/ X0, Y0, Z0, XN1, YN1, ZN1
       COMMON/VV/ NV, V, IFLAG
C
C
       I = ILAYER
       J = NEQ+I
C
       IF ( I.EQ.1) GO TO 20
       IF ( I.EQ.NEQ) GO TO 30
C
       T1=-(Z(I)-Z(I-1))/((X(I)-X(I-1))**2+(X(J)-X(J-1))**2
     &     +(Z(I)-Z(I-1))**2)**0.5/V(I)
       T2= (Z(I+1)-Z(I))/((X(I+1)-X(I))**2+(X(J+1)-X(J))**2
     &     +(Z(I+1)-Z(I))**2) **0.5/V(I+1)
       T3= -((X(I)-X(I-1))**2+(X(J)-X(J-1))**2
     &     +(Z(I)-Z(I-1))**2)**0.5/ V(I)**2
       T4= -( (X(I+1)-X(I))**2+(X(J+1)-X(J))**2
     &     +(Z(I+1)-Z(I))**2) **0.5/V(I+1)**2
C
       GO TO 40
   20  T1= -(Z(I)-Z0)/((X(I)-X0)**2+(X(J)-Y0)**2+(Z(I)-Z0)
     & **2) **0.5/V(I)
       T2= (Z(I+1)-Z(I))/((X(I+1)-X(I))**2+(X(J+1)-X(J))**2
     &    +(Z(I+1)-Z(I))**2) **0.5/V(I+1)
       T3= -((X(I)-X0)**2+(X(J)-Y0)**2+(Z(I)-Z0)**2)
     &  **0.5/ (V(I)**2)
       T4= -( (X(I+1)-X(I))**2 +(X(J+1)-X(J))**2
     &    +(Z(I+1)-Z(I))**2) **0.5/ (V(I+1)**2)
C
       GO TO 40
C
   30  T1=-(Z(I)-Z(I-1))/((X(I)-X(I-1))**2+(X(J)-X(J-1))**2
     &    +(Z(I)-Z(I-1))**2) **0.5/V(I)
      T2= (ZN1-Z(I))/((XN1-X(I))**2+(YN1-X(J))**2
     &   +(ZN1-Z(I))**2) **0.5/V(I+1)
      T3= -((X(I)-X(I-1))**2+(X(J)-X(J-1))**2
     &    +(Z(I)-Z(I-1))**2) **0.5/ (V(I)**2)
      T4= -((XN1-X(I))**2+(YN1-X(J))**2+(ZN1-Z(I))**2)
     &  **0.5/ (V(I+1)**2)
  40  CONTINUE
C
      T12 = T1+T2
      T34 = T3+T4
C
      GO TO (50,60,70), INDEX
  50  NCMAX = 3
      IF (IOFSET.EQ.0) NCMAX=NCMAX-1
      FCN(1) = T12
      FCN(2) = T12*X(I)
      FCN(3) = T34
      GO TO 90
C
  60  NCMAX = 3
      IF (IOFSET.EQ.0) NCMAX=NCMAX-1
      FCN(1) = T12
      FCN(2) = T12*X(J)
      FCN(3) = T34
      GO TO 90
C
  70  NCMAX = 4
      IF (IOFSET.EQ.0) NCMAX=NCMAX-1
      FCN(1) = T12
      FCN(2) = T12 * X(J)
      FCN(3) = T12 * X(I)
      FCN(4) = T34
C
  90  CONTINUE
C
      RETURN
      END
```